

# **Novel Methods for Studying Ras/Erk MAP Kinase**

## **Signaling in Developing T Cells**

Thesis by

Harry Miguel Green

In Partial Fulfillment of the Requirements  
for the Degree of  
Doctor of Philosophy



California Institute of Technology  
Pasadena, California

2006

(Defended August 4, 2005)

© 2006

Harry M. Green

All Rights Reserved

## Acknowledgements

I would like to dedicate this dissertation to my wife, Shelley. Without your constant support and love, this thesis would have never been. You are my everything and without you I have nothing. Thank you also to my family, who has always given me so much support and to which I cannot give enough credit. To my mother and father, thank you for support through my Ph.D., and supporting my decision to do something different. To my many siblings, I hope that I will have more time to spend with each and every one of you.

I would like to thank Pepe Alberola-Ila for his help and support throughout my Ph.D. work. He gave me the opportunity to learn more than I could have possibly imagined in those 5 years. The skills I obtained under his tutelage gave me the critical thinking and survival skills I will need in the future as a practicing clinician. I would also like to thank my other committee members Scott Fraser, Ellen Rothenberg, Pamela Bjorkman, and Mary Kennedy for their helpful comments and suggestions throughout my time at Caltech. I would like to especially acknowledge Scott and Ellen, who went out of their way on many occasions for my benefit.

I would like to thank and acknowledge the members of the Alberola-Ila lab: Micheline Laurent, Gabo Hernandez-Hoyos, Eric Tse, Christie Beel, Susannah Barbee, and Chi Wang. Thanks especially to Micheline for teaching me how to clone and being a great baymate and friend. Special thanks also to Gabo for her help with FTOCs and southern blotting and also for her friendship. And to Eric, who showed me more than anyone that life is too precious to throw away, to appreciate the good things, and not always look at the bad. Wherever you are, my friend, may you be at peace and know that

you will always be in my heart.

I received much help outside of my laboratory that I would like to acknowledge. Thanks to Terry Takahashi for all his advice on protein purification. Thank you also to Randal Bass, who helped me optimize said purification. I would like to thank Mollie Meffert and Joel Pomerantz for some discussions that helped me get on the right track.

Lastly, I'd like to apologize to my friend Patrick Freyne. I'm sure the lengthy title of my thesis comes as a great disappointment.

## Abstract

The Ras/Erk MAPK pathway has been shown to be important in multiple developmental contexts. The development of T cells in the thymus is one such developmental system. Thymocytes undergo positive and negative selection, processes by which they are “chosen” for their ability to recognize MHC molecules loaded with peptide on the surface of cells, but only to react when the peptide is foreign. The Ras/Erk cascade has been shown to be indispensable during the onset of positive selection, but the mechanism of Erk signaling in this process is unknown. In addition, it is unclear if the Ras/Erk cascade is involved in the differentiation phase of positive selection called CD4/CD8 lineage determination, where thymocytes either become CD4<sup>+</sup> or CD8<sup>+</sup> T cells. Furthermore, Erk signaling has been shown to be activated during negative selection, but seems dispensable. In this thesis, we describe novel methods for analyzing Erk signaling by applying new technologies to gain a different perspective on Erk signaling in thymocytes during selection. To this end, we have utilized a technique of intracellular staining to obtain data for single-cell Erk activation in the context of a population of fixed thymocytes. We also pursued the development of FRET-based, genetically-encoded intracellular sensors of Erk activity that could be applied to the analysis of Erk signaling in live thymocytes *in vivo*. To examine the involvement of Ras/Erk signaling during CD4/CD8 lineage determination, we applied a recently described method of lentiviral transgenesis to examine dose-dependent effects of a dominant negative form of Mek, the Erk MAPK kinase, in a single mouse generation. These studies have yielded insights into Erk signaling events and advanced the development of novel techniques to examine signaling during thymocyte selection.

## Contents

<b>Acknowledgements</b> . . . . .	<b>iii</b>
<b>Abstract.</b> . . . . .	<b>v</b>
<b>List of Figures</b> . . . . .	<b>xi</b>
<b>List of Tables</b> . . . . .	<b>xii</b>
<b>1 Introduction</b> . . . . .	<b>1</b>
1.1 T Cells: An Overview of Development and Signaling . . . . .	1
1.1.1 T cells and the immune system . . . . .	1
1.1.2 Developmental path of the T cell . . . . .	3
1.1.3 Ras/Erk MAPK signaling in selection. . . . .	8
1.2 FRET and Fluorescent Probes of Intracellular Signaling Activity . . . . .	14
1.2.1 Fluorescence resonance energy transfer . . . . .	14
1.2.2 Sensors of intracellular signaling utilizing FRET . . . . .	15
1.3 Chapter Overview . . . . .	18
1.3.1 Chapter 2 . . . . .	18
1.3.2 Chapter 3 . . . . .	19
1.3.3 Chapter 4 . . . . .	20
1.4 References . . . . .	21

## 2 Intracellular Staining of Activated Erk MAP Kinase Reveals Switch-Like

<b>Activation Kinetics in Thymocytes . . . . .</b>	<b>32</b>
2.1 Abstract . . . . .	32
2.2 Background . . . . .	33
2.3 Results and Discussion . . . . .	37
2.3.1 Intracellular staining of pErk reveals bimodal distribution of activation upon stimulation with PMA . . . . .	37
2.3.2 Bimodal Erk activation is a function of strength and duration of PMA stimulation . . . . .	43
2.3.3 Optimizing cell surface marker staining under fixation and permeabilization conditions . . . . .	48
2.3.4 Cross-reactivity of cell surface marker antibodies with goat-anti-mouse secondary antibody used for detection of pErk intracellular staining. . .	53
2.3.5 Inability to activate thymocytes with $\alpha$ -CD3 $\epsilon$ or Jurkats with $\alpha$ -hCD3 (OKT3) . . . . .	57
2.4 Future Directions . . . . .	59
2.5 Concluding Remarks . . . . .	60
2.6 Materials and Methods. . . . .	61
2.6.1 Materials. . . . .	61
2.6.2 <i>In vitro</i> stimulations and cell stainings . . . . .	62
2.6.3 Western blotting. . . . .	62
2.7 References . . . . .	63

<b>3 Development of ERK Activity Sensor, an <i>In Vitro</i>, FRET-based Sensor of Extracellular Regulated Kinase Activity . . . . .</b>	<b>67</b>
3.1 Abstract. . . . .	67
3.2 Background. . . . .	68
3.3 Results and Discussion. . . . .	71
3.3.1 Design and model of EAS. . . . .	71
3.3.2 EAS FRET changes in the presence of active ERK2 . . . . .	73
3.3.3 EAS changes in FRET in response to pERK2 require phosphorylation and the ERK binding site . . . . .	74
3.3.4 EAS-3 is not phosphorylated by pSAPK or pp38. . . . .	76
3.4 Conclusions. . . . .	80
3.5 Methods . . . . .	80
3.5.1 EAS constructs . . . . .	80
3.5.2 EAS and active kinase expression. . . . .	81
3.5.3 Kinase assays and fluorimetry. . . . .	82
3.6 References . . . . .	83
<b>4 Exploring Dose-Response Effects of dMek1 and ROG on CD4/CD8 Lineage Determination Using Lentiviral Transgenesis . . . . .</b>	<b>86</b>
4.1 Abstract. . . . .	86
4.2 Background. . . . .	87
4.3 Results and Discussion. . . . .	92
4.3.1 Reproduction of FLckGW mice. . . . .	92
4.3.2 Variegation in lentiviral gene expression is stable . . . . .	96

4.3.3	Analysis of dMek1 and ROG expression in transgenic mice . . . . .	109
4.2.4	Establishing AND <sup>+/+</sup> -Rag2 KO mouse line . . . . .	115
4.4	Future Directions. . . . .	119
4.5	Concluding Remarks . . . . .	120
4.6	Materials and Methods. . . . .	120
4.6.1	Cell staining and flow cytometry . . . . .	120
4.6.2	Production of lentivirus. . . . .	121
4.6.3	Reaggregate fetal thymic organ culture. . . . .	121
4.6.4	Southern blotting of genomic DNA. . . . .	122
4.7	References . . . . .	122
<b>5</b>	<b>A General Approach to Detect Protein Expression <i>In Vivo</i> Using Fluorescent Puromycin Conjugates . . . . .</b>	<b>127</b>
5.1	Abstract. . . . .	127
5.2	Introduction . . . . .	128
5.3	Results . . . . .	131
5.3.1	Design of puromycin conjugates. . . . .	131
5.3.2	Analysis of puromycin-conjugate activity <i>in vitro</i> . . . . .	133
5.3.3	Analysis of puromycin-conjugate activity <i>in vivo</i> . . . . .	134
5.3.4	Mechanism of puromycin conjugate activity <i>in vivo</i> . . . . .	139
5.3.5	Western blot analysis of puromycin conjugate labeling in live cells . . . . .	144
5.4	Discussion . . . . .	145
5.5	Significance . . . . .	148
5.6	Experimental Procedures. . . . .	148

5.6.1 Materials. . . . .148

5.6.2 Puromycin conjugates . . . . . 149

5.6.3 *In vitro* potency determination for puromycin conjugates . . . . .150

5.6.4 Neutravidin capture of *in vitro* translated protein-puromycin-conjugate products . . . . .150

5.6.5 Preparation of MIG<sub>PAC</sub> infected 16610D9 cells . . . . . 151

5.6.6 Enrichment of GFP(+) 16610D9 cells using puromycin and puromycin conjugates . . . . .151

5.6.7 Detection of protein synthesis events *in vivo* using flow cytometry . . .152

5.6.8 Western analysis of 16610D9 cells treated with puromycin conjugates .152

5.7 Acknowledgements. . . . .153

5.8 References . . . . .153

## List of Figures

1-1	T cell development in the thymus . . . . .	4
1-2	Cameleon sensors are Ca <sup>++</sup> -sensitive. . . . .	17
2-1	All-or-none Erk response is triggered by threshold stimulation . . . . .	36
2-2	Differential analysis of 16610D9 cells stimulated with PMA reveals bimodal Erk activation . . . . .	39
2-3	Bimodal Erk activation occurs in both thymocytes and peripheral T cells . . .	41
2-4	Jurkats display graded Erk activation upon PMA stimulation . . . . .	42
2-5	Time course of thymocytes with different PMA concentrations reveals qualitative and quantitative differences in Erk activation . . . . .	45
2-6	Optimizing surface staining under fixation/permeabilization conditions . . . .	50
2-7	Optimizing CD4/CD8 staining under fixation/permeabilization conditions. . .	51
2-8	G $\alpha$ M-bio secondary antibody used for pErk intracellular staining is cross- reactive with $\alpha$ -CD3 . . . . .	55
2-9	G $\alpha$ M-bio secondary antibody used for pErk intracellular staining also cross- reacts with $\alpha$ -CD4, $\alpha$ -CD8, and $\alpha$ -TCR $\beta$ . . . . .	56
2-10	G $\alpha$ R-bio secondary antibody used for pErk intracellular staining shows no cross-reactivity with surface marker antibodies . . . . .	58

3-1	A model for EAS activation and construct design . . . . .	72
3-2	EAS proteins are targets for ERK2 and exhibit decreased FRET efficiency upon phosphorylation. . . . .	75
3-3	Mutation of key residues diminishes EAS-3 phosphorylation by pERK2.77	
3-4	Determination of ERK2 specificity for EAS-3. . . . .	79
4-1	Experimental design for lentiviral transgenic analysis of CD4/CD8 lineage determination. . . . .	88
4-2	The structure of the FLckGW construct and genomic analysis of transgene integrations . . . . .	93
4-3	Thymic analysis of 3 mice from injection panel PN681 for GFP expression .	95
4-4	Splenic analysis of 3 mice from injection panel PN681 for GFP expression .	97
4-5	Experimental design to determine stability of variegation in transgene expression . . . . .	99
4-6	GFP expression in individual fetal thymii from transgenic fetuses . . . . .	100
4-7	C57Bl/6 and B6D2F1 thymocytes can be distinguished by $\alpha$ -CD5.1, but not by $\alpha$ -H-2D <sup>d</sup> . . . . .	102
4-8	GFP analysis of day 7 RgFTOC lobes . . . . .	103
4-9	CD4/CD8 analysis of the GFP <sup>-</sup> population from day 7 RgFTOC lobes . . . .	105
4-10	CD4/CD8 analysis of the GFP <sup>+</sup> population from day 7 RgFTOC lobes. . . .	106
4-11	Day 14 analysis of RgFTOC lobes for GFP expression and host contamination. . . . .	107
4-12	Analysis of FLp(dMek1)IGW mice in a DO11.10 TCR background . . . . .	111

4-13	FLAG-tagged proteins are detectable with intracellular staining, whereas Mek 1/2 are not. . . . .	114
4-14	Mice positive for the ROG transgene showed slight enhancement of both the CD4 and CD8 lineages . . . . .	116
4-15	Determination of homozygosity of the AND TCR gene in AND/Rag2 <sup>o</sup> mice .	118
5-1	Scheme for fluorescent puromycin action . . . . .	130
5-2	Structures of fluorescent puromycin conjugates . . . . .	132
5-3	<i>In vitro</i> activity analysis for various puromycin conjugates . . . . .	135
5-4	Analysis of puromycin conjugate activity in 16610D9 thymocyte cells . . .	138
5-5	Fluorescence shift analysis for puromycin conjugates versus negative control molecules in 16610D9 thymocyte cells . . . . .	140
5-6	Mechanism of action of puromycin and puromycin conjugates in 16610D9 thymocyte cells . . . . .	143
5-7	Western analysis of 16610D9 thymocyte cells treated with a puromycin conjugate and analyzed using an $\alpha$ -fluorescein antibody . . . . .	146

## List of Tables

5-1	The concentration of puromycin conjugate required for 50% inhibition of globin translation (IC <sub>50</sub> ) . . . . .	136
-----	---	-----

# Chapter 1

## Introduction

### 1.1 T Cells: An Overview of Development and Signaling

#### 1.1.1 T cells and the immune system

The mammalian immune system is composed of two distinct parts, the innate and the adaptive. While both parts are derived from the same progenitors, they serve distinct functions in the protection of the organism from outside invasion. The innate immune system offers a first line of defense, where any breach of physical barriers (skin, mucosa) by pathogens immediately activates such players as polymorphonuclear leukocytes (neutrophils, basophils, eosinophils), monocytes/macrophages, and mast cells [1]. These cells are able to stifle many pathogens and, at a minimum, keep them at bay until the adaptive immune system has had sufficient time to mount a response. The adaptive immune system, composed of T and B lymphocytes, then mounts a far more effective response, working in concert with the innate immune system to completely eliminate the pathogen altogether [2]. In this way, an individual can ward off infection and potential life-threatening illnesses. Deficiencies in these processes often lead to chronic or opportunistic infections, which threaten the well-being of the organism.

T and B lymphocytes have the potential to recognize and eradicate any foreign pathogen. The ability to accomplish this feat lies within the genetic coding sequence of the T cell receptor (TCR) and B cell receptor (BCR). While the TCR and BCR have fundamental differences, they both possess a binding region that is derived from a semi-random process called receptor rearrangement [3, 4]. This rearrangement is responsible for the ability of the adaptive immune system to generate cells that can potentially identify any foreign antigen *a priori*. Of these two cell types, T cells are responsible for orchestrating the immune response, directing the other cells of the immune system to effectively respond to a foreign pathogen.

As orchestrators of immune response, T cells must be able to distinguish “self” from “non-self” (i.e., foreign). To achieve this end, T cells must be “educated” throughout their development to be able to scan Major Histocompatibility Complex (MHC)-peptide molecules on antigen presenting cells (APCs) and react if foreign peptides are detected, but remain quiescent if only self-peptides are displayed [5-7]. Portions of this education are stochastic in nature, such as receptor gene rearrangement, and other portions are seemingly instructive. The end result of normal development is a repertoire of T cells, each with a unique receptor that will detect a unique foreign peptide antigen. Faulty development can result in a multitude of disorders, ranging from the complete absence of T cells and therefore no effective adaptive immunity, to autoimmune diseases, when T cells become inappropriately activated by self-antigens and mount a response to host tissues [8, 9]. Either can be catastrophic, allowing infection that can lead to death or extensive damage to multiple organ systems, respectively.

### 1.1.2 Developmental path of the T cell

T cells originate from hematopoietic stem cells (HSCs) in the bone marrow, just as all immune cells do. T cell progenitors exit the bone marrow into the blood and home to the thymus, an organ located rostral to the heart. The thymus has a distinct structure that plays a necessary role in the normal development of thymocytes [10, 11] (Figure 1-1). On the gross histological level, the thymus is separated into two distinct areas called the cortex and the medulla. Aside from the T cell progenitors and thymocytes that occupy the thymus, the cortex is populated by epithelial cells and the medulla is populated by epithelial and bone marrow-derived cells. These cells facilitate the developmental progression of thymocytes, providing distinct developmental signals [10]. The spatial separation of these cell types is also functional, with the earliest developmental stages occurring in the outermost cortex (sub-capsular zone) and moving inward toward the medulla. The progenitors mentioned above exit the bloodstream into the cortex of the thymus and are thus termed thymocytes until they exit into the bloodstream at the end of their development.

At this stage thymocytes reside in the cortex and can be identified by surface markers termed clusters of differentiation (CD) 4 and CD8. These cells are referred to as “double-negative” (DN) because of their lack of CD4 or CD8 TCR-coreceptor expression [12]. This population of thymocytes is usually characterized by 4 sub-populations, termed DN1, DN2, DN3, and DN4. Each DN sub-population is identified by the expression pattern of two cell-surface markers, CD25 and CD44. DN1 cells are CD25<sup>-</sup>/CD44<sup>+</sup>, DN2 cells are CD25<sup>+</sup>/CD44<sup>+</sup>, DN3 are CD25<sup>+</sup>/CD44<sup>-</sup>, and the DN4 stage is CD25<sup>-</sup>/CD44<sup>-</sup> [13]. These phenotypic changes are used to follow developmental

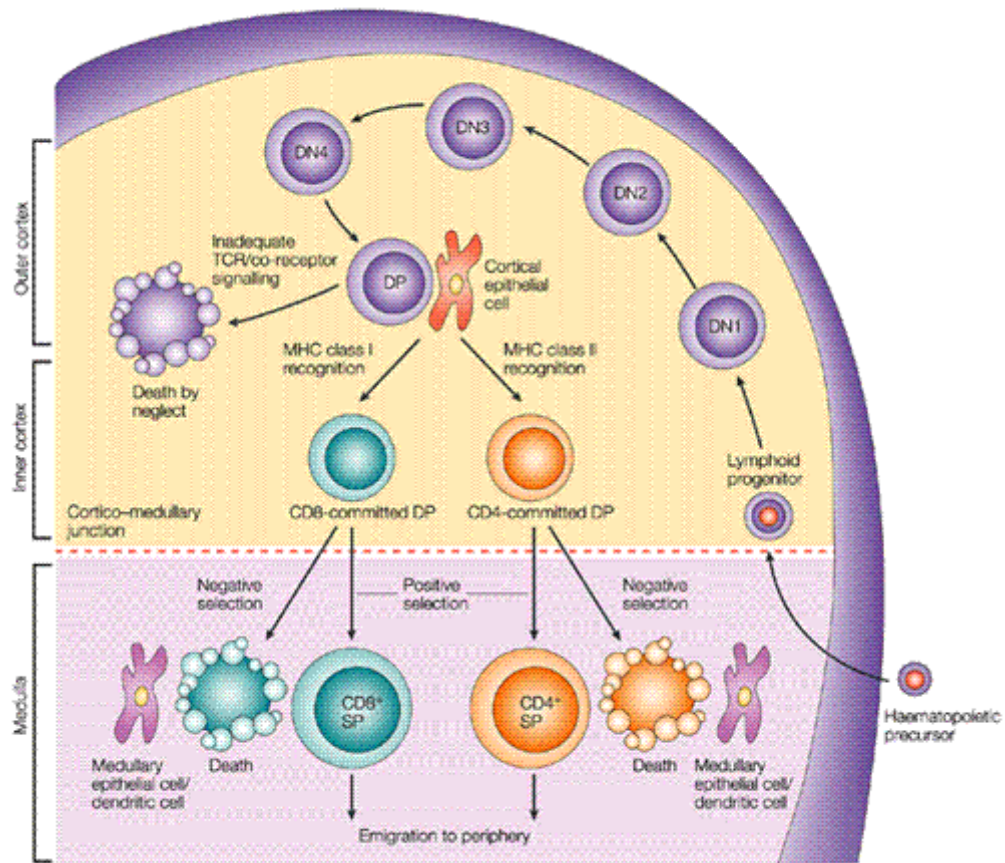


**Figure 1-1. T cell development in the thymus.** T cell progenitors home to the thymus from the bone marrow and enter the thymic cortex. As development progresses through the DN stages, cells move to the outer cortex and to the inner cortex and cortico-medullary junctions at the DP stage. Positive and negative selection ensue as thymocytes migrate into the medulla of the thymus. Final maturation occurs in the medulla, and fully mature T cells migrate out of the thymus through blood vessels in the cortico-medullary junction. Figure from [11].

progress, but are not the only changes in gene expression of these cells.

By the DN3 stage, there is a bifurcation that results in two different types of T cells that are characterized by the type of TCR chains expressed, either  $\alpha\beta$  or  $\gamma\delta$  [14]. These two populations are functionally different and have different developmental paths, and the research we describe here is based on  $\alpha\beta$  T cell development. In the  $\alpha\beta$  lineage, thymocytes have committed to the T cell lineage and begin to rearrange the TCR $\beta$ . The TCR $\beta$ -receptor chain gene locus undergoes a series of recombination events, where small genetically variable regions of the gene are spliced together by RAG recombinases to form an intact receptor (reviewed in [15]). Receptor rearrangement is also inaccurate at the site of gene splicing, which corresponds to the binding region of the translated receptor. The variability produced by both the TCR $\alpha$  (discussed later) and  $\beta$  chains is the basis of foreign antigen recognition [16]. A consequence of generating this variability is that many rearrangements result in either an untranslatable gene product, which produces no receptor at all, or a translated receptor that is unable to recognize MHC molecules on the surface of target cells. In the former case, the thymocyte has two gene copies and is able to rearrange both loci if necessary, giving the cell more than enough opportunity to produce a successfully translatable transcript. The latter case is as useless to the immune system as no receptor at all, since the targets of the TCR are MHC molecules bound to peptides. To achieve an acceptable level of variability within the T cell compartment, this process is incredibly wasteful. It has been estimated that 90% of cells either do not successfully rearrange their receptor or successfully express a receptor that fails to interact with MHC-peptide on the surface of cortical and medullary APCs. These cells fail to receive a signal from the TCR and end up dying by apoptosis [17].

Upon rearrangement of the TCR $\beta$  chain gene locus that yields a full length receptor chain protein product, the TCR $\beta$  receptor chain is integrated into a complex containing an invariant pre-T $\alpha$  chain and CD3, termed the pre-T $\alpha$  receptor complex [18]. The pre-T $\alpha$  chain acts as a surrogate TCR $\alpha$  chain until the actual TCR $\alpha$  chain gene locus has been rearranged, which occurs later in development. CD3 is made up of six receptor chains that form one homodimer (CD3 $\zeta\zeta$ ) and two heterodimers (CD3 $\delta\gamma$  and CD3 $\epsilon\gamma$ ) [19]. Under normal conditions both TCR chains and six CD3 chains form the TCR signaling complex, where CD3 is crucial in forming proper signaling events later in development. This checkpoint, referred to as  $\beta$ -selection, is crucial in thymocyte development, and signals from this complex allow development to proceed. The  $\beta$ -chain locus is prevented from undergoing further rearrangement by allelic exclusion, presumably to prevent further rearrangements on an already translatable receptor [20]. Pre-T $\alpha$  signals also induce cells to undergo several rounds of division and upregulate the coreceptors CD4 and CD8 [17]. We utilize co-expression of CD4 and CD8 as phenotypic markers indicating that the  $\beta$ -selection checkpoint has been passed and refer to these cells as double-positive (DP).

The majority of DN development occurs in the cortex of the thymus (Figure 1-1) [21]. As thymocytes progress through the DN stages, they gradually move inward toward the medulla. At the DP stage, they have moved through the cortex to the cortico-medullary junction, where they begin to receive selection signals. The process of selection is thought to be an “education” of thymocytes and is the basis for the ability of T cells to scan peptides loaded on MHC molecules, reacting to MHC bound to foreign peptides but not to self-peptides bound to MHC. MHC molecules are expressed on the

surface of APCs and are loaded with peptides, derived from either intracellular proteins on MHC class I or extracellular proteins on MHC class II. T cells must be capable of interacting with MHC/peptide complexes with enough affinity/avidity to scan them in the presence of peptide. This interaction, however, must be weak enough to not elicit a response if only self-peptide is present. A thymocyte with a TCR that binds MHC/self-peptide with too high affinity/avidity could potentially react to tissues out in the periphery and cause auto-immune disease [9]. To this end, selection has been characterized by two processes, termed positive selection and negative selection.

Positive selection is the survival and maturation of DPs due to intermediate affinity/avidity interactions between the TCR and MHC/peptides. Phenotypically they are identified by the expression of CD69 and heat stable antigen (HSA) [22, 23]. Those cells that have TCRs that interact too weakly with or cannot bind MHC/peptide do not receive the proper intracellular signals to promote survival. These cells then “die by neglect” meaning they apoptose due to the lack of signal. Positive selection is counter-balanced by negative selection, the process by which potentially auto-reactive thymocytes are removed from the T cell repertoire. Thymocytes that recombine their TCR chains such that the receptor binds too strongly to MHC/self-peptide receive strong intracellular signals. These thymocytes are deleted from the maturing population by apoptosis, avoiding the production of T cells that could possibly react to self [24, 25].

Positive selection also encompasses lineage determination, which is the maturation stage where thymocytes are driven to become either CD4 or CD8 “single-positives” (SPs). These cells complete their maturation in the medulla, where negative selection is strongest. Expression of CD69 and HSA is down-regulated in these cells just

prior to exit, and phenotypically demarcate the most mature thymocytes. It is estimated that only 5% of cells that begin development in the thymus reach this final mature stage [26, 27]. The cells exit through the same cortico-medullary blood vessels that they entered the thymus from, and enter the periphery as fully mature naïve T cells.

### **1.1.3 Ras/Erk MAPK signaling in selection**

The Ras/Erk MAPK signaling pathway has been shown to be important in a multitude of different systems. Many developmental processes require this cascade, such as eye development in *Drosophila* and vulval development in *C. elegans* [28, 29]. Ras is involved in the development of many cancers as well, indicative of the pivotal role the Ras/Erk cascade plays in normal cell cycle regulation, growth, and development [30]. For a proper adaptive immune response to pathogens, intact Ras/Erk signaling is required for the activation of T cells [31]. Not surprisingly, signaling through this pathway is also required for proper T cell development in the thymus.

Ras signaling through Erk involves a multi-level kinase cascade. Activated Ras, a 21 kD small GTP-binding protein, recruits the MAP kinase kinase kinase (MAPKKK) Raf to the membrane. Raf, in turn, phosphorylates and activates Mek, the MAP kinase kinase (MAPKK), which activates Erk MAPK. Erk has many downstream targets that include Ets-family transcription factors, c-fos, and Egr1. Erk also targets other kinases, such as ribosomal-S6-kinase, and targets some of the mediators of its own activation, such as the protein tyrosine kinase p56<sup>lck</sup> (Lck) and the membrane-bound adaptor molecule linker of activated T cells (LAT) [32, 33].

Analysis of the Erk-1 knockout mouse revealed a decrease in SP percentages,

indicating a deficit in positive selection [34]. However knockouts of H-Ras and N-Ras, yield no observed immune cell deficiency, and the K-Ras knockout results in embryonic lethality [35]. To side-step this difficulty, an effective way of studying the involvement of this pathway in selection has been the use of dominant negative forms of Ras (dnRas), Raf, and Mek (dMek1). Under the direction of tissue-specific promoters that target expression to positively selecting thymocytes, transgenic mice expressing dnRas or dMek1 had severe blocks in positive selection [36-38]. When these transgenes were combined by cross-breeding, mice expressing both dnRas and dMek1 exhibited a complete block in positive selection. Data from transgenic mouse studies using dominant-negative Raf also showed a deficit in positive selection in a transgenic TCR background [39]. It is important to note, however, that none of these dominant-negative signaling molecules alone are enough to completely block positive selection [37, 39]. Data from transgenic mice expressing dnRas and a constitutively active form of Mek1 or the hypersensitive mutant Erk<sup>sem</sup> did not show complete rescue of positive selection [40]. These two sets of data reveal that other factors downstream of Ras are also involved in positive selection. Other studies have looked at Erk signaling in selection using pharmacological inhibition of the Erk pathway. The inhibitors PD98059 and UO126, which target Mek, inhibited positive selection consistent with transgenic data discussed above. The results from some of these inhibitor studies, however, also implicated the Ras/Erk pathway in negative selection, which was inconsistent with data from transgenic mice expressing the dnRas and dMek [26, 41, 42]. Another study, however, did not see this effect [43].

One transgenic system that establishes Erk activation in the presence of negative

selecting stimulus involved the expression of a TCR $\alpha$  chain with the connecting-peptide motif mutated [44]. This not only established that differential signaling is induced by different components of the TCR/CD3 complex, but also that positively and negatively selecting stimuli yield of different Erk activation kinetics. The negative selecting stimulus elicited a high level of Erk activation that was short-lived. The positively selecting stimulus yielded Erk activation that was weaker, but of much longer duration. This may be indicative differential signaling kinetics similar to that seen in PC12 activation with epidermal growth factor (EGF) and nerve growth factor (NGF) [45]. EGF stimulation of these cells stimulates proliferation, eliciting a strong but transient Erk activation. NGF, however, stimulates differentiation of PC12 cells but yields a weaker activation of Erk that maintains itself over a long period of time. This differential signaling has been linked to hyperphosphorylation of c-fos, increasing its lifetime and transcriptional activity. This effect has recently been shown in mature T cells as well [46]. Further examination of transcriptional regulators activated by Erk changes overall gene expression during positive selection, and the feedback loops involved in Erk regulation may shed light on the mechanism of this differential signaling.

#### **1.1.4 CD4/CD8 lineage determination models**

The onset of positive selection signals survival and maturation in DP thymocytes. In the latter stages of positive selection, DP thymocytes downregulate either CD4 or CD8 coreceptor expression, in a process termed CD4/CD8 lineage determination. In normal development, lineage determination is directed by the interaction of the TCR with MHC on thymic antigen presenting cells. TCR interaction with MHC class II drives the

development of CD4<sup>+</sup> T cells, whereas interaction with MHC class I drives CD8<sup>+</sup> development. Once the cell has made this determination, expression of the unwanted coreceptor is eliminated, and the cell enters the final stage of maturation as a single-positive (SP) thymocyte before exiting into the periphery.

Several models have been put forth in order to explain the mechanism of lineage determination. The stochastic model states that the downregulation of either CD4 or CD8 gene expression is a random event [47-49]. Once a DP thymocyte has received positive selection signals, it begins to downregulate one of the coreceptors. If the incorrectly matched coreceptor is downregulated first, then the thymocyte continues maturation due to the signaling provided by the correctly matched coreceptor on the cell surface. If the correctly matched coreceptor is downregulated initially, the cell lacks the proper signal because the unmatched coreceptor can not engage the TCR/MHC complex. While the former situation induces survival and maturation, the latter results in death of the thymocyte due to the coreceptor/TCR mismatch. For example, if a thymocyte bearing an MHC II-restricted TCR downregulates CD8, then CD4 remains on the cell surface and can provide signals for survival and further maturation. If this same cell downregulates CD4, then the remaining CD8 molecules can not engage the TCR/MHC complex, and lack of signal causes the thymocyte to apoptose.

Another model of CD4/CD8 lineage determination is an instructive model that states that lineage determination is driven by differential TCR/coreceptor signals. In this model, the strength/duration of signaling drives maturation into either a CD4<sup>+</sup> or CD8<sup>+</sup> SP. This model theorizes that strong/long duration signals elicit CD4<sup>+</sup> maturation, and weak/short duration signals elicit CD8<sup>+</sup>. Lck has been shown to bind to the intracellular

tail of CD4 with higher efficiency than CD8 [50], and therefore it is postulated that signaling initiated by CD4 is stronger than CD8. It has also been shown in a two-step culture system that thymocytes expressing an MHC I-restricted TCR developed into CD8<sup>+</sup> SPs with short duration signals, whereas longer duration signals caused these same cells to develop into CD4 SP thymocytes [51].

Yet a third model that has been recently proposed is the kinetic signaling model of CD4/CD8 lineage determination. This model proposes that once positive selection has been initiated, thymocytes automatically downregulate CD8 coreceptor expression (reviewed in [52]). The resultant CD4<sup>+</sup>CD8<sup>lo</sup> population then undergoes lineage determination by either the continuation or cessation of signaling. If the TCR is MHC II-restricted and requires CD4 coreceptor engagement or is coreceptor independent, signaling continues even though the CD8 coreceptor has been downregulated and results in the maturation of the thymocyte into a CD4 SP. In contrast, should the TCR be MHC I-restricted and require CD8 coreceptor engagement, the cessation of signaling due to the loss of the CD8 would drive the silencing of CD4 and the re-expression of CD8. This process has been termed coreceptor reversal, and the result is development of the thymocyte into a CD8 SP.

#### **1.1.4 Ras/Erk signaling in CD4/CD8 lineage determination**

The involvement of signaling through the Ras/Erk MAPK pathway in fate choice of DPs is unclear. Many of the investigations into lineage determination have concentrated on the protein tyrosine kinase Lck, which is a known activator of the Ras/Erk pathway. Lck has been shown to bind to both CD4 and CD8 coreceptors, as

mentioned above, and is essential in initiating TCR signaling events that control  $\beta$ -selection [53, 54] and positive selection [55-58]. Lck's involvement in lineage determination has been suggested to differentially signal CD4 or CD8 development based on the strength of the signal elicited. This is apparently due to the Lck's preferential affinity for the cytoplasmic tail of CD4 over CD8. The intracellular portion of CD4 binds to a far greater percentage of the Lck pool than does CD8 [50]. Mice expressing a chimeric transgene composed of the CD8 extracellular domain and CD4 cytoplasmic tail show favored development of CD4 in a MHC class I-restricted background [58, 59]. In addition, constitutively active and dominant negative mutants of Lck have been shown to direct CD4 development in a class I-restricted background and CD8 development in a class II-restricted background, respectively [55]. It should be noted, however, that Lck activation is pivotal in most downstream signaling elicited by the TCR and is by no means restricted to Ras/Erk activation.

Several studies have examined the role of Ras/Erk in lineage commitment directly by transgenic or pharmacological means. In most of these studies, it was evident that dnRas and dMek affected the development of both CD4 and CD8 lineages equally [36-38]. Only one study in mice expressing Erk<sup>sem</sup> suggested that increased Erk activity improved the production of CD4 SPs [42]. In studies using PMA and ionomycin as pharmacological stimulators, DP thymocytes could be induced to develop into CD8 SPs with low dose/short duration stimulation and into CD4 SPs with high dose/long duration stimulation [60-62]. Conversely, pharmacological inhibition of the Ras/Erk pathway has shown a marked deficiency in the production of CD4 SPs but not CD8 SPs in FTOCs [41, 42, 63]. These latter studies, however, rely on pharmacological inhibitors that may

influence other signaling pathways and therefore may be the result of inhibition of parallel signaling pathways that are truly involved in lineage determination.

## **1.2 FRET and Fluorescent Probes of Intracellular Signaling Activity**

### **1.2.1 Fluorescence resonance energy transfer**

Fluorescence resonance energy transfer (FRET) is a phenomenon by which the dipoles of two fluorescent molecules interact, transferring energy from one to another. One fluorescent molecule, the donor, absorbs incident light energy consistent with its absorption spectrum. The dipole of the donor influences the dipole of the second fluorescent molecule, termed the acceptor, transferring energy to the acceptor, which is given off as light energy in the emission spectrum of the acceptor. An analogy of this process is the interaction of two tuning forks. If one tuning fork is struck and placed closely to a second with similar resonance qualities, energy in the form of sound vibrations will transfer to the second fork and cause it to resonate. It is important to note that this phenomenon is not the emission of a photon by the donor, which is then absorbed by the acceptor molecule, but rather a transfer of energy by dipole interactions.

Many factors determine whether or not FRET can occur between two fluorescent molecules. The two most important factors are: 1) that the distance between the two molecules is 10-100Å and 2) that the emission spectrum of the donor and excitation spectrum of the acceptor overlaps. The distance requirement poses some difficulty with the design and development of biomolecules tethered to fluorescent molecules if the minimum 100Å distance cannot be maintained. On the other hand, this distance requirement allows for the detection of close molecular interactions with conventional

light microscopy, even though the interactions themselves are well beyond the theoretical resolution limit of the light microscope. The latter spectral requirement is relatively easy to fulfill, due to the development of a vast number of small-molecule fluorescent compounds that can be chemically conjugated to many biomolecules and the development of spectrally shifted variants of green fluorescent protein (GFP). Another, more minor factor affecting FRET efficiency is the angle between the dipoles of the two molecules. FRET is most efficient when the dipoles are parallel and most inefficient when the dipoles are  $90^\circ$  to one another. Other factors affecting FRET efficiency are the index of refraction of the medium and the fluorescence quantum yield of the donor fluorescent molecule.

### **1.2.2 Sensors of intracellular signaling utilizing FRET**

Some of the first applications of FRET to biological research involved the chemical conjugation of fluorescent molecules to biomolecules for proximity measurements [64, 65]. Since that time, a plethora of biological applications have been explored utilizing this phenomenon as a sensor of proximity and as a biomolecular ruler [66]. One application that has only recently been established is the use of FRET to study intracellular signaling events. These studies have utilized the ease of molecular cloning and the development of spectral variants of GFP to create protein-based sensors of intracellular activity. These sensors take advantage of fluorescence detection, which has become exquisitely sensitive with new technologies. Another key advantage is that these sensors are genetically encoded, allowing the easy delivery of these sensors into live cells to monitor intracellular signaling events taking place with spatial and temporal resolution.

Some of the first developed sensors of intracellular activity were the “cameleon” sensors of intracellular calcium flux [67] (Figure 1-2). These sensors were designed with two GFP variant pairs, either blue fluorescent protein (BFP) and GFP or cyan fluorescent protein (CFP) and yellow fluorescent protein (YFP). These pairs were coupled together by a linker containing a portion of the C-terminus of the calcium-dependent binding protein calmodulin fused to the M13 peptide, the 26-residue calmodulin-binding peptide of myosin light-chain kinase. The result was sensors capable of detecting the presence of  $\text{Ca}^{++}$  by an increase in FRET efficiency, due to the formation of a globular complex by calmodulin bound to  $\text{Ca}^{++}$  and the M13 peptide that brought the BFP/GFP or CFP/YFP into close proximity. These sensors were not only active in *in vitro* analysis with the addition of  $\text{Ca}^{++}$ , but also could be used to study calcium flux in HeLa cells. Since the initial development of these sensors, they have been used for a myriad of studies, including calcium signaling in the endoplasmic reticulum [68], pancreatic  $\beta$ -cells [69], and zebrafish neurons [70].

Many other FRET-based sensors of intracellular signaling have since been developed to look at other signaling events. Sensors of caspase activity, for instance, allow real-time monitoring of apoptosis signaling [71, 72]. Pertinent to the topic of this thesis is the development of sensors sensitive to kinase activity. Some have involved receptor tyrosine kinases such as epidermal growth factor receptor (EGFR) and insulin receptor (IR) [73]. Quite a number of sensors of cytosolic kinases have also been developed, including sensors specific for protein kinases A and C [74-76], Abl, and Src [77]. To study small GTP-binding protein activity, sensors for Ras and Rap1 that are

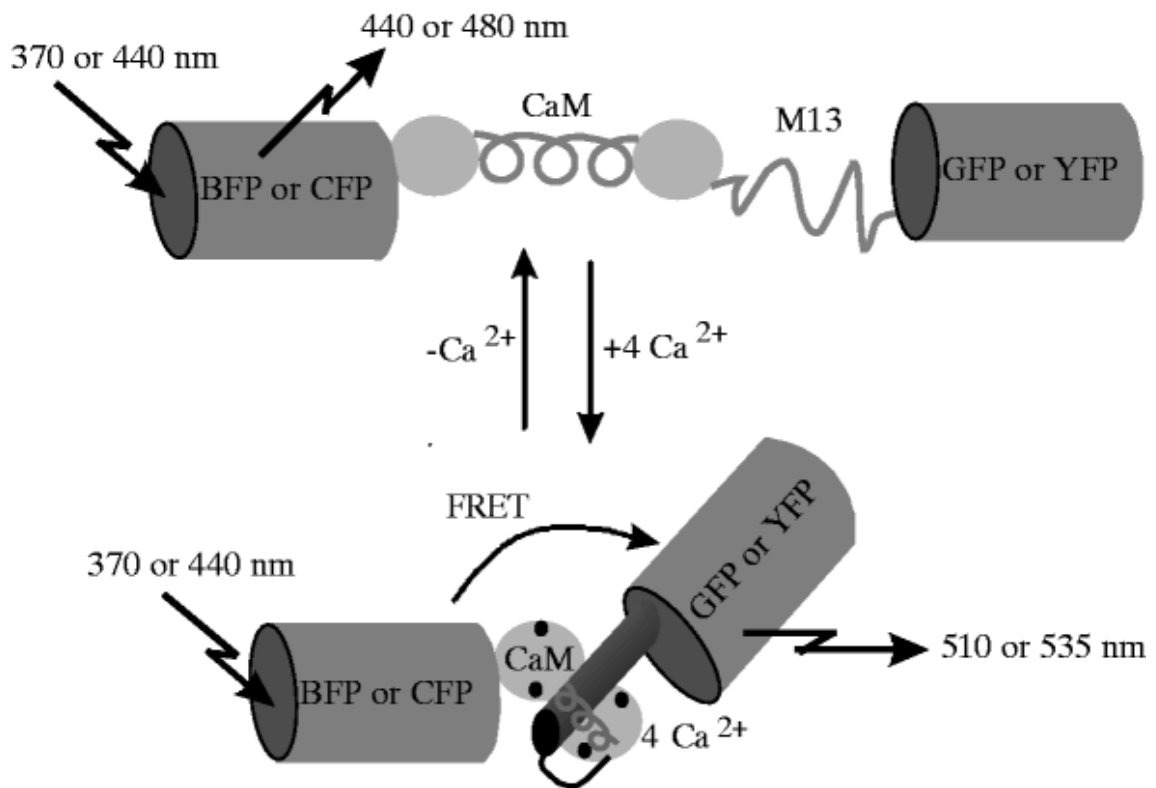


**Figure 1-2. Cameleon sensors are Ca<sup>++</sup>-sensitive.** Fluorescent proteins linked by Ca<sup>++</sup>-sensitive Calmodulin binding domain and the M13 peptide. Upon Ca<sup>++</sup> binding, orientation and distance between the fluorescent proteins changes, increasing energy transfer between the donor and acceptor molecules. Figure from [67].

active in cells have also been introduced [78]. This growing family of live-cell sensors will allow for the study of intracellular signaling dynamics that has thus far not been possible.

## **1.3 Chapter Overview**

### **1.3.1 Chapter 2**

Chapter 2 examines the mechanistic activation of the mitogen activated protein kinase (MAPK) extracellular-signal regulated kinases (Erk) 1 and 2 in thymocytes and peripheral T cells. Erk activity is critical for DP cells to be positively selected, but their role in negative selection is still debatable. Up to now, studies regarding Erk have relied mostly on the analysis of activation by western blot for activated Erk. A caveat of this analysis is that it requires samples to be homogenized populations of cells to obtain enough protein for detection. Erk activation, however, has been shown to act as an ultrasensitive switch in one system, meaning that once a threshold of activation has been reached, all the Erk MAPK in a given cell is activated. Until that threshold is attained the entire cellular pool of Erk remains inactive. This is a plausible mechanism for the “life or death” decision that DPs must make at that developmental checkpoint.

To be able to analyze DP thymocytes on a single cell level, we utilized a technique of intracellular staining followed by single-cell fluorescence detection using flow cytometry. Using this method we were able to analyze single-cell phospho-Erk (pErk) levels and population dynamics under different time and dose conditions. Although we were limited to pharmacological stimulation of Erk using PMA, we were able to establish bimodal activation that occurs in a dose- and time-dependent manner.

Our data also suggested that strong activation signals led to a higher level of activation than under weaker stimulation conditions, and that the kinetics of activation were different with different dose levels. This technique provided us with some insight into single-cell and population dynamics of Erk activation and could potentially lead to further understanding of Erk activation during positive and negative selection of thymocytes.

### 1.3.2 Chapter 3

The technique of intracellular staining discussed in chapter 2 allowed us look at Erk activation under different stimulation conditions, but with the caveat that cells must be fixed and permeabilized prior to analysis. This meant that Erk activation in thymocytes could not be monitored in live cells in real time. To address this issue, we attempted to develop a fluorescent reporter of Erk activation utilizing the phenomenon of fluorescence resonance energy transfer (FRET) [79]. Using two variants of GFP connected by a peptide sensitive to Erk MAPK phosphorylation, we created a genetically encoded sensor of Erk activity. CFP and YFP were used in conjunction with Erk-sensitive peptides derived from the transcription factors Ets1 and Elk1. Our proposed use of this reporter was to examine thymocytes undergoing selection and follow Erk activation in these cells using epifluorescence or confocal laser scanning microscopy.

Initial *in vitro* analysis of several constructs, which we named Erk Activity Sensors (EASs), yielded changes in FRET upon incubation with purified pErk. It was evident from this data, however, that peptides derived from shorter sequences yielded maximal changes in FRET upon phosphorylation. Further examination of the EAS-3

construct, which demonstrated the largest change in FRET, showed that the change in FRET was dependent on two consensus Erk phosphorylation sites and the MAPK binding domain. This construct was also shown to be highly specific for Erk MAPK over two other prominent MAPKs, p38 and stress-activated protein kinase (SAPK; also known as Jun N-terminal kinase (JNK)). The use of this construct in live cells, however, yielded no FRET change and was determined to be due to intracellular phosphatase activity. We therefore were unable to utilize our developed sensor, in its current form, for *in vivo* analysis of thymocyte signaling during selection. To address this difficulty, we have entered into a collaboration in an effort to derive a phospho-peptide specific binding domain by an mRNA-display selection process.

### **1.3.3 Chapter 4**

Our efforts turned to analyzing Erk signaling during CD4/CD8 lineage commitment stage of positive selection using the dominant negative form of Mek1 (dMek1), the Erk MAPK kinase. To this end, we utilized a new technique to create transgenic mice. Recently, there was a report regarding the use of lentivirus as a delivery method of transgenes [80]. This method of transgenesis results in the generation of mouse litters in which each pup potentially carries a different copy number, ranging from 0-30 copies. Due to transgene delivery driven by viral mechanisms, integrations also occur throughout the genome and can potentiate the level of transgene expression. The combinatorial effect is that each litter represents a dose response experiment, with transgene expression levels varying from mouse to mouse over a dose spectrum. In addition, it was shown that transgenes delivered by lentiviruses can also be targeted to

certain tissues by tissue-specific promoters, including the Lck proximal promoter that directs expression to the thymus.

Before beginning our analysis of the effect of dMek1 on lineage determination we had to establish that transgene expression correlated with copy number and that the variegation in gene expression seen in the report above was stable. We first showed that, indeed, the percentage of cells expressing the transgene and the overall level of fluorescence in thymocytes expressing a GFP transgene did correlate with copy number. We were then able to demonstrate that the variegation of transgene expression was stable using sorted transgenic thymocyte populations and by following their development in reaggregated fetal thymic organ culture (RgFTOC). We then made mice using a lentiviral vector containing dMek1 followed by an internal ribosome entry site (IRES) and GFP, in a DO11.10 transgenic TCR background. Our goal was to use GFP as a marker of transgene-expressing cells, but unfortunately GFP was not expressed even in thymocytes from a high copy number mouse. Mice positive for the transgene did appear to have an effect on positive selection, but there was no effect on CD4/CD8 lineage decision. We also tried over-expression of the transcription factor repressor of GATA to induce a lineage switch, but that too showed no effect. Recapitulation of past transgenic experiments may be the key to circumventing the technical difficulties we have encountered with this method.

## 1.4 References

1. Janeway CA, Jr., Medzhitov R: **Innate immune recognition**. *Annu Rev Immunol* 2002, **20**:197-216.

2. Schnare M, Barton GM, Holt AC, Takeda K, Akira S, Medzhitov R: **Toll-like receptors control activation of adaptive immune responses.** *Nat Immunol* 2001, **2**(10):947-950.
3. Paige CJ, Wu GE: **The B cell repertoire.** *Faseb J* 1989, **3**(7):1818-1824.
4. Strominger JL: **Developmental biology of T cell receptors.** *Science* 1989, **244**(4907):943-950.
5. Austyn JM: **Antigen uptake and presentation by dendritic leukocytes.** *Semin Immunol* 1992, **4**(4):227-236.
6. Cotner T: **Factors governing the binding and recognition of foreign and self-peptides by MHC class II.** *Autoimmunity* 1993, **16**(1):57-67.
7. Rubin RL, Kretz-Rommel A: **Linkage of immune self-tolerance with the positive selection of T cells.** *Crit Rev Immunol* 1999, **19**(3):199-218.
8. Lovik M: **The SCID (severe combined immunodeficiency) mouse--its biology and use in immunotoxicological research.** *Arch Toxicol Suppl* 1995, **17**:455-467.
9. Ohashi PS: **Negative selection and autoimmunity.** *Curr Opin Immunol* 2003, **15**(6):668-676.
10. Crivellato E, Vacca A, Ribatti D: **Setting the stage: an anatomist's view of the immune system.** *Trends Immunol* 2004, **25**(4):210-217.
11. Germain RN: **T-cell development and the CD4-CD8 lineage decision.** *Nat Rev Immunol* 2002, **2**(5):309-322.
12. Ceredig R, Rolink T: **A positive look at double-negative thymocytes.** *Nat Rev Immunol* 2002, **2**(11):888-897.

13. Godfrey DI, Kennedy J, Suda T, Zlotnik A: **A developmental pathway involving four phenotypically and functionally distinct subsets of CD3-CD4-CD8-triple-negative adult mouse thymocytes defined by CD44 and CD25 expression.** *J Immunol* 1993, **150**(10):4244-4252.
14. MacDonald HR, Radtke F, Wilson A: **T cell fate specification and alphabeta/gammadelta lineage commitment.** *Curr Opin Immunol* 2001, **13**(2):219-224.
15. Grawunder U, West RB, Lieber MR: **Antigen receptor gene rearrangement.** *Curr Opin Immunol* 1998, **10**(2):172-180.
16. Kim DR, Park SJ, Oettinger MA: **V(D)J recombination: site-specific cleavage and repair.** *Mol Cells* 2000, **10**(4):367-374.
17. Fehling HJ, von Boehmer H: **Early alpha beta T cell development in the thymus of normal and genetically altered mice.** *Curr Opin Immunol* 1997, **9**(2):263-275.
18. Groettrup M, Ungewiss K, Azogui O, Palacios R, Owen MJ, Hayday AC, von Boehmer H: **A novel disulfide-linked heterodimer on pre-T cells consists of the T cell receptor beta chain and a 33 kd glycoprotein.** *Cell* 1993, **75**(2):283-294.
19. Hayes SM, Shores EW, Love PE: **An architectural perspective on signaling by the pre-, alphabeta and gammadelta T cell receptors.** *Immunol Rev* 2003, **191**:28-37.
20. Uematsu Y, Ryser S, Dembic Z, Borgulya P, Krimpenfort P, Berns A, von Boehmer H, Steinmetz M: **In transgenic mice the introduced functional T cell**

- receptor beta gene prevents expression of endogenous beta genes. *Cell* 1988, **52**(6):831-841.
21. Anderson G, Jenkinson EJ: **Lymphostromal interactions in thymic development and function.** *Nat Rev Immunol* 2001, **1**(1):31-40.
  22. Bendelac A, Matzinger P, Seder RA, Paul WE, Schwartz RH: **Activation events during thymic selection.** *J Exp Med* 1992, **175**(3):731-742.
  23. Yamashita I, Nagata T, Tada T, Nakayama T: **CD69 cell surface expression identifies developing thymocytes which audition for T cell antigen receptor-mediated positive selection.** *Int Immunol* 1993, **5**(9):1139-1150.
  24. Barton GM, Rudensky AY: **Evaluating peptide repertoires within the context of thymocyte development.** *Semin Immunol* 1999, **11**(6):417-422.
  25. Barton GM, Rudensky AY: **Requirement for diverse, low-abundance peptides in positive selection of T cells.** *Science* 1999, **283**(5398):67-70.
  26. Mariathasan S, Jones RG, Ohashi PS: **Signals involved in thymocyte positive and negative selection.** *Semin Immunol* 1999, **11**(4):263-272.
  27. Palmer E: **Negative selection--clearing out the bad apples from the T-cell repertoire.** *Nat Rev Immunol* 2003, **3**(5):383-391.
  28. Rubin GM, Chang HC, Karim F, Laverty T, Michaud NR, Morrison DK, Rebay I, Tang A, Therrien M, Wassarman DA: **Signal transduction downstream from Ras in Drosophila.** *Cold Spring Harb Symp Quant Biol* 1997, **62**:347-352.
  29. Sternberg PW, Han M: **Genetics of RAS signaling in C. elegans.** *Trends Genet* 1998, **14**(11):466-472.

30. Duursma AM, Agami R: **Ras interference as cancer therapy.** *Semin Cancer Biol* 2003, **13**(4):267-273.
31. Dong C, Davis RJ, Flavell RA: **MAP kinases in the immune response.** *Annu Rev Immunol* 2002, **20**:55-72.
32. Chang L, Karin M: **Mammalian MAP kinase signalling cascades.** *Nature* 2001, **410**(6824):37-40.
33. Rincon M: **MAP-kinase signaling pathways in T cells.** *Curr Opin Immunol* 2001, **13**(3):339-345.
34. Pages G, Guerin S, Grall D, Bonino F, Smith A, Anjuere F, Auberger P, Pouyssegur J: **Defective thymocyte maturation in p44 MAP kinase (Erk 1) knockout mice.** *Science* 1999, **286**(5443):1374-1377.
35. Esteban LM, Vicario-Abejon C, Fernandez-Salguero P, Fernandez-Medarde A, Swaminathan N, Yienger K, Lopez E, Malumbres M, McKay R, Ward JM *et al*: **Targeted genomic disruption of H-ras and N-ras, individually or in combination, reveals the dispensability of both loci for mouse growth and development.** *Mol Cell Biol* 2001, **21**(5):1444-1452.
36. Alberola-Ila J, Forbush KA, Seger R, Krebs EG, Perlmutter RM: **Selective requirement for MAP kinase activation in thymocyte differentiation.** *Nature* 1995, **373**(6515):620-623.
37. Alberola-Ila J, Hogquist KA, Swan KA, Bevan MJ, Perlmutter RM: **Positive and negative selection invoke distinct signaling pathways.** *J Exp Med* 1996, **184**(1):9-18.

38. Swan KA, Alberola-Ila J, Gross JA, Appleby MW, Forbush KA, Thomas JF, Perlmutter RM: **Involvement of p21ras distinguishes positive and negative selection in thymocytes.** *Embo J* 1995, **14**(2):276-285.
39. O'Shea CC, Crompton T, Rosewell IR, Hayday AC, Owen MJ: **Raf regulates positive selection.** *Eur J Immunol* 1996, **26**(10):2350-2355.
40. Alberola-Ila J, Hernandez-Hoyos G: **The Ras/MAPK cascade and the control of positive selection.** *Immunol Rev* 2003, **191**:79-96.
41. Bommhardt U, Scheuring Y, Bickel C, Zamoyska R, Hunig T: **MEK activity regulates negative selection of immature CD4+CD8+ thymocytes.** *J Immunol* 2000, **164**(5):2326-2337.
42. Sharp LL, Schwarz DA, Bott CM, Marshall CJ, Hedrick SM: **The influence of the MAPK pathway on T cell lineage commitment.** *Immunity* 1997, **7**(5):609-618.
43. Sugawara T, Moriguchi T, Nishida E, Takahama Y: **Differential roles of ERK and p38 MAP kinase pathways in positive and negative selection of T lymphocytes.** *Immunity* 1998, **9**(4):565-574.
44. Werlen G, Hausmann B, Palmer E: **A motif in the alphabeta T-cell receptor controls positive selection by modulating ERK activity.** *Nature* 2000, **406**(6794):422-426.
45. Murphy LO, Smith S, Chen RH, Fingar DC, Blenis J: **Molecular interpretation of ERK signal duration by immediate early gene products.** *Nat Cell Biol* 2002, **4**(8):556-564.

46. Schade AE, Levine AD: **Cutting edge: extracellular signal-regulated kinases 1/2 function as integrators of TCR signal strength.** *J Immunol* 2004, **172**(10):5828-5832.
47. Chan SH, Cosgrove D, Waltzinger C, Benoist C, Mathis D: **Another view of the selective model of thymocyte selection.** *Cell* 1993, **73**(2):225-236.
48. Davis CB, Killeen N, Crooks ME, Raulet D, Littman DR: **Evidence for a stochastic mechanism in the differentiation of mature subsets of T lymphocytes.** *Cell* 1993, **73**(2):237-247.
49. van Meerwijk JP, Germain RN: **Development of mature CD8+ thymocytes: selection rather than instruction?** *Science* 1993, **261**(5123):911-915.
50. Wiest DL, Yuan L, Jefferson J, Benveniste P, Tsokos M, Klausner RD, Glimcher LH, Samelson LE, Singer A: **Regulation of T cell receptor expression in immature CD4+CD8+ thymocytes by p56lck tyrosine kinase: basis for differential signaling by CD4 and CD8 in immature thymocytes expressing both coreceptor molecules.** *J Exp Med* 1993, **178**(5):1701-1712.
51. Yasutomo K, Doyle C, Miele L, Fuchs C, Germain RN: **The duration of antigen receptor signalling determines CD4+ versus CD8+ T-cell lineage fate.** *Nature* 2000, **404**(6777):506-510.
52. Singer A: **New perspectives on a developmental dilemma: the kinetic signaling model and the importance of signal duration for the CD4/CD8 lineage decision.** *Curr Opin Immunol* 2002, **14**(2):207-215.
53. Fehling HJ, Iritani BM, Krotkova A, Forbush KA, Laplace C, Perlmutter RM, von Boehmer H: **Restoration of thymopoiesis in pT alpha-/- mice by anti-**

- CD3epsilon antibody treatment or with transgenes encoding activated Lck or tailless pT alpha.** *Immunity* 1997, **6**(6):703-714.
54. Page ST, van Oers NS, Perlmutter RM, Weiss A, Pullen AM: **Differential contribution of Lck and Fyn protein tyrosine kinases to intraepithelial lymphocyte development.** *Eur J Immunol* 1997, **27**(2):554-562.
55. Hernandez-Hoyos G, Sohn SJ, Rothenberg EV, Alberola-Ila J: **Lck activity controls CD4/CD8 T cell lineage commitment.** *Immunity* 2000, **12**(3):313-322.
56. Legname G, Seddon B, Lovatt M, Tomlinson P, Sarner N, Tolaini M, Williams K, Norton T, Kioussis D, Zamoyska R: **Inducible expression of a p56Lck transgene reveals a central role for Lck in the differentiation of CD4 SP thymocytes.** *Immunity* 2000, **12**(5):537-546.
57. Molina TJ, Kishihara K, Siderovski DP, van Ewijk W, Narendran A, Timms E, Wakeham A, Paige CJ, Hartmann KU, Veillette A *et al*: **Profound block in thymocyte development in mice lacking p56lck.** *Nature* 1992, **357**(6374):161-164.
58. Seong RH, Chamberlain JW, Parnes JR: **Signal for T-cell differentiation to a CD4 cell lineage is delivered by CD4 transmembrane region and/or cytoplasmic tail.** *Nature* 1992, **356**(6371):718-720.
59. Itano A, Salmon P, Kioussis D, Tolaini M, Corbella P, Robey E: **The cytoplasmic domain of CD4 promotes the development of CD4 lineage T cells.** *J Exp Med* 1996, **183**(3):731-741.

60. Adachi S, Iwata M: **Duration of calcineurin and Erk signals regulates CD4/CD8 lineage commitment of thymocytes.** *Cell Immunol* 2002, **215**(1):45-53.
61. Iwata M, Kuwata T, Mukai M, Tozawa Y, Yokoyama M: **Differential induction of helper and killer T cells from isolated CD4+CD8+ thymocytes in suspension culture.** *Eur J Immunol* 1996, **26**(9):2081-2086.
62. Wilkinson B, Kaye J: **Requirement for sustained MAPK signaling in both CD4 and CD8 lineage commitment: a threshold model.** *Cell Immunol* 2001, **211**(2):86-95.
63. Basson MA, Zamoyska R: **The CD4/CD8 lineage decision: integration of signalling pathways.** *Immunol Today* 2000, **21**(10):509-514.
64. Cantley LC, Hammes GG: **Characterization of sulfhydryl groups on chloroplast coupling factor 1 exposed by heat activation.** *Biochemistry* 1976, **15**(1):9-14.
65. Uster PS, Deamer DW: **Fusion competence of phosphatidylserine-containing liposomes quantitatively measured by a fluorescence resonance energy transfer assay.** *Arch Biochem Biophys* 1981, **209**(2):385-395.
66. Stryer L: **Fluorescence energy transfer as a spectroscopic ruler.** *Annu Rev Biochem* 1978, **47**:819-846.
67. Miyawaki A, Llopis J, Heim R, McCaffery JM, Adams JA, Ikura M, Tsien RY: **Fluorescent indicators for Ca<sup>2+</sup> based on green fluorescent proteins and calmodulin.** *Nature* 1997, **388**(6645):882-887.

68. Demaurex N, Frieden M: **Measurements of the free luminal ER Ca(2+) concentration with targeted "cameleon" fluorescent proteins.** *Cell Calcium* 2003, **34**(2):109-119.
69. Graves TK, Hinkle PM: **Ca(2+)-induced Ca(2+) release in the pancreatic beta-cell: direct evidence of endoplasmic reticulum Ca(2+) release.** *Endocrinology* 2003, **144**(8):3565-3574.
70. Higashijima S, Masino MA, Mandel G, Fetcho JR: **Imaging neuronal activity during zebrafish behavior with a genetically encoded calcium indicator.** *J Neurophysiol* 2003, **90**(6):3986-3997.
71. Onuki R, Nagasaki A, Kawasaki H, Baba T, Uyeda TQ, Taira K: **Confirmation by FRET in individual living cells of the absence of significant amyloid beta - mediated caspase 8 activation.** *Proc Natl Acad Sci U S A* 2002, **99**(23):14716-14721.
72. Xu X, Gerard AL, Huang BC, Anderson DC, Payan DG, Luo Y: **Detection of programmed cell death using fluorescence energy transfer.** *Nucleic Acids Res* 1998, **26**(8):2034-2035.
73. Sato M, Ozawa T, Inukai K, Asano T, Umezawa Y: **Fluorescent indicators for imaging protein phosphorylation in single living cells.** *Nat Biotechnol* 2002, **20**(3):287-294.
74. Nagai Y, Miyazaki M, Aoki R, Zama T, Inouye S, Hirose K, Iino M, Hagiwara M: **A fluorescent indicator for visualizing cAMP-induced phosphorylation in vivo.** *Nat Biotechnol* 2000, **18**(3):313-316.

75. Violin JD, Zhang J, Tsien RY, Newton AC: **A genetically encoded fluorescent reporter reveals oscillatory phosphorylation by protein kinase C.** *J Cell Biol* 2003, **161**(5):899-909.
76. Zhang J, Ma Y, Taylor SS, Tsien RY: **Genetically encoded reporters of protein kinase A activity reveal impact of substrate tethering.** *Proc Natl Acad Sci U S A* 2001, **98**(26):14997-15002.
77. Ting AY, Kain KH, Klemke RL, Tsien RY: **Genetically encoded fluorescent reporters of protein tyrosine kinase activities in living cells.** *Proc Natl Acad Sci U S A* 2001, **98**(26):15003-15008.
78. Mochizuki N, Yamashita S, Kurokawa K, Ohba Y, Nagai T, Miyawaki A, Matsuda M: **Spatio-temporal images of growth-factor-induced activation of Ras and Rap1.** *Nature* 2001, **411**(6841):1065-1068.
79. Green HM, Alberola-Ila J: **Development of ERK activity sensors, an in vitro, FRET-based sensor of extracellular regulated kinase activity.** *BMC Chem Biol* 2005, **5**(1):1.
80. Lois C, Hong EJ, Pease S, Brown EJ, Baltimore D: **Germline transmission and tissue-specific expression of transgenes delivered by lentiviral vectors.** *Science* 2002, **295**(5556):868-872.

## **Chapter 2**

# **Intracellular Staining of Activated Erk MAP Kinase Reveals Switch-Like Activation Kinetics in Thymocytes**

### **2.1 Abstract**

The importance of the Ras/Erk MAP Kinase signaling pathway in the positive selection of double-positive thymocytes has been established. However, the mechanism by which Erk signaling conveys the signal to survive and mature is unknown. In this chapter, we propose that Erk acts as an ultrasensitive “switch-like” mechanism where a threshold stimulus activates the entire intracellular pool of Erk. To investigate the plausibility of this hypothesis, we utilized antibodies specific for the phosphorylated form of Erk and a method of fluorescence intracellular staining to analyze both single-cell and population Erk activation dynamics. Pharmacological stimulation of Erk revealed bimodal activation of Erk in 16610D9 cells, primary thymocytes, and primary T cells. The Jurkat human T cell line, however, demonstrated a graded Erk response to increasing stimulus. Our time-course analysis also revealed a quantitative effect on Erk activation that was dependent on the level of stimulation. To further characterize subpopulations of thymocytes, rigorous optimization of cell surface marker staining for compatibility with intracellular staining protocols was performed. These preliminary experiments have

provided us with insight into Erk activation dynamics that can be studied under more physiological conditions.

## **2.2 Background**

Cell-fate determination in any developmental context relies on the concerted action of extracellular stimuli and intracellular response [1-4]. Cells receive information from their surroundings through cell-cell contact and exocrine/paracrine factors, which direct the intracellular production of second messengers and activation of kinase cascades. In turn, these complex responses elicit changes in gene expression that direct the developmental outcome of the cell. In addition, cells express cell surface proteins and secrete factors that affect the developmental processes of surrounding cells. In many tissues of the body, development terminates at the conclusion of sexual maturation, and cells enter a state of maintenance, with no further development. Cells of the immune system, however, are constantly renewing themselves from sources of hematopoietic stem cells in the bone marrow. The existence of countless parasitic organisms in the environment requires that the immune system be highly adaptable and also have an extremely high turnover (i.e., wasteful). This “wastefulness” is not only a function of the actual immune response elicited by exogenous invaders, but is key to production of the T and B cell repertoires. In the thymus, for instance, it is estimated that only about 5% of the thymic progenitors that enter the thymus successfully mature and exit the thymus as naïve T cells [5, 6]. There are several checkpoints during thymocyte development, such as  $\beta$ -selection, positive selection, and negative selection, which the cells must pass through to achieve maturation. Failure at any one of these checkpoints results in death of

the thymocyte. In a manner of speaking, the developmental outcome at each checkpoint is either life or death.

The process of positive selection, as discussed earlier, dictates this life or death outcome. Insufficient engagement of the T cell receptor (TCR) with self-Major Histocompatibility Complex (MHC) causes “death by neglect” due to inadequate signaling downstream of the TCR [7-9]. The positively selected thymocyte can engage MHC bound to self-peptide, and the resulting signal triggers survival. It has been shown that one of the necessary signaling pathways involved in positive selection is the Ras/Erk MAPK pathway [7, 10]. The mechanism by which the Ras/Erk pathway directs this process is unclear, however. While much of the above data have suggested that Erk signaling is involved only in negative selection, there is also data to suggest that the strength and duration of Erk signaling can signal either survival by positive selection or death by negative selection [11].

The dynamics of Erk activation during positive selection are unclear as well. It is conceivable that Erk activation is a graded response, where strength and duration of signal dictate the percentage of intracellular Erk molecules that are activated and for how long. This “rheostat” response would then rely heavily on downstream effectors and feedback mechanisms to determine the final qualitative developmental outcome. Another possible mechanism of Erk activation is as an ultrasensitive, “switch-like” response. In this scenario, the entire intracellular pool of Erk molecules would remain dephosphorylated until a threshold of activation is reached. Once the signaling threshold is reached, the entire pool of Erk is activated. This “all-or-none” response could mean the difference between life and death during positive selection.

Evidence for ultrasensitivity in the Ras/Erk MAPK pathway comes from experiments conducted in *Xenopus* oocytes (Figure 2-1). In 1998, Ferrell and Machleder demonstrated that Erk MAP Kinase acts as an all-or-none signaling member in maturation of *Xenopus* oocytes [12]. This is a departure from the long-believed mechanism that intensity of stimulus conveys intensity of signal. *Xenopus* oocytes mature upon exposure to progesterone, where the oocytes move from a G2 arrest and progress to metaphase of meiosis II, where they arrest once again. Intermediate stages of this transition are highly transient. Once a threshold level of stimulus is achieved, all MAPK in the cell becomes phosphorylated, and maturation of the oocyte progresses. When examined on a single-cell basis by western blot, either >90% or <10% of MAPK in each cell was phosphorylated.

This analysis utilizes the key advantage that *Xenopus* oocytes are extremely large single cells. This offers the possibility of doing single-cell biochemical assays, such as western blotting in Figure 2-1B. Since the threshold of progesterone stimulation is different for each oocyte, a study of MAPK activation across a homogenized population of oocytes would have indicated a combination of phosphorylated and dephosphorylated Erk. To study these ultrasensitive systems it is necessary to be able to detect activation in a single cell and not in populations. Therefore, examining the mechanism of Erk signaling in thymocytes poses a significant problem. Thymocytes are in general quite small and have very little cytoplasm. While antibodies for Erk and phospho-Erk (pErk) are quite robust, and western blotting is a relatively sensitive technique, the size and protein composition of thymocytes make single-cell analysis prohibitive. To solve this problem, we have utilized a technique of intracellular staining using phospho-specific Erk

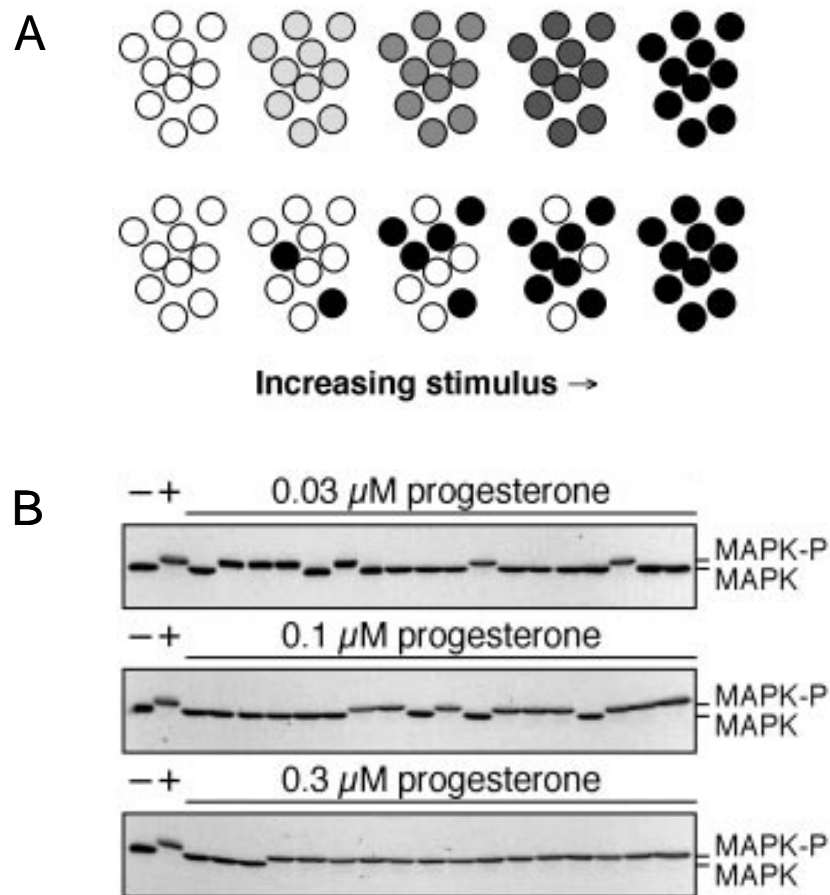


**Figure 2-1. All-or-none Erk response is triggered by threshold stimulation.** A) The model of all-or-none versus graded activation responses suggests that Erk activation is either graded and increasing stimulus correlates positively to the percentage of Erk activated in a given cell (top panel) or that Erk activation is switch-like and requires threshold stimulus to activate (bottom panel). B) Single-cell western blots for MAPK reveal that *Xenopus* oocytes treated with progesterone are either fully activated or inactivated dependent on threshold stimulation. As stimulus increases, a greater percentage of oocytes are fully activated. Each lane corresponds to a single oocyte. This figure was adapted from [12].

antibodies and flow cytometry to study single cells over an entire population. This has given us some insight into the mechanism of Erk activation in both thymocytes and peripheral T cells.

## **2.3 Results and Discussion**

### **2.3.1 Intracellular staining of pErk reveals bimodal distribution of activation upon stimulation with PMA**

To determine the efficacy of this approach, our initial experiments were conducted in the 16610D9 cell line. These cells are similar to developing thymocytes, as they were derived from a CD4<sup>+</sup>/CD8<sup>+</sup> double-positive (DP) murine thymoma [13]. While we concede that only guarded conclusions about *in vivo* mechanisms can be derived from a cell line such as this, these cells were a more appropriate starting point than other, more commonly used, cell lines such as NIH-3T3 or HEK-293 cells. These latter cell lines are derived from connective tissue, and their developmental processes and intracellular signaling in response to extracellular stimulation are likely quite different than thymocytes.

16610D9 cells express abundant amounts of both the CD4 and CD8 coreceptor, but have very low levels of surface CD3 expression and do not respond well to  $\alpha$ -CD3 stimulation [14]. Therefore, we could not induce downstream Erk activation by cross-linking CD3 using  $\alpha$ -CD3 antibodies. Instead, we used the phorbol ester phorbol-myristate-12,13-acetate (PMA) as a pharmacological activator of the Ras/Erk pathway. PMA mimics the action of diacylglycerol (DAG), which is produced mainly by Phospholipase C- $\gamma$  (PLC- $\gamma$ ), and usually activates the Erk pathway by binding to and

activating members of the Protein Kinase C (PKC) family [15, 16]. In thymocytes and T cells, however, the mode of activation is likely through the Ras guanine nucleotide exchange factor (RasGEF), RasGRP [17]. RasGRP has a regulatory DAG binding site, which PMA may bind to and facilitate activation. Recent data, however, also suggests that RasGRP activation by PMA is mediated by a member of the PKC family, PKC $\delta$ , which is activated directly by PMA and activates RasGRP by phosphorylation [18]. Once RasGRP is activated, it in turn activates small GTP binding proteins, such as Ras, and induces downstream Erk phosphorylation.

PMA is an extremely potent activator of Erk [19]. In thymocytes, full Erk activation can be accomplished with a 6 nM PMA treatment for 10 minutes at 37°C (data not shown). Therefore, to analyze this activation it was necessary to perform a very tight dose response from no treatment to 6 nM PMA. Canonical analysis of a homogenized population of 16610D9 cells by western blot reveals a dose-dependent increase in pErk that appeared to be a graded response to stimulation with PMA (Figure 2-2A). With this method, increasing concentrations of PMA gave rise to positively correlative increases in total pErk protein. In contrast, 16610D9 cells analyzed by flow cytometry demonstrated a bimodal distribution of pErk intracellular staining when doses of PMA were increased by 1 nM increments (Figure 2-2B). At each successive dose there appeared to be a decrease in the number of cells in the “inactive” state and an increase in “activated” cells (arrows). This illustrated the advantage of analyzing Erk on the single-cell level, rather than on the level of the entire population.

The results obtained in 16610D9 cells prompted us to look at Erk activation dynamics in thymocytes. Since we were particularly interested in Erk activation during

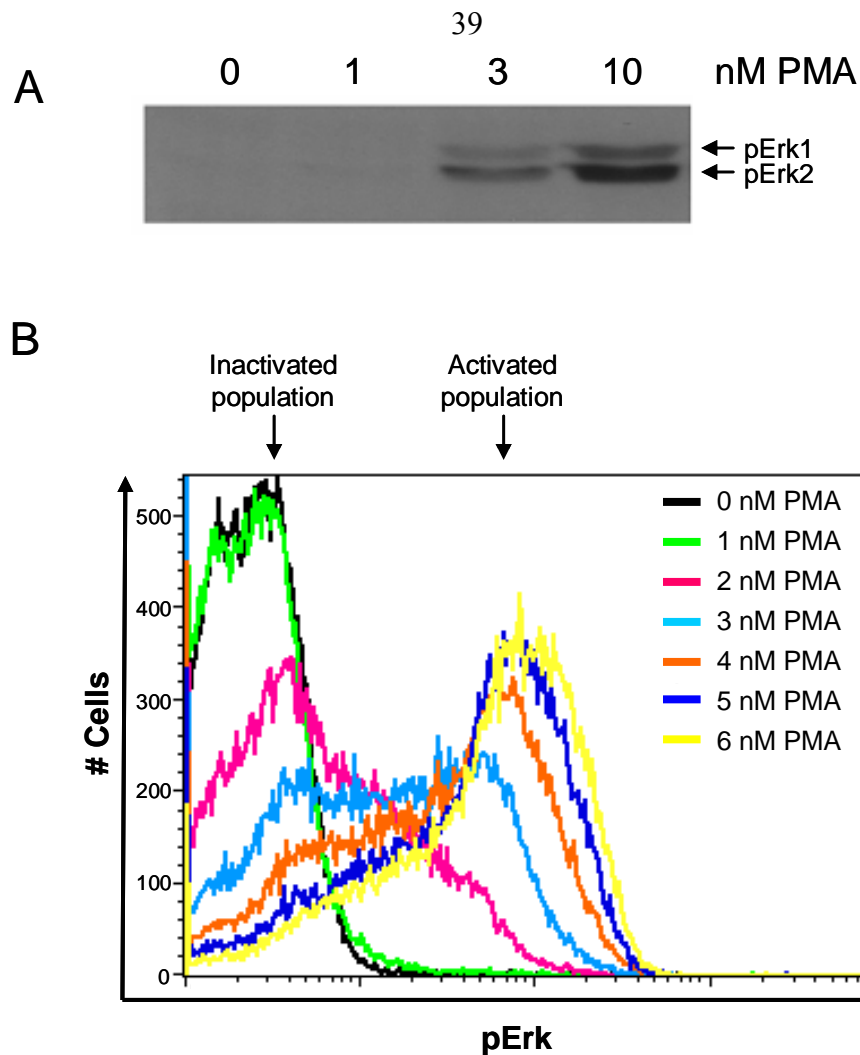


**Figure 2-2. Differential analysis of 16610D9 cells stimulated with PMA reveals bimodal Erk activation.** A)  $1 \times 10^5$  16610D9 cells were treated for 10 minutes with increasing amounts of PMA as indicated. The cells were lysed and cytosolic fraction analyzed by western blot with  $\alpha$ -pErk. B) 16610D9 cells were treated with indicated amounts of PMA for 10 minutes, fixed with 2% formaldehyde, permeabilized with MeOH, and stained for pErk. These two techniques illustrate the advantage of intracellular staining over western blotting of cell lysate. By western blot, treatment appears to stimulate a graded Erk activation whereas bimodal activation is apparent by intracellular staining and analysis by flow cytometry.

positive selection, we used thymocytes derived from a C57Bl/6 MHC null ( $MHC^{-/-}$ ) mouse. As previously discussed, thymocytes require TCR-MHC interactions to undergo selection and consequently arrest at the DP stage in an  $MHC^{-/-}$  mouse. These thymocytes were treated with very low doses of PMA, again due to the exquisite sensitivity of thymocytes to PMA. We found that thymocytes were even more sensitive to Erk activation with PMA than 16610D9 cells, but showed a remarkably similar bimodal distribution with 1 nM PMA stimulation (Figure 2-3A). Interestingly, the entire population of thymocytes treated with as little as 2 nM PMA showed maximal Erk activation, suggesting that the range of threshold of activation is quite narrow.

We were also interested in comparing the above data in 16610D9 cells and thymocytes with the Erk activation in peripheral T cells. The threshold of Erk activation through TCR-MHC interaction is lower in DP thymocytes than in naïve, peripheral T cells [20]. When we treated wild-type C57Bl/6 splenocytes with PMA, we found the same bimodal distribution of  $CD5^{+}$  cells with Erk in the inactive and active state (Figure 2-3B). Consistent with higher sensitivity found in DP thymocytes, peripheral cells needed at minimum 2 nM PMA for bimodal activation, and even 3 nM was not enough to activate the entire population.

To gain perspective on these experiments with regard to human T cells, we treated Jurkat cells, which are human cells derived from an acute T cell lymphoma (Figure 2-4). We found a striking disparity with the results discussed in Figure 2-3. With increasing PMA concentrations, there is an increased pErk staining of the entire population, with a positive correlation between the amount of staining and the treatment dose. This pattern is indicative of the graded response, discussed above, with the percentage of Erk that is

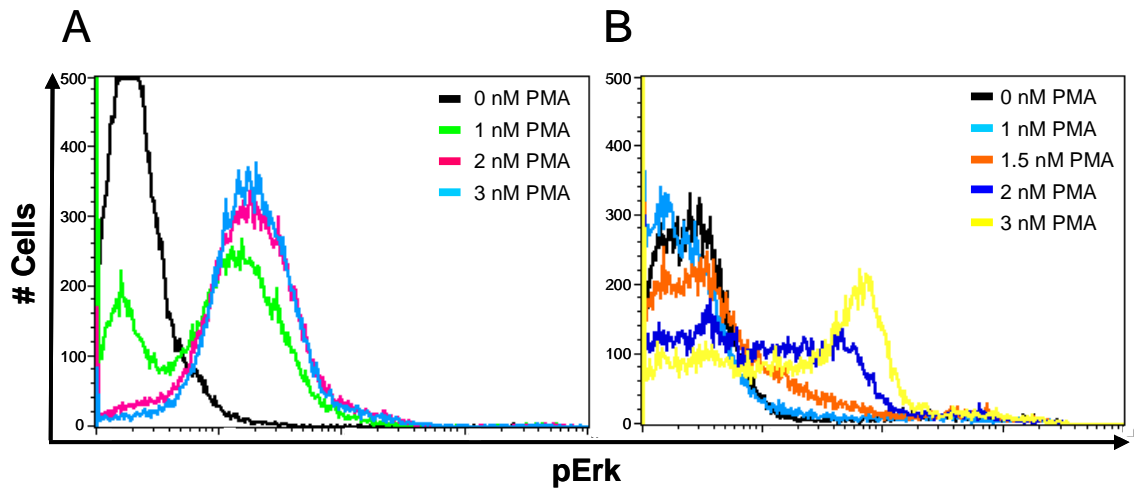


**Figure 2-3. Bimodal Erk activation occurs in both thymocytes and peripheral T cells.** A) Thymocytes from an MHC<sup>-/-</sup> mouse were treated with indicated doses of PMA for 10 minutes. Treatment with 1nM PMA obviously exhibits bimodal activation, indicating that threshold levels of PMA occur between 1 and 2 nM. B) CD5<sup>+</sup> Splenocytes from a wt C57Bl/6 mouse also exhibited bimodal activation, with slightly higher threshold levels that was consistent with threshold of activation being higher in mature T cells than in DP thymocytes.

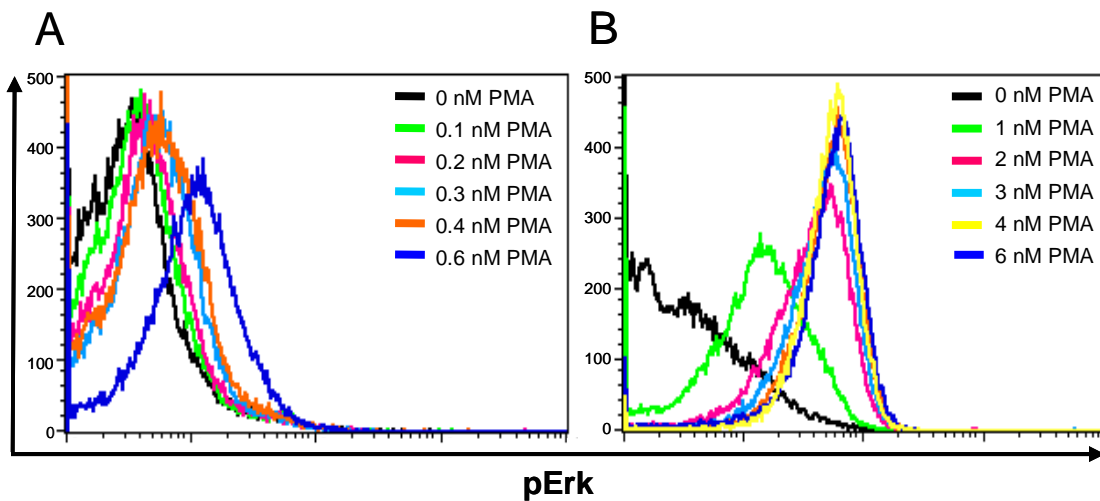


**Figure 2-4. Jurkats display graded Erk activation upon PMA stimulation.** As PMA dose increases, each cell activates an increasing percentage of intracellular Erk. The result is a gradual peak shift of the entire population as dose increases, which is different than what is seen in 16610D9 cells,  $MHC^{-/-}$  thymocytes, and wt splenocytes.

phosphorylated within the cell increasing as a function of increasing stimulation.

This final result raises some thought-provoking questions. Is this graded response to stimulation in Jurkats a residual response that occurs in normal human T cells, indicating a fundamental difference in mouse versus human T cells and possibly thymocytes? Jurkats are a transformed cell line that has been around since 1980 [21]. Is this result simply a byproduct of transformation and long term cell culture? While testing Erk activation in human thymocytes presents a problem with obtaining tissue samples, the testing of human T cells extracted from whole blood is conceivable. This, in conjunction with further characterization of the Erk response, could give us clues not only to the mechanism of Erk activation in thymocytes and T cells, but also to the differences between our mouse model and these processes in humans. It is sometimes easy to lose the perspective that the final goal of these types of studies is to better understand human immunity and to use that understanding for the treatment of human disease.

### **2.3.2 Bimodal Erk activation is a function of strength and duration of PMA stimulation**

The above results gave us a starting point to understand and analyze Erk signaling under different conditions. Two aspects we were particularly interested in exploring were the dynamics of strength and duration of stimulus, as well as how they affect downstream Erk activation. It has been long debated as to how signal/duration of TCR engagement directs positive and negative selection and CD4/CD8 lineage determination, and which downstream players are responsible for the final developmental outcome [22].

While it has been argued that Erk signaling is involved only in positive selection and not in negative selection [7, 10], it has also been suggested that a short but strong TCR signal results in negative selection and a weaker but sustained signal yields positive selection [11].

We looked at the levels of pErk in MHC<sup>-/-</sup> thymocytes treated with different levels of PMA over the course of several hours. This gave us an opportunity to not only track the bimodality of Erk activation, but also gave us insight into the dynamics over time. Previously, it was shown by western blot that Erk would become activated quickly upon PMA stimulation, and then pErk levels would decrease to near pre-stimulation levels over the course of several hours [23]. Using intracellular staining of pErk allowed us to analyze single-cell levels of pErk over a period of time, giving us a glimpse at the kinetics of Erk activation, and to determine if the bimodal distribution of Erk activation was constant over several hours. In addition, by following pErk over time at several dose levels, we could gain insight into the effects of weak and strong activation signals on the status of Erk activity in thymocytes.

Our 10-minute dose response results in Figure 2-3 suggested that full activation Erk by PMA occurred over 0-3 nM. We chose 5 different doses over this range and followed pErk levels at 10 minutes, 30 minutes, 1 hour, 3 hours, and 6 hours. We chose not to follow levels after 6 hours because thymocytes begin to die after a short time in culture without feeder-cell support. The results showed that the status of Erk activation is dependent upon both the PMA treatment dose and the time of exposure (Figure 2-5). At the low doses of 0.1 nM and 0.3 nM, activation of Erk only appears after 6 hours of treatment. For 1 nM PMA treatment, bimodal distribution of Erk activation at 30 minutes

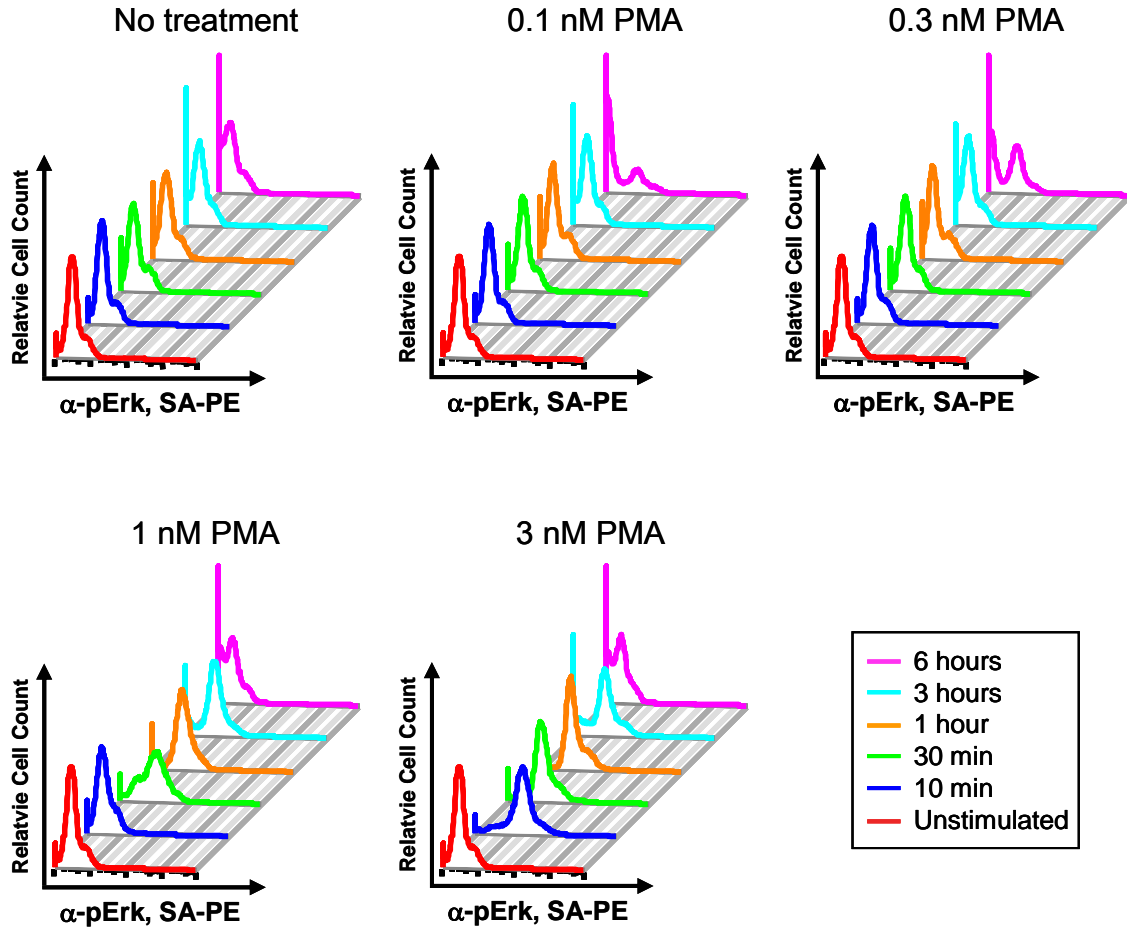


**Figure 2-5. Time course of thymocytes with different PMA concentrations reveals qualitative and quantitative differences in Erk activation.** At low PMA concentrations (0.1 and 0.3 nM), cells maintain a pool of inactive Erk until the 6-hour time-point, suggesting that duration of stimulation is important in Erk activation. At higher PMA concentrations (1 and 3 nM), activation occurs much earlier, but a correlation remains between strength of signal and duration of signal to elicit Erk phosphorylation. In addition, strong stimulation with 3 nM PMA elicits a “hyperactivation” of Erk at 10 minutes, which is reduced and maintained to the 3-hour time-point. Eventually, Erk is completely deactivated, suggesting that a negative feedback loop is initiated once Erk is activated.

was evident. At 1 hour, however, the entire population was activated, and this level of activation was observed up to 3 hours. At 6 hours, all the cells in the population had pre-stimulation levels of pErk, suggesting that the entire pool of Erk in each cell had been deactivated. At the highest dose of PMA (3 nM) used in this time course, the pattern of activation was different than the other doses that were tested. The initial reading taken at 10 minutes showed higher peak fluorescence than at subsequent time points. At 30 minutes, levels of pErk dropped to an intermediate level of activation, and this level of activation was maintained at 1 hour and 3 hours. As was seen with 1 nM treatment, pErk appeared completely deactivated by 6 hours.

These results indicated that the threshold of stimulus for bimodal Erk activation could not only be dependent on dose, but also the duration of stimulus. This was particularly evident at the lower doses of 0.1 nM and 0.3 nM, where stimulation did not induce Erk activation until the 6-hour time-point. In addition, the percentage of activated cells correlated positively with an increase in dose. At 1 nM, Erk was activated in approximately two-thirds of the population at 30 minutes, but at 1 hour the entire population was activated. These results suggested that weak activation signals are capable of initiating Erk activation if they are sustained. Stronger signals, such as the 3 nM treatment, induce a strong initial response, but the cell is then desensitized to further Erk activation.

The dynamics of Erk activation under the 3 nM PMA condition differed from lower doses in the early phase of activation. The initial 10-minute post-stimulation staining had a high level of activation for the entire population of thymocytes. At 30 minutes, the peak had shifted to a lower level of fluorescence, indicating that there was

less pErk in the cells. There is further shift, albeit slight, at 1 hour and the activation state maintains itself until 3 hours. As with 1 nM treatment, levels of pErk had returned to basal levels by 6 hours. It should be noted, however, that whole Erk intracellular staining was not performed in these experiments and would be a critical control in future studies.

These changes in activation dynamics suggest a mechanism of Erk activation in positively selecting thymocytes. On one hand, thymocytes could individually have a threshold level of activation, and the intracellular pool of Erk stays inactive until that threshold is reached. Once a given cell has received an above-threshold signal through TCR/MHC interactions, a large percentage of the intracellular pool of Erk is activated in a switch-like manner. Beyond this threshold, there may be a quantitative component to Erk activation, as observed in the 1 nM vs. 3 nM PMA treatments. The 1 nM treatment yielded a moderate level of activation that was maintained and then shut off. The 3 nM treatment yielded an initial pulse of higher activation that then fell to the lower level seen in the 1 nM treatment. These observations are not only consistent with data that have suggested that differential Erk activation occurs with positively and negatively selecting signal [11], but also suggest a new component of the activation that may be the initial signal for survival in DP thymocytes undergoing positive selection.

These preliminary experiments provided us with an overall picture of Erk activation in thymocytes and T cells with pharmacological stimulation, but did not distinguish the multitude of subpopulations within each tissue sample. Thymocytes, in particular, have many developmental stages that are characterized by their surface staining, and our primary interest lies with DP thymocytes that are undergoing selection. To distinguish these subpopulations, cells are stained with multiple antibodies to selected

cell surface antigens. Each of these antibodies is conjugated to a different fluorochrome and can be distinguished in a flow cytometer. Analysis of these combinations is the long-standing, canonical method of distinguishing subpopulations of immune cells.

### **2.3.3 Optimizing cell surface marker staining under fixation and permeabilization conditions**

Intracellular staining of pErk requires fixation and permeabilization. The permeabilization method we used to strip the cell membranes away required the use of methanol (MeOH). MeOH fixation is very effective, but quite harsh and often results in the destruction of certain protein epitopes. The proteins that are primarily affected are those that are associated with cellular membranes, including those cell surface markers that are usually used for subpopulation identification. Therefore, it was necessary for us to optimize staining conditions for cell surface markers in conjunction with our fixation and permeabilization protocol.

Subsets of thymocytes that are at different developmental stages can be characterized by cell surface staining of several different markers. Examples of commonly used markers are CD4, CD8, TCR $\beta$ , CD25, CD44, and CD5. In fact, the three main subsets of thymocytes are named for the surface expression of, or lack thereof, the TCR co-receptors CD4 and CD8. Thymocytes negative for both CD4 and CD8, referred to as double-negative (DN) thymocytes, represent the earliest developmental subset and can be further subdivided by their surface expression of CD44 and CD25. Early DN cells have not rearranged their TCR loci and therefore do not express TCR $\beta$ . TCR $\beta$  expression initiates with  $\beta$ -selection, increases at the DP stage, and reaches a maximum

at the SP stage. CD5 expression can be used to distinguish T cells from most B cells when analyzing the white blood cell (WBC) component from splenic extraction, as can TCR $\beta$  expression.

We first tested splenocytes under three staining conditions: 1) antibody staining before fixation and permeabilization, 2) antibody staining after fixation, but before permeabilization, and 3) antibody staining after fixation and permeabilization. For this initial test, we stained with  $\alpha$ -CD5-PE,  $\alpha$ -CD3-FITC,  $\alpha$ -CD3-CyC,  $\alpha$ -TCR $\beta$ -PE, and  $\alpha$ -TCR $\beta$ -APC under the conditions mentioned above. Our results indicate that the only effective condition for CD5 staining was to stain after both fixation and permeabilization (Figure 2-6A). In contrast, CD3 staining was most effective prior to both fixation and permeabilization with the FITC conjugate (Figure 2-6B). The  $\alpha$ -CD3-CyC conjugate seemed to be ineffective under all conditions, with only a slight shoulder representing the CD3<sup>+</sup> population in the sample stained before fixation and permeabilization. TCR $\beta$  staining revealed effective staining both after fixation and permeabilization with the PE conjugate and before fixation with the APC conjugate (Figure 2-6C).

We also tested staining conditions for CD4 and CD8 in thymocytes, due to the importance of these markers in thymocyte analysis. Staining condition 2 was eliminated because results in splenocytes indicated no real advantage of this staining condition over condition 1 or 3. Two conjugates to  $\alpha$ -CD4 and four conjugates to  $\alpha$ -CD8 were tested (Figure 2-7).  $\alpha$ -CD4-PE was ineffective under all staining conditions, whereas staining with  $\alpha$ -CD4-CyC prior to fixation/permeabilization gave a characteristic staining pattern of thymocytes from a wild-type C57Bl/6 mouse (Figure 2-7A). For CD8 staining, all conjugates except for the PE conjugate were effective at staining before

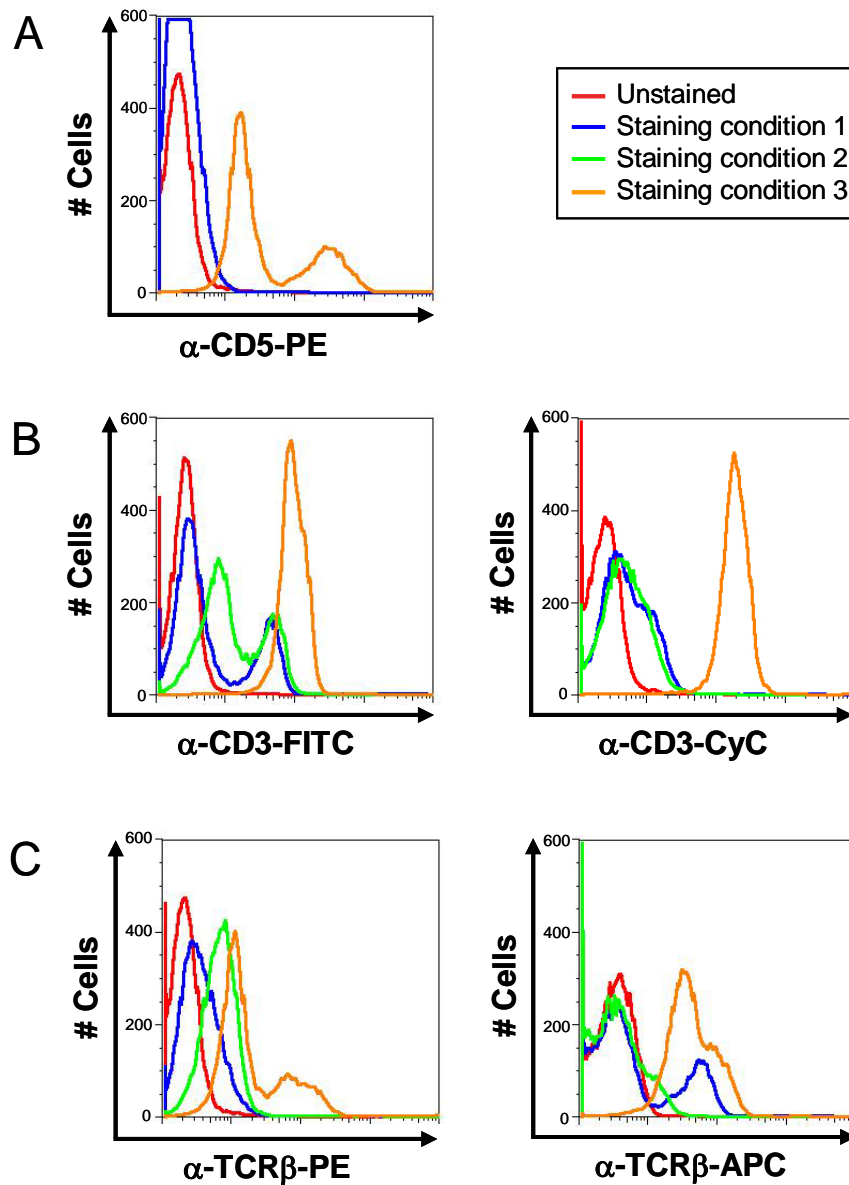


**Figure 2-6. Optimizing surface staining under fixation/permeabilization conditions.**

A) Testing of  $\alpha$ -CD5-PE conjugate. B) Testing of  $\alpha$ -CD3-FITC and -CyC conjugates. C) Testing of  $\alpha$ -TCR $\beta$ -PE and -APC conjugates. Splenocytes were stained under 3 conditions: 1. antibody staining, followed by fixation and permeabilization, 2. fixation followed by staining and permeabilization, and 3. fixation and permeabilization followed by staining. It is apparent that staining conditions are not only dependent on the antibody, but also the fluorescent conjugate. For example,  $\alpha$ -CD3-FITC stained under condition 2 gives robust staining, whereas the -CyC conjugate does not.

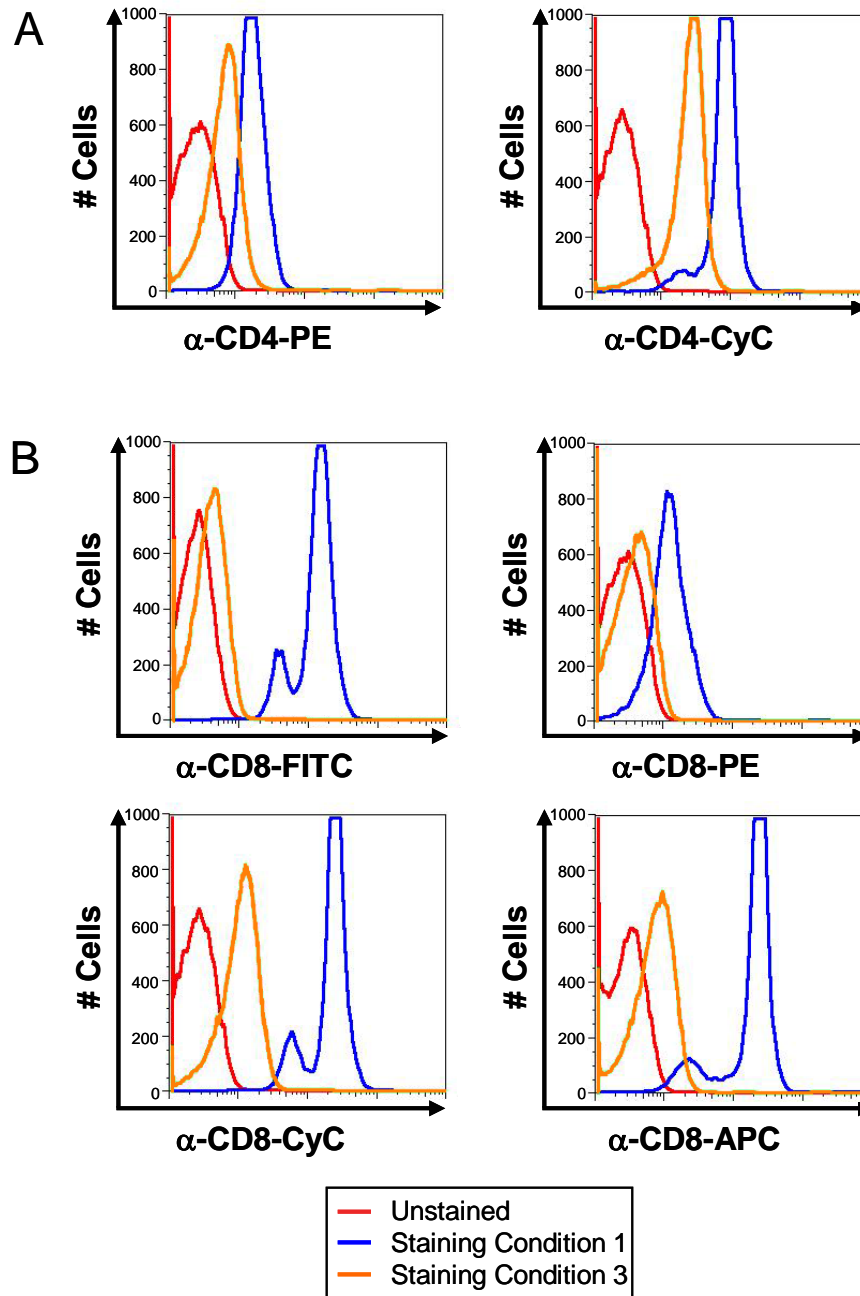


**Figure 2-7. Optimizing CD4/CD8 staining under fixation/permeabilization conditions.** A) Testing of  $\alpha$ -CD4-PE and -CyC conjugate. B) Testing of  $\alpha$ -CD8-FITC, -PE, -CyC, and -APC conjugates. Thymocyte samples were stained under conditions 1 and 3 as described in Figure 6. It is apparent that both the CD4 and CD8 epitopes are destroyed upon permeabilization with MeOH, but can be stained prior to fixation and permeabilization. This data also suggests that PE does not survive permeabilization.

fixation/permeabilization, but not after (Figure 2-7B). As with CD4, no staining condition with  $\alpha$ -CD8-PE conjugate yielded the characteristic thymocyte staining pattern for CD8.

The results from Figures 2-6 and 2-7 provided some insight as to which cell surface marker epitopes are preserved during the fixation/permeabilization process. This destruction is most likely due to the MeOH permeabilization step, as illustrated in Fig 2-6B and 6C where staining conditions 1 and 2 gave similar results. Fixation may play a role, however, as samples stained between fixation and permeabilization all show altered staining when compared with the other staining conditions. It was apparent that CD4, CD8, and CD3 all required staining prior to fixation and permeabilization, presumably because the epitopes that their respective antibodies recognize were destroyed. TCR $\beta$ , on the other hand, appeared to stain well after permeabilization with  $\alpha$ -TCR $\beta$ -PE and prior to fixation with  $\alpha$ -TCR $\beta$ -APC. This would suggest that the TCR $\beta$  epitope is still accessible after MeOH treatment. It is also clear from this data that PE can not withstand permeabilization with MeOH, as all PE signal was lost if staining was performed before fixation.  $\alpha$ -TCR $\beta$ - and  $\alpha$ -CD5- PE conjugates were only effective if staining was performed after permeabilization, and  $\alpha$ -CD4- and  $\alpha$ -CD8- PE conjugates did not retain signal when the staining was done before fixation. As such, we reserved PE for detection of pErk after permeabilization.

These experiments illustrate the importance of optimization of cell surface staining in conjunction with intracellular staining. By no means have we covered the gamut of surface markers, and any future work in this area warrants the optimization of staining conditions prior to conducting complex experiments. Testing of several different

conjugates to each antibody would be recommended, given that some conjugates (e.g., CD8-APC and TCR $\beta$ -APC) appear to give better staining than others.

#### **2.3.4 Cross-reactivity of cell surface marker antibodies with goat-anti-mouse secondary antibody used for detection of pErk intracellular staining**

The next logical step in our analysis of Erk activation in thymocytes was to initiate Erk signaling with a more physiologically relevant stimulus than PMA. The simplest way to accomplish this is by *ex vivo* stimulation by cross-linking of the TCR/CD3 complex with  $\alpha$ -CD3 $\epsilon$  antibodies [24]. This simulates the aggregation of TCR/CD3 complexes when interacting with MHC molecules on the surface of an antigen presenting cell. Thymocytes are incubated with  $\alpha$ -CD3 $\epsilon$  antibodies that are derived from Armenian hamster, which provides primary cross-linking of TCR/CD3 complexes. To strengthen the aggregation, and thereby increase downstream signaling,  $\alpha$ -armenian hamster secondary antibodies are used to cross-link the  $\alpha$ -CD3 $\epsilon$ . However, we were using a biotinylated goat-anti-mouse (G $\alpha$ M-biotin) secondary antibody for our intracellular pErk staining, and we were concerned about cross-reactivity between this secondary and the  $\alpha$ -CD3 $\epsilon$ , as many commercially available anti-mouse antibodies cross-react with armenian hamster.

Most cell surface marker antibodies are commercially available, already conjugated to a variety of fluorochromes, and cross-reactivity is rarely an issue. However, our antibodies to pErk are not primarily used for immunohistochemistry and are not available directly conjugated to fluorescent molecules. It is possible to purchase antibody labeling kits, but these are expensive, take time to optimize conjugation

conditions, and are rather inefficient. The most efficient and economical method to detect pErk is using commercially available secondary antibody. These antibodies can be purchased conjugated to fluorochromes for direct detection, or to biotin, for detection using streptavidin (SA) conjugated to a fluorochrome. This latter method of detection is most effective because of the three-step signal amplification achieved by having a primary antibody specific for the intracellular target, multiple secondary antibodies recognizing each primary antibody, and several SA molecules binding to each secondary antibody. Cross-reactivity of the secondary to a different target antibody, however, will result in the non-specific labeling with the fluorescent SA conjugate.

We took wild-type thymocytes from a C57Bl/6 mouse and stained samples using various staining conditions (Figure 2-8). Our results showed that the G $\alpha$ M-biotin secondary we were using for pErk staining was cross-reactive with the  $\alpha$ -CD3 derived from armenian hamster. Not surprisingly, when combined with pErk staining under stimulated and non-stimulated conditions, the fluorescence profile appears to be a combination of pErk and CD3 staining. This led to further suspicion that other antibodies we would be using for surface staining would also be cross-reactive. The TCR $\beta$ -chain antibodies at our disposal were also derived from armenian hamster, and the  $\alpha$ -CD4 and  $\alpha$ -CD8 conjugates were monoclonal antibodies derived from rat. Rats are also closely related to mice, and antibody cross-reactivity is likely.

We tested rat  $\alpha$ -CD4-CyC, rat  $\alpha$ -CD8-FITC, and armenian hamster  $\alpha$ -TCR $\beta$ -APC antibody conjugates with our G $\alpha$ M-biotin secondary antibody (Figure 2-9). As with the  $\alpha$ -CD3, all conjugates showed cross-reactivity, and pErk staining was befuddled. Our options at this point were limited to changing our pErk staining. Many of the

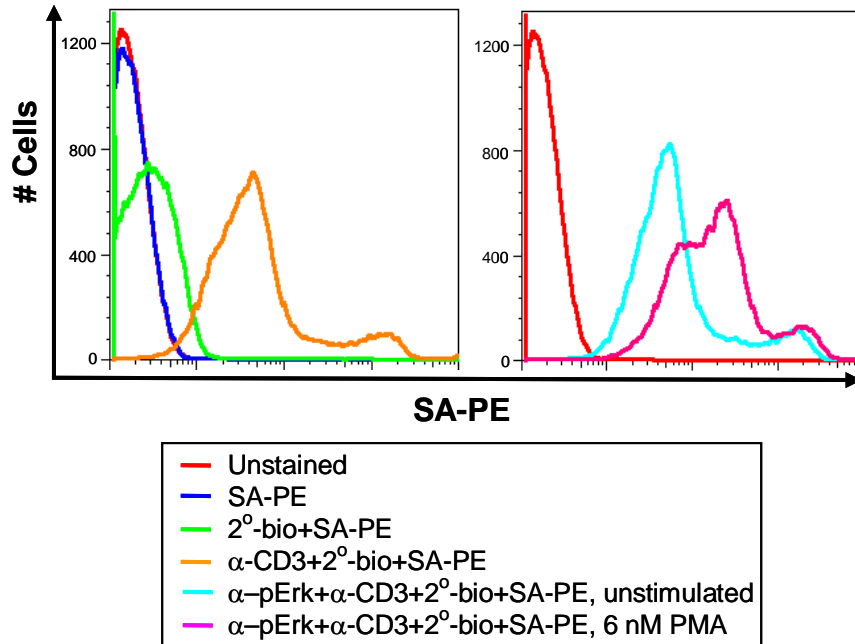


**Figure 2-8. G $\alpha$ M-bio secondary antibody used for pErk intracellular staining is cross-reactive with  $\alpha$ -CD3.** Unconjugated  $\alpha$ -CD3 that is used for stimulations by cross-linking TCR/CD3 complexes was tested with a biotinylated G $\alpha$ M secondary (2 $^{\circ}$ ) used for intracellular staining. Thymocytes stained with 2 $^{\circ}$  + SA-PE had limited background staining (left panel). When combined with  $\alpha$ -CD3, cross-reactivity is evident by its characteristic CD3 staining pattern. Unstimulated and stimulated thymocytes were fixed and permeabilized and stained with the combination of  $\alpha$ -pErk,  $\alpha$ -CD3, 2 $^{\circ}$ , and SA-PE (right panel). The stimulated sample appears to be a combination of CD3 staining and pErk staining.

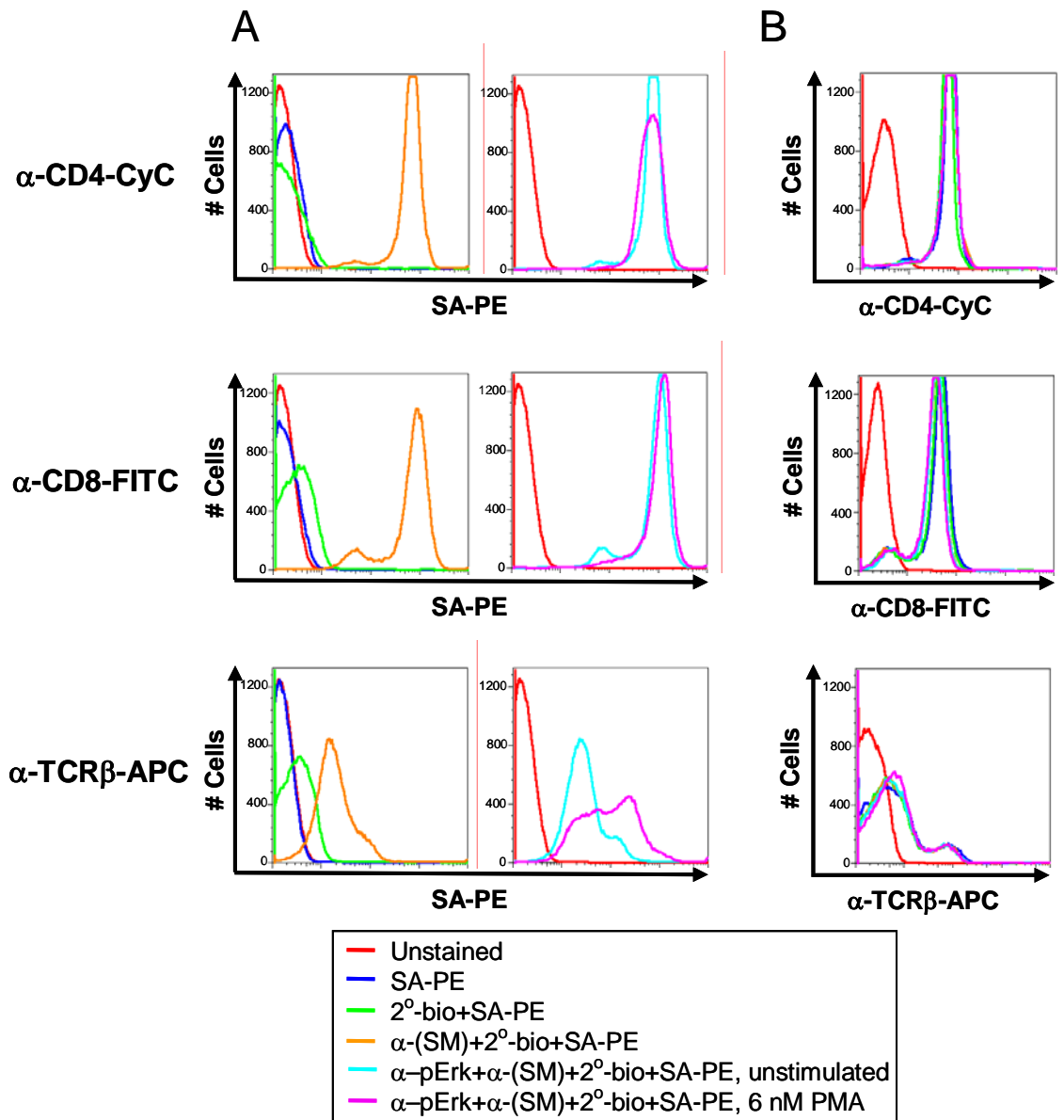


**Figure 2-9.**  $\text{GaM-bio}$  secondary antibody used for pErk intracellular staining also cross-reacts with  $\alpha$ -CD4,  $\alpha$ -CD8, and  $\alpha$ -TCR $\beta$ . A) Similar to results with  $\alpha$ -CD3, the  $\text{GaM-bio}$  2<sup>o</sup> cross-reacted with  $\alpha$ -CD4-CyC,  $\alpha$ -CD8-FITC, and  $\alpha$ -TCR $\beta$ -APC (left panels). The staining pattern was befuddled when samples were dual stained with  $\alpha$ -pErk and a surface marker antibody ( $\alpha$ -(SM)) (right panels). B) Surface staining patterns were normal for each surface marker antibody in its respective fluorescence channel (FL-3 for  $\alpha$ -CD4-CyC, FL-1 for  $\alpha$ -CD8-FITC, and FL-4 for  $\alpha$ -TCR $\beta$ -APC).

commercially available cell surface antibodies are derived from rat, mouse, and armenian hamster, and trying to avoid cross-reactivity by switching to different antibodies was prohibitive. An unconjugated G $\alpha$ M could potentially have been used as a blocking agent, but would have been costly, added an extra step to an already long staining procedure, and may not have been as sensitive. Our solution was to switch to a rabbit polyclonal antibody to pErk, and to test a biotinylated goat-anti-rabbit (G $\alpha$ R-biotin) secondary for cross-reactivity. We again tested unconjugated  $\alpha$ -CD3,  $\alpha$ -CD4-CyC,  $\alpha$ -CD8-FITC, and  $\alpha$ -TCR $\beta$ -APC. Our results indicated that no cross-reactivity could be detected when secondary G $\alpha$ R-biotin and SA-PE were used in the absence of pErk antibody (Figure 2-10). Dual staining of pErk and surface markers under untreated and treated conditions was comparable to pErk staining alone (Figure 2-10A, second column).

### **2.3.5 Inability to activate thymocytes with $\alpha$ -CD3 $\epsilon$ or Jurkats with $\alpha$ -hCD3 (OKT3)**

As mentioned above, the next logical step in pursuing the analysis of Erk activation was to stimulate thymocytes and Jurkats by cross-linking TCR/CD3 complexes. Multiple trials were attempted to activate thymocytes with  $\alpha$ -CD3 $\epsilon$  antibodies and Jurkats with OKT3, a monoclonal antibody to human CD3 [25]. In the thymocyte case, further CD3 cross-linking was provided by a secondary anti-armenian hamster antibody. In neither case were we able to elicit downstream Erk activation (data not shown). This led us to pursue an alternative method for detecting Erk activation in live cells, which is the topic of the Chapter 3.

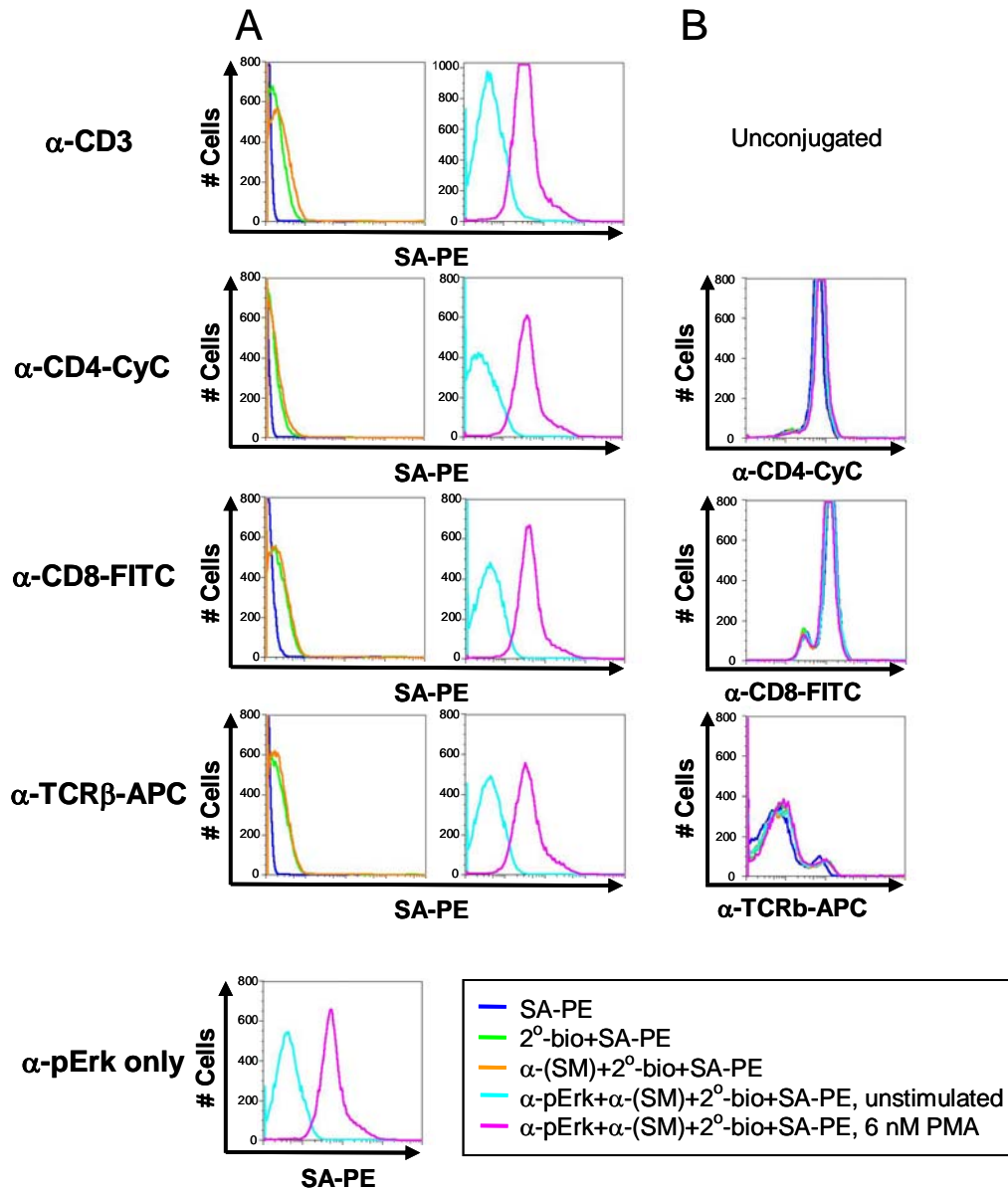


**Figure 2-10.  $G\alpha R$ -bio secondary antibody used for pErk intracellular staining shows no cross-reactivity with surface marker antibodies.** A) Only background staining was observed when thymocytes were surface-stained followed by biotinylated  $G\alpha R$   $2^{\circ}$  antibody staining (left panels). pErk staining under stimulated and unstimulated conditions were all similar to the  $\alpha$ -pErk staining only control (right panels). B) Surface staining patterns were normal for each surface marker antibody in its respective fluorescence channel (FL-3 for  $\alpha$ -CD4-CyC, FL-1 for  $\alpha$ -CD8-FITC, and FL-4 for  $\alpha$ -TCR $\beta$ -APC).

## 2.4 Future Directions

Although we were unable to successfully stimulate thymocytes or Jurkats with  $\alpha$ -CD3, there are alternative methods of activating thymocytes in culture. One option would be to use polymer beads that are pre-coated with  $\alpha$ -CD3. This would eliminate the need for a secondary cross-linking antibody because the polymer would keep the antibodies bound and clustered statically. Another option would be to use a cell line such as P388D1, a transformed macrophage cell line that expresses  $F_c$  receptor [26]. These cells can effectively activate thymocytes when pre-incubated with  $\alpha$ -CD3. While these methods have been less used than canonical  $\alpha$ -CD3 stimulation, they may provide a viable alternative.

Another more physiological condition would be to utilize mice expressing a transgenic TCR to analyze Erk activation under more controlled conditions. We would accomplish this by using physiologically relevant peptide presentation as the source of stimulation. For example, the OT-1 transgenic TCR is MHC class I-restricted and specific for a peptide derived from ovalbumin [27]. Under normal developmental conditions OT-1 induces the development of  $CD8^+$  T cells, as well as in FTOC [27]. The agonist for this TCR is an octameric peptide with the amino acid sequence SIINFEKL, which induces negative selection of thymocytes. A single-point mutation at position one of the peptide (S $\rightarrow$ E) produces a positively selecting peptide of the sequence EIINFEKL. Thymocytes could then be incubated with  $\beta 2$ -microglobulin deficient ( $\beta 2M^{-/-}$ ) antigen presenting cells that can be loaded with either of these peptides or in the absence of peptide to simulate non-selecting, positive-selecting, and negative-selecting conditions. Within the positive-selecting and negative-selecting conditions one can look at cell

viability with increasing peptide concentration. Analysis of pErk by intracellular staining could give us clues as to Erk activation dynamics under positively and negatively selecting conditions.

A more advanced approach may be to analyze Erk activation in thymocytes developing in fetal thymic organ cultures (FTOCs) using 2-photon confocal microscopy. Several groups have been able to track fluorescently labeled thymocytes in FTOCs using this microscopy technique [28]. For our purposes, we would only be able to analyze fixed and permeabilized samples, which may prove a technical challenge with the size and 3-dimensional structure of a reaggregated FTOC. Penetration of formaldehyde, the fixation agent, may not be effective, and MeOH treatment of a reaggregated lobe might destroy the 3-D structure. Staining might also prove difficult due to ineffective penetration of antibodies. Regardless, it might prove useful and informative to visualize the Erk activation status of thymocytes in an environment that is similar to the thymus.

## **2.5 Concluding Remarks**

We have established that Erk activation is switch-like with pharmacological stimulation. This observation was dependent on using intracellular staining to analyze single-cell activation states. The major drawback that this technique presents is that intracellular staining is most easily accomplished by cell fixation and permeabilization by stripping away the cell membrane. This is the only way to provide access for the relatively large antibody specific for a given target. While it is possible to gently permeabilize cells with saponin, thus avoiding fixation and harsh permeabilization but still allowing antibody entry, it is likely that this treatment would have a severe impact on

the homeostasis of the cell. In addition, the introduction of a large macromolecule (i.e., an antibody) that binds pErk could present an artificial accumulation of phosphorylated Erk, due to the protection of the phospho-threonine and phospho-tyrosine of activated Erk from phosphatase activity. This technique, while a useful method of looking at the activation status of Erk in individual cells, only provides static information from one point in time. To analyze Erk activation in real time, we looked to develop a sensor that could be introduced into cells and provide a spatiotemporal readout of Erk activity in developing thymocytes.

## **2.6 Materials and Methods**

### **2.6.1 Materials**

16610D9 (gift from Dr. C. Murre) and Jurkat (gift from Dr. J. Pomerantz) were cultured in complete RPMI medium (Invitrogen) supplemented with 10% v/v fetal calf serum (FCS) (Omega Scientific). Thymocytes and erythrocyte-free spleen cell suspensions were harvested from 6-8 week-old adult mice from thymus and spleen, respectively. Staining antibodies (BD-Pharmingen; eBiosciences) were used in various concentrations optimized for flow cytometry. pErk antibodies (Cell Signaling Technology) were used at 1:200 v/v for intracellular staining and 1:2000 for western blotting. Secondary G $\alpha$ M and G $\alpha$ R antibodies and streptavidin-conjugates were used at 1:200 v/v for intracellular staining. Secondary G $\alpha$ M antibodies conjugated to horseradish peroxidase (HRP) were used at a concentration of 1:10,000. Enhanced Chemiluminescent (ECL) substrate (Amersham) was used for western blot detection.

### **2.6.2 *In vitro* stimulations and cell stainings**

One million cells were resuspended in 175  $\mu$ l of 1X Phosphate Buffered Solution (PBS) supplemented with 4% FCS (P4F) and indicated PMA concentrations. After 10-minute incubation at 37°C, cells were fixed by adding 25  $\mu$ l of 16% formaldehyde (Ted Pella) to each sample. Samples were incubated again for 10 minutes at 37°C and transferred to flow cytometry tubes. To permeabilize fixed cells, ice-cold MeOH (1.8 ml) was added to each sample tube while vortexing and samples were incubated on ice for 30 minutes. Samples were spun at 500 x g for 5 minutes, and the supernatant was removed and washed with 2 ml of P4F. Samples were spun again as described above, the supernatant was removed, and samples were resuspended in 100  $\mu$ l of P4F containing indicated antibodies. Samples were incubated on ice for 15 minutes and washed with 2 ml of P4F, and 100  $\mu$ l of P4F containing secondary antibody was added. Incubations and washes were repeated for streptavidin conjugates, and samples were resuspended in P4F for flow cytometry analysis. Cell surface staining was performed in 100  $\mu$ l P4F for 10 minutes on ice either before fixation, between fixation and permeabilization, or after permeabilization steps described above. Flow cytometry was conducted on either a FACScalibur or a FACScan (Becton Dickinson) and analyzed using Flowjo software (TreeStar). All unlabeled axes are based on a log-scale relative fluorescence.

### **2.6.3 Western blotting**

Whole-cell extracts were prepared from  $1 \times 10^5$  cells, electrophoresed in 10% SDS-PAGE gels, and blotted onto nitrocellulose membranes. All further described incubations were at room temperature. Membranes were blocked in 5% skim milk in

PBS-T (0.05% Tween-20) for 1 hour and incubated in 1% milk/PBS-T with 1:2000 pErk antibody. Membranes were washed 3 x 15 minutes with PBS-T and incubated with GaM-HRP secondary antibody for 1 hour. Membranes were washed again as described above, incubated with ECL substrate for 5 minutes, and exposed to X-ray film.

## 2.7 References

1. Gronemeyer H: **Control of transcription activation by steroid hormone receptors.** *Faseb J* 1992, **6**(8):2524-2529.
2. Ingber D: **Extracellular matrix and cell shape: potential control points for inhibition of angiogenesis.** *J Cell Biochem* 1991, **47**(3):236-241.
3. Mattson MP: **Cellular signaling mechanisms common to the development and degeneration of neuroarchitecture. A review.** *Mech Ageing Dev* 1989, **50**(2):103-157.
4. Rothenberg EV, Chen D, Diamond RA, Dohadwala M, Novak TJ, White PM, Yang-Snyder JA: **Acquisition of mature functional responsiveness in T cells: programming for function via signaling.** *Adv Exp Med Biol* 1991, **292**:71-83.
5. Mariathasan S, Jones RG, Ohashi PS: **Signals involved in thymocyte positive and negative selection.** *Semin Immunol* 1999, **11**(4):263-272.
6. Palmer E: **Negative selection--clearing out the bad apples from the T-cell repertoire.** *Nat Rev Immunol* 2003, **3**(5):383-391.
7. Alberola-Ila J, Forbush KA, Seger R, Krebs EG, Perlmutter RM: **Selective requirement for MAP kinase activation in thymocyte differentiation.** *Nature* 1995, **373**(6515):620-623.

8. O'Shea CC, Crompton T, Rosewell IR, Hayday AC, Owen MJ: **Raf regulates positive selection.** *Eur J Immunol* 1996, **26**(10):2350-2355.
9. Swan KA, Alberola-Ila J, Gross JA, Appleby MW, Forbush KA, Thomas JF, Perlmutter RM: **Involvement of p21ras distinguishes positive and negative selection in thymocytes.** *Embo J* 1995, **14**(2):276-285.
10. Alberola-Ila J, Hogquist KA, Swan KA, Bevan MJ, Perlmutter RM: **Positive and negative selection invoke distinct signaling pathways.** *J Exp Med* 1996, **184**(1):9-18.
11. Werlen G, Hausmann B, Palmer E: **A motif in the alphabeta T-cell receptor controls positive selection by modulating ERK activity.** *Nature* 2000, **406**(6794):422-426.
12. Ferrell JE, Jr., Machleder EM: **The biochemical basis of an all-or-none cell fate switch in *Xenopus* oocytes.** *Science* 1998, **280**(5365):895-898.
13. Bain G, Quong MW, Soloff RS, Hedrick SM, Murre C: **Thymocyte maturation is regulated by the activity of the helix-loop-helix protein, E47.** *J Exp Med* 1999, **190**(11):1605-1616.
14. Ko M, Jang J, Ahn J, Lee K, Chung H, Jeon SH, Seong RH: **T cell receptor signaling inhibits glucocorticoid-induced apoptosis by repressing the SRG3 expression via Ras activation.** *J Biol Chem* 2004, **279**(21):21903-21915.
15. Liu WS, Heckman CA: **The sevenfold way of PKC regulation.** *Cell Signal* 1998, **10**(8):529-542.
16. Toker A: **Signaling through protein kinase C.** *Front Biosci* 1998, **3**:D1134-1147.

17. Priatel JJ, Teh SJ, Dower NA, Stone JC, Teh HS: **RasGRP1 transduces low-grade TCR signals which are critical for T cell development, homeostasis, and differentiation.** *Immunity* 2002, **17**(5):617-627.
18. Brodie C, Steinhart R, Kazimirsky G, Rubinfeld H, Hyman T, Ayres JN, Hur GM, Toth A, Yang D, Garfield SH *et al*: **PKCdelta associates with and is involved in the phosphorylation of RasGRP3 in response to phorbol esters.** *Mol Pharmacol* 2004, **66**(1):76-84.
19. Chen RH, Sarnecki C, Blenis J: **Nuclear localization and regulation of erk- and rsk-encoded protein kinases.** *Mol Cell Biol* 1992, **12**(3):915-927.
20. Davey GM, Schober SL, Endrizzi BT, Dutcher AK, Jameson SC, Hogquist KA: **Preselection thymocytes are more sensitive to T cell receptor stimulation than mature T cells.** *J Exp Med* 1998, **188**(10):1867-1874.
21. Gillis S, Watson J: **Biochemical and biological characterization of lymphocyte regulatory molecules. V. Identification of an interleukin 2-producing human leukemia T cell line.** *J Exp Med* 1980, **152**(6):1709-1719.
22. Alberola-Ila J, Hernandez-Hoyos G: **The Ras/MAPK cascade and the control of positive selection.** *Immunol Rev* 2003, **191**:79-96.
23. Ku H, Meier KE: **Phosphorylation of paxillin via the ERK mitogen-activated protein kinase cascade in EL4 thymoma cells.** *J Biol Chem* 2000, **275**(15):11333-11340.
24. Whitehurst CE, Boulton TG, Cobb MH, Geppert TD: **Extracellular signal-regulated kinases in T cells. Anti-CD3 and 4 beta-phorbol 12-myristate 13-**

- acetate-induced phosphorylation and activation. *J Immunol* 1992, **148**(10):3230-3237.
25. Paz PE, Wang S, Clarke H, Lu X, Stokoe D, Abo A: **Mapping the Zap-70 phosphorylation sites on LAT (linker for activation of T cells) required for recruitment and activation of signalling proteins in T cells.** *Biochem J* 2001, **356**(Pt 2):461-471.
26. Nishida T, Matsuki Y, Ono T, Oguma T, Tsujimoto K, Sato M, Tadakuma T: **The novel murine CD4+CD8+ thymocyte cell line exhibits lineage commitment into both CD4+ and CD8+ T cells by altering the intensity and the duration of anti-CD3 stimulation in vitro.** *J Immunol* 2004, **172**(11):6634-6641.
27. Hogquist KA, Jameson SC, Heath WR, Howard JL, Bevan MJ, Carbone FR: **T cell receptor antagonist peptides induce positive selection.** *Cell* 1994, **76**(1):17-27.
28. Jacobelli J, Andres PG, Boisvert J, Krummel MF: **New views of the immunological synapse: variations in assembly and function.** *Curr Opin Immunol* 2004, **16**(3):345-352.

## Chapter 3

# Development of ERK Activity Sensor, an *In Vitro*, FRET-based Sensor of Extracellular Regulated Kinase Activity

This chapter has previously appeared as: Green HM, Alberola-Ila J: **Development of ERK activity sensors, an in vitro, FRET-based sensor of extracellular regulated kinase activity.** *BMC Chem Biol* 2005, **5**(1):1. The formatting of this paper has been adapted to this thesis, while content remains unchanged.

### 3.1 Abstract

Study of ERK activation has thus far relied on biochemical assays that are limited to the use of phospho-specific antibodies and radioactivity *in vitro*, and analysis of whole cell populations *in vivo*. As with many systems, fluorescence resonance energy transfer (FRET) can be utilized to make highly sensitive detectors of molecular activity. Here we introduce FRET-based ERK Activity Sensors, which utilize variants of Enhanced Green Fluorescent Protein fused by an ERK-specific peptide linker to detect ERK2 activity.

ERK Activity Sensors display varying changes in FRET upon phosphorylation by active ERK2 *in vitro* depending on the composition of ERK-specific peptide linker sequences derived from known *in vivo* ERK targets, Ets1 and Elk1. Analysis of point mutations reveals specific residues involved in ERK binding and phosphorylation of ERK Activity Sensor 3. ERK2 also shows high *in vitro* specificity for these sensors over two other major MAP Kinases, p38 and pSAPK/JNK. EAS's are a convenient, non-radioactive alternative to study ERK dynamics *in vitro*. They can be utilized to study ERK activity in real-time. This new technology can be applied to studying ERK kinetics *in vitro*, analysis of ERK activity in whole cell extracts, and high-throughput screening technologies.

### 3.2 Background

Traditional methods for studying signal transduction cascades have been based solely on biochemical analysis of whole cell populations and homogenized tissues (e.g., radioassays, western blots, etc.). In addition, *in vitro* studies have required the use of radioactive isotopes for biochemical characterization of kinases. These methods are time consuming, produce large quantities of radioactive waste, and do not allow for the study of real-time kinase dynamics.

Recently, sensors for studying signal molecules *in vitro*, as well as cascade dynamics in single cells, have been developed utilizing fluorescent proteins and the phenomenon of fluorescence resonance energy transfer (FRET). FRET is a phenomenon by which energy is transferred from one fluorescent molecule to another by way of dipole-dipole interactions during excitation of the donor molecule. FRET efficiency is

given by the equation:

$$\text{FRET efficiency} = \frac{1}{1 + (R/R_o)^6}$$

where R is the donor-acceptor radius and R<sub>o</sub> is the radius at which FRET efficiency is 50% (Förster radius). Small changes in R (1-2Å) and small orientation changes between the donor and acceptor fluorophores can dramatically affect the efficiency of FRET, making very small changes in structure easily detectable. The limitation, however, is that FRET is effective only between 10-100Å, and therefore the donor and acceptor must be maintained in close proximity. Genetically encoded fluorescent proteins fused by linker peptide sequences have been utilized to address proximity limitations, as well as facilitate the delivery of the sensor into live cells.

Some of the earliest work done with these sensors includes genetically encoded sensors of caspase activity, in which caspase-3 and caspase-8 sensitive linker peptides were fused between the different variants of Enhanced Green Fluorescent Protein (EGFP) [1]. These studies allowed the characterization of apoptosis in single living cells with spatio-temporal resolution. Other types of FRET signaling sensors have since evolved, including sensors for calcium signaling [2], receptor tyrosine kinases [3, 4], intracellular kinases [4-7], and histone methylation [8]. These sensors have been shown to be useful in *in vitro* assays, as well as to allow the study of signaling events in a single cell, in real time [4].

The Ras/ERK cascade controls differentiation and proliferation in many different cell types and organisms. In this signal transduction pathway, activated Ras (Ras-GTP) binds directly to Raf-1 and recruits it to the membrane where Raf becomes activated. Raf

then phosphorylates and activates Mek-1 and Mek-2 (the MAPK kinase), which in turn phosphorylates the MAPKs ERK-1 and ERK-2. Activated ERKs translocate to the nucleus and directly phosphorylate transcriptional regulatory proteins (including members of the Ets family of transcription factors, and the bZIP factors Fos and Jun) (reviewed in [9]). Kinetics and *in vivo* dynamics of ERK MAP kinase activity are not completely understood. Traditionally, the level of ERK activation has been thought to be relative to the strength of the upstream signal. Some data suggest, however, that ERK activation is “switch-like,” requiring a threshold of activation, above which all ERK molecules within the cell become activated [10]. Computational models of MAPK signaling mechanisms can fit both possibilities [11, 12]. Therefore, the development of new tools to study these dynamics is essential to determine the biochemical nature of ERK signaling.

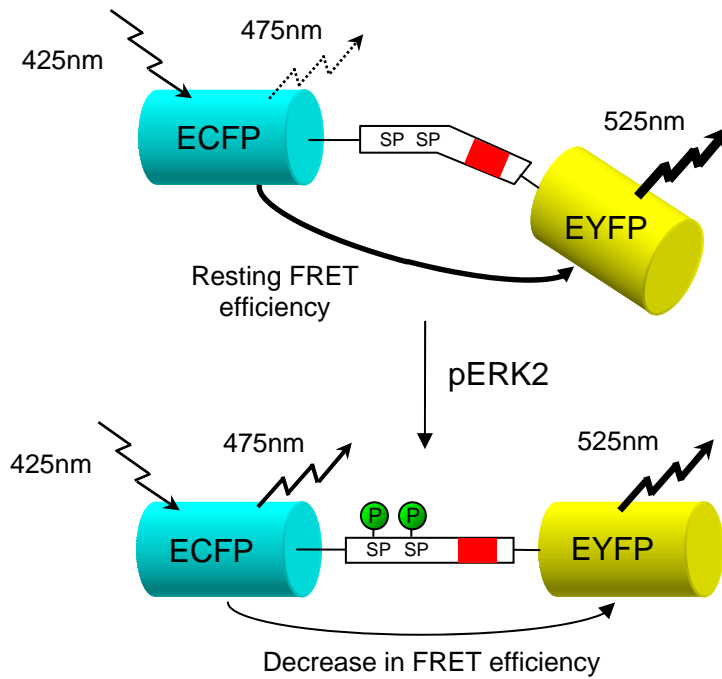
In this manuscript, we describe the development of several FRET-based sensors of MAP kinase activity, which we have called ERK Activity Sensors (EAS). Peptide linker sequences taken from the Ets family transcription family members Ets1 and Elk1, both ERK targets, were fused between cyan and yellow variants of EGFP (ECFP and EYFP, respectively). Several of our constructs respond to phosphorylation by activated ERK with changes in FRET, and at least one of them, EAS-3, is specific for active Extracellular Regulated Kinase (ERK) as opposed to two other MAP kinases, p38 and SAPK/JNK. Therefore, EAS-3 is a viable, non-radioactive sensor of ERK MAPK activity *in vitro*.

### 3.3 Results and Discussion

#### 3.3.1 Design and model of EAS

EAS was designed to have a short peptide linker sequence sensitive to phosphorylation by ERK fused between ECFP and EYFP. ECFP and EYFP were chosen as a FRET pair because of the good spectral overlap between the emission of ECFP and the excitation of EYFP. We hypothesized that phosphorylation would result in changes in secondary structure of the linker peptide that would alter FRET efficiency for the protein (Figure 3-1A). Since it was unclear which factors would contribute to forming a suitable FRET sensor, we prepared several different constructs with peptide linker sequences containing ERK phosphorylation sites taken from Ets1 and Elk1 transcription factors, which are physiological substrates of the ERK MAPKs (Figure 3-1B). EAS-2, derived from mouse Ets1, has a rather large linker peptide, due to the discovery that the MAP Kinase binding site (D-domain) is approximately 90 amino acids downstream of the target serine [13]. The linker sequences for EAS 3-5 were taken from human Elk1, which has been shown to have the DEF domain (FXFP amino-acid motif), a known MAPK binding site, near the C-terminus. These peptides also contain two Serine-Proline (SP) motifs (consensus MAPK phosphorylation sites) corresponding to serines 383 and 389 of Elk1, which have been shown to be targets of MAP kinases. Phosphorylation of these serines has also been shown to be directed specifically by the DEF domain [14]. EAS-Neg is a negative control construct with a short peptide linker derived from Ets1, containing a consensus MAPK phosphorylation site, but no MAPK binding site.

A



B

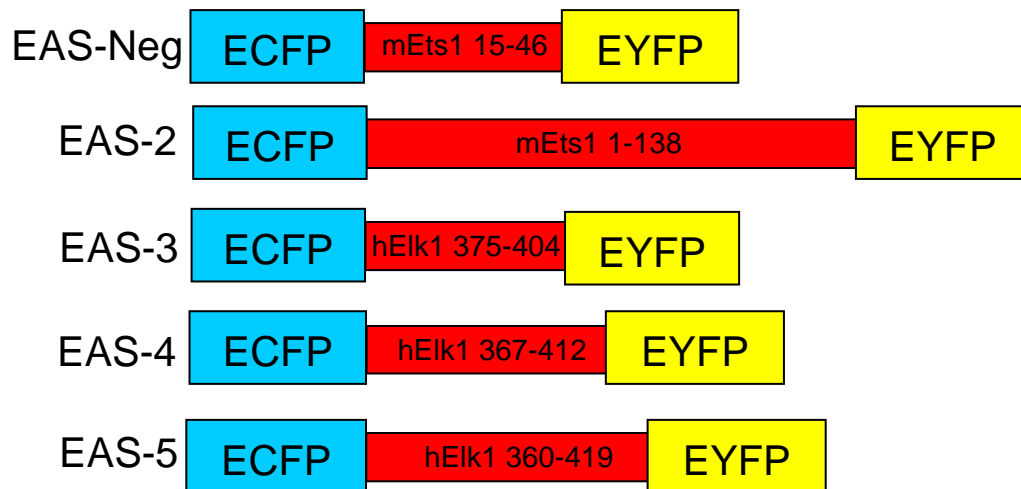


**Figure 3-1. A model for EAS activation and construct design.** See next page for caption text.

**Figure 3-1 cont'd.** (A) Our inferred model indicates that upon pERK2 phosphorylation a conformational change in the linker peptide of EAS decreases the efficiency of FRET. The red area in the linker peptide indicates the relative position of either D-domain (EAS-2) or DEF domain (EAS-3, -4, -5), and the SP motifs denote the consensus phosphorylation sites. (B) The gene constructs include EAS-Neg and EAS-2, which are derived from mouse Ets1. EAS 3-5 contain peptide linkers derived from human Elk1. The composition of each linker peptide is indicated by the primary sequence positions derived from Ets1 and Elk1, respectively.

---

### **3.3.2 EAS FRET changes in the presence of active ERK2**

We expected a change in energy transfer between ECFP and EYFP upon incubation with active ERK2 (pERK2) for EAS to be effective as a real time sensor. This would indicate that a phosphorylation event had affected the distance and orientation between the two fluorophores. Each EAS construct was incubated with pERK2 in a fluorimeter (30°C), and readings were taken prior to addition of ATP. Upon the addition of ATP, all EAS constructs, with the exception of EAS-Neg, showed a decrease of energy transfer indicated by an increase in donor (ECFP) emission (475 nm) with a concomitant decrease in acceptor (EYFP) emission (525 nm) after 40 minutes (Figure 3-2A). Therefore, a decrease in FRET efficiency correlates with phosphorylation of EAS by pERK2. The resultant change in ECFP/EYFP emission ratio is comparable to or exceeds that of similar FRET-based signal transduction sensors [4-6]. Under the same conditions, EAS-Neg showed no change in FRET over the course of 30 minutes, confirming the specificity of ERK2 for EAS 2-5 and the requirement of a

phosphorylation event to induce a change in FRET. Figure 3-2B shows the absolute change in ECFP/EYFP ratio over a 40-minute time course for each construct. EAS-3 and EAS-4 show the greatest absolute decrease in EYFP/ECFP emission ratio, with EAS-5 having an intermediate change in emission ratio. EAS-2 showed very little change in FRET. Phosphorylation was also confirmed by an *in vitro* kinase  $^{32}\text{P}$  phosphorylation assay using recombinant pERK2 (Figure 3-2C). EAS 2-5 sensors were efficiently phosphorylated as compared to the non-specific control, EAS-Neg, and Myelin Basic Protein (MBP), a common target of activated MAPKs for *in vitro* studies. Based on the robust FRET signal change and radioassay results, further studies focused on EAS-3.

### **3.3.3 EAS changes in FRET in response to pERK2 require phosphorylation and the ERK binding site**

Mutants of EAS-3 were utilized to validate the structural features of EAS essential for decreased FRET efficiency upon incubation with pERK2. We refined EAS-3 by replacing the bulky N-terminal GST-purification tag (Glutathione-S-Transferase) with a Histidine-10 tag on the C-terminus. This reduced the possibility that the large purification tag would interfere with FRET efficiency changes. In addition, we mutated alanine 207 and alanine 487 to lysine. As previously reported, this prevents EGFP dimerization [15]. This latter modification reduced co-purification of truncation products with full-length EAS (data not shown).

To further characterize EAS-3, we generated different constructs targeting critical residues and analyzed their ability to serve as substrates for pERK2. Mutants EAS3-S286A, EAS3-S292A, and the double mutant EAS3-S(286,292)A eliminated consensus

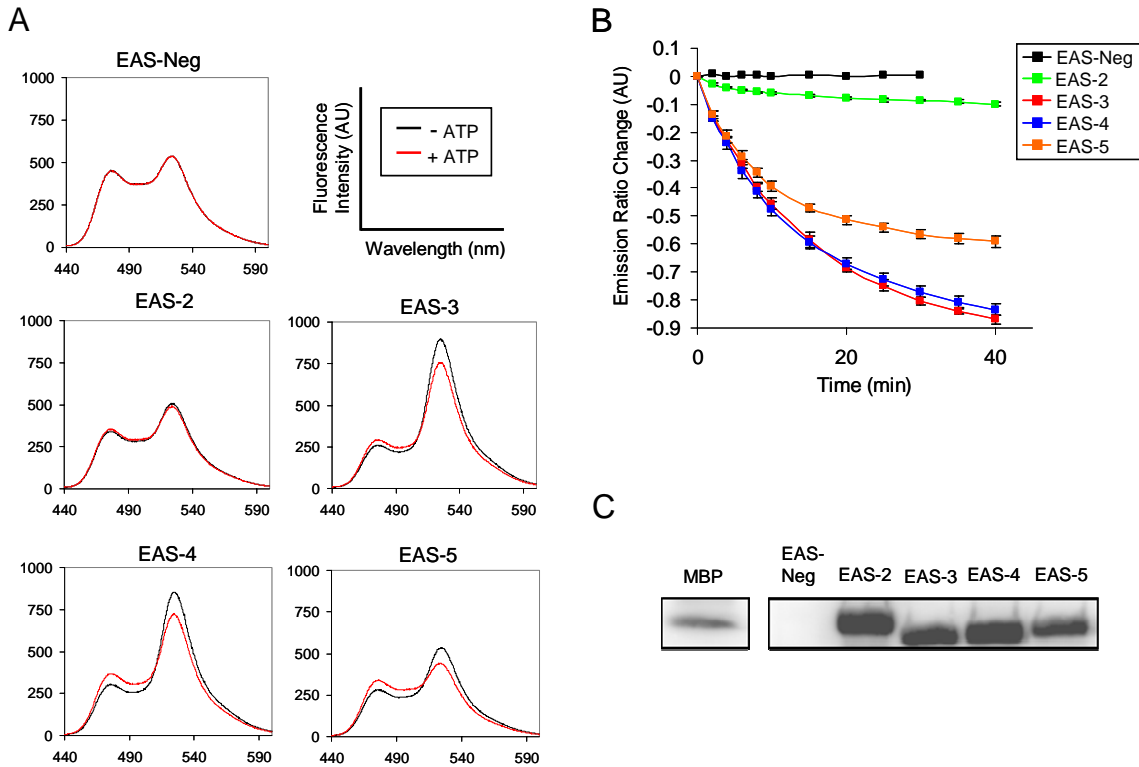


**Figure 3-2. EAS proteins are targets for ERK2 and exhibit decreased FRET efficiency upon phosphorylation.** (A) Emission spectra indicate the effective FRET change for each EAS protein sensor. Time course fluorimetry with EAS-Neg shows that pERK2 induces no FRET change 30 minutes after ATP addition. All other EAS proteins show varying gains in ECFP emission (475 nm) and losses in EYFP emission (525 nm) 40 minutes after ATP addition. (B) Absolute change in the ratio of EYFP/ECFP emission for EAS-Neg is zero over a 30-minute time course, whereas a decrease in ratio for EAS-3, EAS-4, and EAS-5 is readily detectable at 2 minutes, and continues to decay exponentially over the time course. EAS-2 has a detectable change in emission ratio, but the change is minimal as compared to other EAS proteins. Error analysis was determined from three independent experiments. (C) EAS proteins (EAS-2, -3, -4, and -5) are phosphorylated by pERK2 in the presence of  $\gamma$ -[ $^{32}$ P]ATP. This confirms that EAS proteins are targets of pERK2 as compared with MBP, a known ERK2 substrate. As expected, EAS-Neg is not phosphorylated by pERK2.

phosphorylation sites (Figure 3-2A). The dead binding domain mutant (EAS3-DBD) eliminated the DEF domain by replacing the two key phenylalanines with alanines, creating an AXAP motif (Figure 3-3A). As Figure 3-3B demonstrates, all five mutants have decreased phosphorylation compared to the wild type sensor. As expected, the EAS3-S(286,292)A mutant had the lowest level of phosphate incorporation due to absence of both serine-proline consensus phosphorylation sites required by MAP Kinases. A decrease in phosphorylation of EAS-DBD is also consistent with the requirement of MAPKs to bind targets for efficient phosphorylation (reviewed in [16]). Differences between wild-type EAS-3 and mutants are also reflected in change of FRET efficiency when treated with pERK2 in fluorimeter experiments (Figure 3-3C). These relative changes in FRET efficiency are consistent with the radioassay data.

### **3.3.4 EAS-3 is not phosphorylated by pSAPK or pp38**

Distinguishing the activation of different MAP kinases within the cell is essential since each MAPK pathway is activated by multiple mitogens and external environmental factors to varying degrees (reviewed in [17]). Furthermore, there is extensive cross-talk between the different MAP kinase pathways. Detection methods must effectively isolate the signal of the target kinase from other family members to elucidate the contributions of these different pathways to a given cellular process.

The target peptide linkers were designed to impart specificity for ERK. Elk1 and Ets1 were chosen because of their seemingly specific interaction with ERK relative to p38 or SAPK/JNK (reviewed in [18]). To determine whether EAS-3 acted as a specific substrate for ERK, we performed *in vitro* phosphorylation assays to quantify the ability of

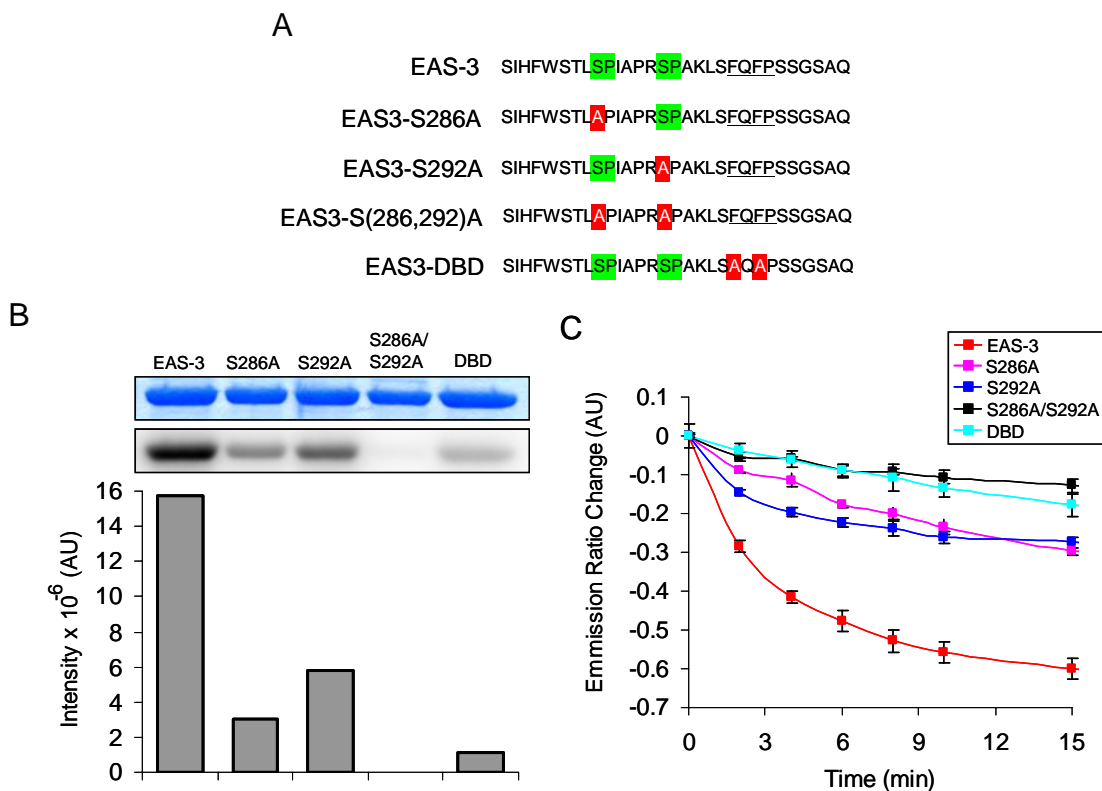


**Figure 3-3. Mutation of key residues diminishes EAS-3 phosphorylation by pERK2.** (A) Primary sequences of EAS-3 and EAS-3 mutant linker peptides are shown with consensus phosphorylation sites (highlighted in green) and ERK binding sites (underlined). Residue mutations to alanine are highlighted in red. (B) Analysis of mutant EAS-3 proteins by  $\gamma$ -[<sup>32</sup>P]ATP phosphorylation shows complete loss of pERK2 phosphorylation of the S(286,292)A mutant as compared to wild-type EAS-3. Decreased <sup>32</sup>P-phosphorylation of site-specific mutants also indicates the involvement of both Ser286 and Ser292 for pERK2 activity. Requirement of the ERK binding domain for efficient phosphorylation is evident from decreased phosphorylation of the EAS3-DBD mutant. Band intensities were quantitated by densitometry and are shown graphically. Equal protein loading is shown by Coomassie staining of EAS-3 and EAS-3 mutants, and phosphorylation assay was terminated after 15 minutes at 30°C. (C) Fluorimetry data for EAS-3 and EAS-3 mutants reveal that the FRET efficiency change is reduced with various mutations, consistent with the phosphorylation assay in B.

pERK2, pp38, and pSAPK/JNK to phosphorylate EAS-3 (Figure 3-4). As shown in Figure 3-4A, EAS-3 is an approximately 2000-fold more specific target for pERK2 than pp38, and 50-fold more specific for pERK2 than pSAPK/JNK. Activities of pERK2, pp38, and pSAPK/JNK were confirmed by using known substrates specific for each kinase (Figure 3-4B). MBP was used in conjunction with pERK2, GST-ATF2 with pp38, and GST-c-Jun with pSAPK/JNK. Specificity of these kinases for EAS-3 was also confirmed by FRET in a fluorimeter (Figure 3-4C). It is clear that the change in FRET was dramatic when EAS-3 was incubated with pERK2, but showed little or no response when incubated with pp38 or pSAPK/JNK. This is consistent with the results found in 4A. Given the similarity of these kinases, this also suggests that EAS-3 would be specifically acted upon by pERK2 even in the presence of other activated intracellular kinases.

The demonstrated specificity of pERK2 for EAS-3 phosphorylation suggests that this sensor is a candidate for *in vivo* studies of ERK signaling. However, our preliminary experiments in NIH-3T3 cells indicated that EAS-3 was susceptible to intracellular phosphatase activity (data not shown). We surmise that this is due to the absence of a protective phospho-specific binding domain within the EAS-3 construct. Such binding domains have been crucial in the development of other FRET-based signaling sensors of kinase activity [2-4,6,7]. These binding domains, however, are taken from naturally occurring domains that are specific for each target sequence. Unfortunately, no known phospho-specific binding domain exists for Elk1 in the region of Ser383/389. Therefore, we are using a semi-rational approach to develop a phospho-specific binding domain that acts to protect the phosphorylated EAS-3 linker from intracellular phosphatases. This

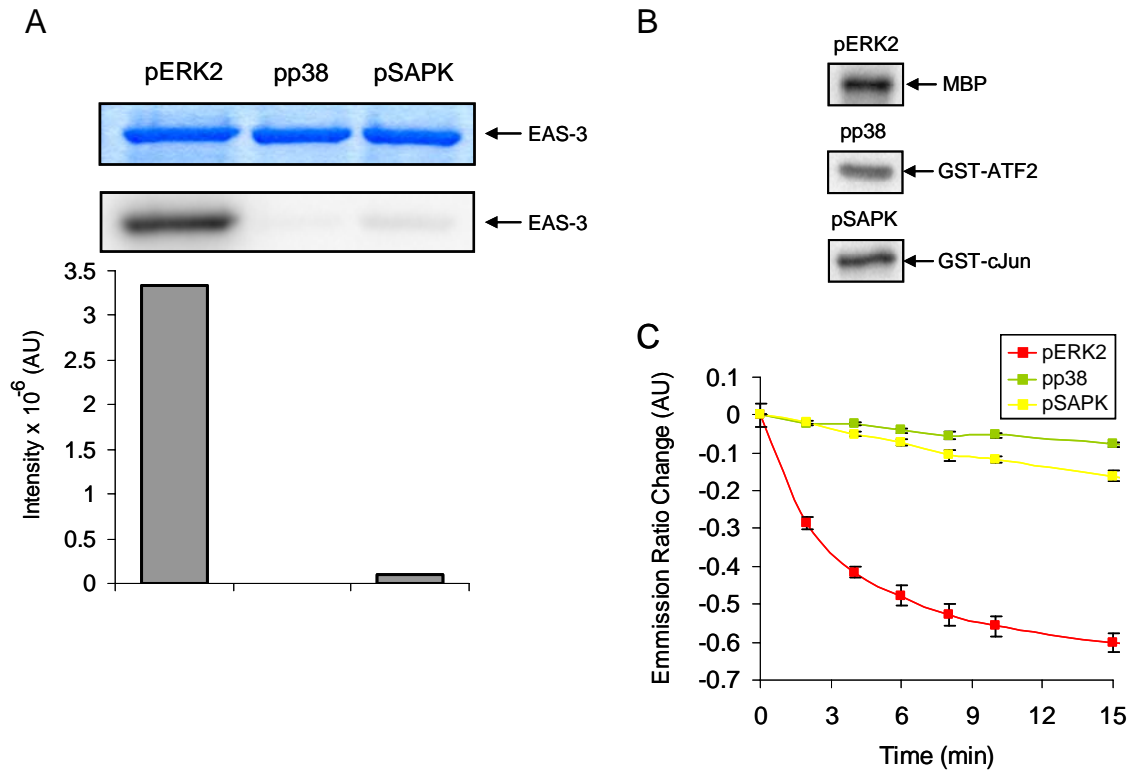


**Figure 3-4. Determination of ERK2 specificity for EAS-3.** (A) Phosphorylation of EAS-3 is efficient with pERK2, but not pp38 or pSAPK. pp38 and pSAPK incorporate little or no  $^{32}\text{P}$  into EAS-3 at the same relative specific activity as pERK2. Band intensities were quantitated by densitometry and are shown graphically. Equal protein loading of EAS-3 is shown by Coomassie staining. (B) Specific targets for pERK2 (MBP), pp38 (GST-ATF2), and pSAPK (GST-cJun) are efficiently phosphorylated in the presence of  $\gamma\text{-}[^{32}\text{P}]\text{ATP}$ . The amounts of active kinase used in A were based on the relative incorporation of  $^{32}\text{P}$  into each cognate substrate by the respective kinase. (C) Fluorimetry of EAS-3 with MAPKs shows that the FRET efficiency change is significantly diminished in the presence of pp38 or pSAPK as compared to pERK2. This is consistent with the phosphorylation assay in A.

will enable us to adapt the EAS-3 sensor for use in live cells.

### **3.4 Conclusions**

These results show that our novel ERK Activity Sensors provide real-time *in vitro* detection of MAP kinase activity. This method can be applied to studying kinetics of ERK activity in real time, as well as detection of ERK activity in unknown cell lysate fractions. There is also the potential to use these sensors for high-throughput screening of ERK kinase activity with fluorescence plate readers. This method is more direct and convenient to monitor ERK activation *in vitro* than conventional assays that either use radioactivity for detection or rely on indirect detection using phospho-specific antibodies for MAPK targets.

### **3.5 Methods**

#### **3.5.1 EAS constructs**

DNA coding for peptide linkers was amplified by PCR with primers designed with Bgl II and BamHI sites at the 5' and 3' ends, respectively. The products were cloned into pECFP-C1 (Clontech), and EYFP from pEYFP-N1 was subsequently cloned in frame to create EAS constructs. EAS's were cloned into pGEX-2T (Amersham) in frame with GST for expression and purification purposes. These GST-tagged constructs were used for initial fluorimetry experiment of EAS constructs. Other versions of EAS's were constructed using ECFP and EYFP with mutation A(207,487)K, which eliminates dimerization of GFPs, and cloned into pET21a (Novagen) with a Histidine-10 tag. These His10-tagged constructs were used for mutant and specificity experiments. EAS-3 linker

mutants were made by Quickchange Site Directed Mutagenesis (Stratagene) to make either single or double point mutation within the peptide linker. For expression in NIH-3T3 cells, EAS's were cloned into the pECFP vector backbone without tags.

### **3.5.2 EAS and active kinase expression**

BL21(DE3) cells were transformed with EAS constructs and plated on LB agar supplemented with 100 g/ml ampicillin. Colonies were picked into 4ml LB-Amp and shaken overnight at 30°C. 250ml LB was inoculated with starter culture, grown to A<sub>600</sub> of 0.6, and induced with 0.1mM IPTG for 18 hours. Cells were spun down, lysed by French press, and cell fragments were spun down at 18,000 rpm in a Beckman JA-20 rotor for 30 minutes. Proteins were purified from lysates over Ni-NTA Superflow (Qiagen) or Glutathione Sepharose 4B (Amersham).

Activated kinases were purified as described [19]. pERK2 was either purchased (NEB) or purified from bacteria transformed with a plasmid containing both constitutively active MEK1\* and His-tagged ERK2. Phosphorylation of ERK2 by MEK1\* occurred in bacteria prior to lysis. BL21(DE3) cells were electroporated with MEK1\*/ERK2 construct and grown overnight at 37°C on LB-Amp agar plates. Several colonies were picked and incubated in 4ml of TB supplemented with 100 g/ml carbenicillin. The starter culture was added to 1L of TB, grown to A<sub>600</sub> of 0.35, and then induced with 0.25mM IPTG for 12 hours at 30°C. Cells were harvested and lysed as above and purified over Ni-NTA Superflow. Activated p38 and SAPK/JNK were purified from bacteria electroporated with two plasmids, one coding for constitutively active MEK kinase 4 (MEKK4\*) and another coding for MEK4 and either His-tagged

p38 or His-tagged SAPK/JNK. These constructs were grown and purified as above, except with both carbenicillin and kanamycin (50 g/ml). Protein concentration and buffer exchange performed with Centriplus, Centricon, and Microcon ultrafiltration membranes (Millipore).

### **3.5.3 Kinase assays and fluorimetry**

Radioactive kinase assays were performed in 25  $\mu$ l in 12.5 mM MOPS pH 7.5, 12.5 mM  $\beta$ -glycerophosphate pH 7.3, 7.5 mM  $MgCl_2$ , 500  $\mu$ M NaOrthovanadate, 500  $\mu$ M NaF, and 9.7 nM DTT. Amounts of kinase and substrate added to reactions are indicated in figure legends. Finally, ATP supplemented with 0.2 nmol [ $\gamma$ - $^{32}P$ ]ATP (6000 mCi/mmol, Molecular Bioproducts) was added to a final concentration of 1 mM. Reactions were incubated at 30°C for 15 minutes, 8.3  $\mu$ l of 4x protein sample buffer (SB) were added, and samples were boiled for 5 minutes. Samples were analyzed with 10% or 12% SDS-PAGE (BioRad Mini-Protean II) and transferred to a nitrocellulose membrane. The membrane was exposed to a phosphoscreen and scanned on a Storm 860 (Molecular Dynamics). Quantitative densitometry of bands was performed using ImageQuant 5.0 (Molecular Dynamics).

Fluorimetry was performed in a Shimadzu Spectrofluorophotometer RF-5301PC. Assays were performed in same buffer as above in a volume of 2.5 ml. The final concentration of EAS constructs was 250 nM, and final concentration of pERK2 was 50nM. The reaction was incubated in fluorimeter and warmed to 30°C. Excitation was set at 425nm to excite ECFP and avoid excitation of EYFP, and readings were taken in 0.2nm increments. An initial reading was taken prior to ATP addition. To initiate

reaction, ATP was added to a final concentration of 1  $\mu$ M, a spinner was activated for 1 minute, and the first reading taken at 2 minutes. EYFP to ECFP ratios were calculated by dividing EYFP peak emission by ECFP peak emission. Peak emissions were defined as an average intensity of EYFP between 524.6-525.4 nm and of ECFP between 474.6-475.4 nm.

### 3.6 References

1. Xu X, Gerard AL, Huang BC, Anderson DC, Payan DG, Luo Y: **Detection of programmed cell death using fluorescence energy transfer.** *Nucleic Acids Res* 1998, **26**(8):2034-2035.
2. Miyawaki A, Llopis J, Heim R, McCaffery JM, Adams JA, Ikura M, Tsien RY: **Fluorescent indicators for Ca<sup>2+</sup> based on green fluorescent proteins and calmodulin.** *Nature* 1997, **388**(6645):882-887.
3. Sato M, Ozawa T, Inukai K, Asano T, Umezawa Y: **Fluorescent indicators for imaging protein phosphorylation in single living cells.** *Nat Biotechnol* 2002, **20**(3):287-294.
4. Ting AY, Kain KH, Klemke RL, Tsien RY: **Genetically encoded fluorescent reporters of protein tyrosine kinase activities in living cells.** *Proc Natl Acad Sci U S A* 2001, **98**(26):15003-15008.
5. Nagai Y, Miyazaki M, Aoki R, Zama T, Inouye S, Hirose K, Iino M, Hagiwara M: **A fluorescent indicator for visualizing cAMP-induced phosphorylation in**

- vivo**. *Nat Biotechnol* 2000, **18**(3):313-316.
6. Zhang J, Ma Y, Taylor SS, Tsien RY: **Genetically encoded reporters of protein kinase A activity reveal impact of substrate tethering**. *Proc Natl Acad Sci U S A* 2001, **98**(26):14997-15002.
  7. Violin JD, Zhang J, Tsien RY, Newton AC: **A genetically encoded fluorescent reporter reveals oscillatory phosphorylation by protein kinase C**. *J Cell Biol* 2003, **161**(5):899-909.
  8. Lin Z, Suzow JG, Fontaine JM, Naylor EW: **A high throughput beta-globin genotyping method by multiplexed melting temperature analysis**. *Mol Genet Metab* 2004, **81**(3):237-243.
  9. Chang L, Karin M: **Mammalian MAP kinase signalling cascades**. *Nature* 2001, **410**(6824):37-40.
  10. Ferrell JE, Jr., Machleder EM: **The biochemical basis of an all-or-none cell fate switch in *Xenopus* oocytes**. *Science* 1998, **280**(5365):895-898.
  11. Levchenko A, Bruck J, Sternberg PW: **Scaffold proteins may biphasically affect the levels of mitogen-activated protein kinase signaling and reduce its threshold properties**. *Proc Natl Acad Sci U S A* 2000, **97**(11):5818-5823.
  12. Huang CY, Ferrell JE, Jr.: **Ultrasensitivity in the mitogen-activated protein kinase cascade**. *Proc Natl Acad Sci U S A* 1996, **93**(19):10078-10083.
  13. Seidel JJ, Graves BJ: **An ERK2 docking site in the Pointed domain**

- distinguishes a subset of ETS transcription factors.** *Genes Dev* 2002, **16**(1):127-137.
14. Fantz DA, Jacobs D, Glossip D, Kornfeld K: **Docking sites on substrate proteins direct extracellular signal-regulated kinase to phosphorylate specific residues.** *J Biol Chem* 2001, **276**(29):27256-27265.
  15. Zacharias DA, Violin JD, Newton AC, Tsien RY: **Partitioning of lipid-modified monomeric GFPs into membrane microdomains of live cells.** *Science* 2002, **296**(5569):913-916.
  16. Sharrocks AD, Yang SH, Galanis A: **Docking domains and substrate-specificity determination for MAP kinases.** *Trends Biochem Sci* 2000, **25**(9):448-453.
  17. Johnson GL, Lapadat R: **Mitogen-activated protein kinase pathways mediated by ERK, JNK, and p38 protein kinases.** *Science* 2002, **298**(5600):1911-1912.
  18. Biondi RM, Nebreda AR: **Signalling specificity of Ser/Thr protein kinases through docking-site-mediated interactions.** *Biochem J* 2003, **372**(Pt 1):1-13.
  19. Khokhlatchev A, Xu S, English J, Wu P, Schaefer E, Cobb MH: **Reconstitution of mitogen-activated protein kinase phosphorylation cascades in bacteria. Efficient synthesis of active protein kinases.** *J Biol Chem* 1997, **272**(17):11057-11062.

## **Chapter 4**

# **Exploring Dose-Response Effects of dMek1 and ROG on CD4/CD8 Lineage Determination Using Lentiviral Transgenesis**

### **4.1 Abstract**

A double-positive thymocyte must make a decision to become either a CD4<sup>+</sup> or CD8<sup>+</sup> mature T cell during the differentiation phase of positive selection. While it is clear that this choice is directed by the interaction of the T cell receptor with either MHC class I (CD8<sup>+</sup>) or class II (CD4<sup>+</sup>), the involvement of Ras/Erk MAP kinase signaling in this process is unclear. In this chapter, we describe an application of a recently described method of transgenesis using lentiviral vectors in an effort to study the dose-effects of dMek1 expression in thymocytes in a single generation of mice. We initially established a rough correlation of transgene expression and transgene copy number. We were also able to show that the variegation in transgene expression seen in the initial report was stable, demonstrating the viability of our approach in studying the effects of transgenes on the development in the thymus. Data from dMek1 mice suggested no effect in CD4/CD8 lineage determination by reducing Erk signaling. These data, however, were

incomplete as we were unable to identify transgene expressing cells. We expressed the repressor ROG in thymocytes and also observed no effect. These results may be indicative of technical difficulties with this novel approach for studying lineage determination. Future experiments should focus on trouble-shooting this technique by recapitulating results from previous studies.

## 4.2 Background

Coherent Ras/Erk signaling is crucial during the onset of positive selection of thymocytes (reviewed in [1]). The role of this signaling pathway in CD4/CD8 lineage determination, however, remains unclear. Experiments affecting TCR signaling through Lck have lent support to a strength-of-signal model [2, 3]. One study indicated calcineurin and Erk MAPK signaling in lineage commitment [4], although this study relied completely on pharmacological stimulation in culture rather than on a more physiological method. There is also evidence that Erk<sup>sem</sup>, a hypersensitive form of Erk2, increased CD4<sup>+</sup> development, but the effect was modest [5]. To address this issue, we developed a system that would allow for genetic manipulation of the Ras/Erk pathway and study the dose-dependent effects of a dominant negative form of Mek1 (dMek1) on lineage determination (Figure 4-1). Our aim was to utilize the relatively new technique of lentiviral transgenesis to create transgenic animals for analysis, as opposed to the canonical method of creating transgenic animals by pronuclear injection.

Microinjection of foreign DNA into the male pronucleus of mouse zygotes is the standard and established method to make transgenic animals that was first introduced by Gordon and Ruddle [6]. A gene construct is introduced with a gene-of-interest (GOI)

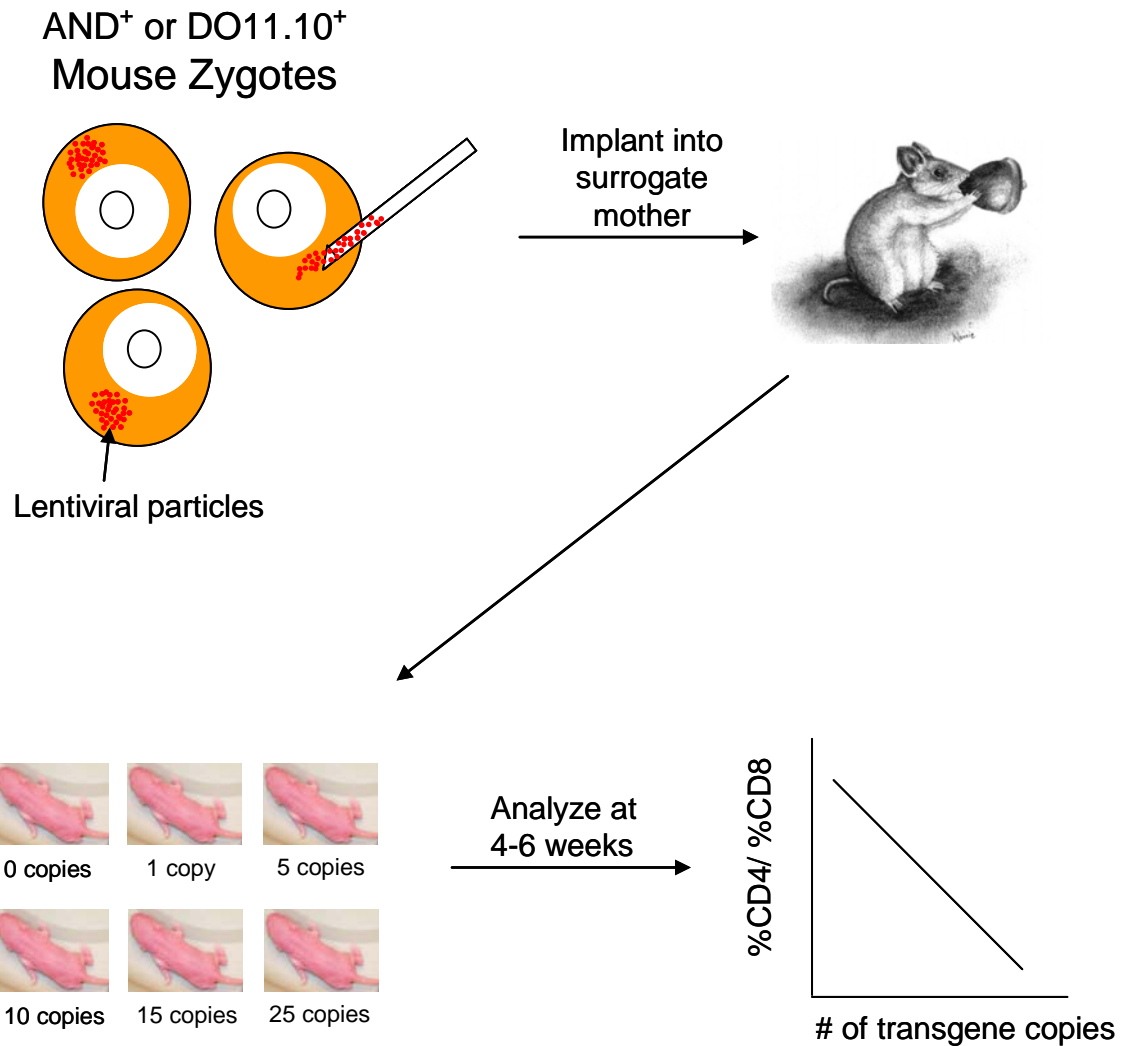


**Figure 4-1. Experimental design for lentiviral transgenic analysis of CD4/CD8 lineage determination.** AND<sup>+</sup> or DO11.10<sup>+</sup> embryos were harvested <24 hours after mating, and concentrated lentivirus was microinjected into the perivitelline space. Injected embryos were then implanted into a surrogate mother and allowed to litter. Transgenic mice were analyzed for transgene integration by southern blot of genomic DNA purified from tail tissue. Thymii and/or spleens were harvested from selected mice between 4 and 6 weeks of age and were analyzed for dose-dependent lineage choice switch from CD4 SP to CD8 SP.

controlled by promoter/enhancer sequences. Several copies of the gene (1-100) integrate into the genome, and the efficiency of integration and number of copies integrated are dependent on many factors. Such factors include DNA concentration, construct size, timing of the injection, and how proficient the technician is with microinjection. Several advancements have been made in an effort to fine tune this process for increased efficiency, but the overall process has changed little since its discovery. The end result is the integration of the foreign DNA into the host genome. Copy number alone, however, rarely correlates the gene expression level in founder mice. The transgenic protein expressed in each founder is dependent on many factors, including copy number (more copies can sometimes decrease expression) and the specific site of integration [7].

One cannot, therefore, deduce the level of protein expression solely by detecting the transgene copy number by southern blot of mouse genomic DNA. To determine protein expression levels, each founder must be mated and a line established. Some offspring would be used for analysis, while others would be mated to continue the established line. This process is further lengthened by the fact that it is often necessary to use zygotes derived from the mating of two different mouse strains. Backcrossing to establish a syngeneic line is considered complete at 14 generations, which takes over 2 years assuming a 2-3 month generation time. To determine a transgenic dose response, one would have to establish many different founders, analyze each individually for protein expression levels, and backcross each individual line to obtain syngeneic lines. The resources required for such a project are prohibitive. Our lentiviral approach, however, allows for dose-dependent analysis of transgene expression in a single generation, decreasing time and monetary costs significantly.

Silencing of retroviral expression is a common problem in infection of stem cells. After initial infection and integration, gene expression is often quickly silenced by a combination of histone deacetylation, chromatin rearrangement, and CpG methylation [8, 9]. Lentiviruses, however, are often less susceptible to similar silencing effects [10, 11], and have been successfully implemented in the treatment of genetic disease [12]. Recently, a novel method of creating transgenic animals has been described [13]. Using a self-inactivating (SIN) lentiviral vector coding for EGFP as the gene-of-interest, the authors were able to infect mouse and rat zygotes with a replication-incompetent virus. Under ubiquitin promoter control, EGFP was expressed in every tissue examined by the authors. In addition, the authors were able to direct EGFP expression to specific tissues of transgenic animals. The Lck proximal promoter was able to direct EGFP expression to thymocytes specifically. Similarly, the myogenin promoter directed EGFP expression to skeletal muscle. The authors also examined germ-line transmission and found that the viral transgene could indeed be transmitted to further generations.

This novel method to create transgenic animals, however, does have a few shortcomings. Traditionally, transgenesis is performed by intracellular injection of transgenic DNA. Concatamers of the transgenic vector often integrate together, resulting in multiple copies of the transgene that are confined to one genomic locus. Germ-line transmission of the transgene is stable because either all the copies of the transgene are passed on or none are. Retroviral insertions, in contrast, occur randomly throughout the genome. The resulting germ-line transmission would be diluted over several generations. Another shortcoming is that mice expressing GFP under the Lck proximal promoter exhibit variegation in gene expression ([13], supplemental data). The stability of this

variegation, however, was not explored by the authors and required our attention if this method were to be viable. This topic is discussed later in this chapter.

Although there are apparent pitfalls with using this system, there are specific advantages we sought to utilize. Due to variations in the amount of concentrated virus delivered per injection and the statistical variability of infection, each embryo will receive a different number of transgene copies. Given the random integration of the viral genome, there is likely a rough correlation between transgene copy number and actual protein expression. Each pup in the resulting litter will have a different number of transgene copies, and therefore will harbor different levels of transgene expression. Each litter will therefore not only give information for each individual transgenic mouse, but will also give us dose-dependence data as a whole. This is clearly an advantage over attempting to establish several different transgenic lines by traditional transgenesis.

To specifically study the role of the Ras/Erk cascade in CD4/CD8 lineage determination, we needed to use a transgenic TCR animal model. A model already successfully used to study the role of Lck in lineage determination is the AND transgenic TCR [2]. This TCR is specific for a pigeon Cytochrome C peptide in the context of I-E<sup>k</sup> and is MHC class II restricted, which under normal developmental conditions yields CD4<sup>+</sup> T cells [14]. Importantly, the AND TCR is co-receptor independent, allowing for the characterization of functionally mature T cells in the absence of co-receptor binding [15, 16]. Our expectation, then, would be that we could drive the development of CD8<sup>+</sup> T cells with dominant negative forms of Ras or Mek1 (dnRas or dMek1, respectively) in an AND TCR background if the Ras/Erk pathway plays a role in CD4/CD8 lineage determination.

## 4.3 Results and Discussion

### 4.3.1 Reproduction of FLckGW mice

To verify the efficacy of lentiviral transgenesis and to familiarize ourselves with the technical aspects of making these mice, we began by reproducing a portion of the experiment described by Lois, et al. [13]. Being that our interests lay in the thymus, the most appropriate construct to use was the FLckGW construct, which coded for GFP expression under the Lck proximal promoter. Lentivirus was packaged in the HEK-293 cell line, concentrated by ultracentrifugation, and administered to newly fertilized C57Bl/6 embryos by perivitelline injection. Progeny were analyzed by southern blot of genomic tail DNA to determine integration and estimate gene copy number. Based on this analysis, three mice were chosen with 0, low, and high copy and analyzed for GFP expression in the thymus and spleen.

Genomic DNA was purified from tail tissue from each of the 18 progeny resulting from the FLckGW lentiviral infection of mouse embryos. Each sample was digested by PstI restriction endonuclease, transferred to Hybond-N<sup>+</sup> membrane, and probed with a radiolabeled DNA probe specific for a portion of GFP. The results are shown in Figure 4-2B. It is apparent that each mouse received a different pattern and number of integrations, consistent with the previous report [13]. This was a key feature to using lentiviral transgenesis to study dose effects of dMek1 on lineage determination, as we expected variable gene expression in these mice. Mouse PN681-1 (\*\*\*), mouse PN681-5 (\*\*), and mouse PN684-13 (\*) were used to analyze variation in gene expression as a corollary to gene copy number and to confirm variegation in transgene

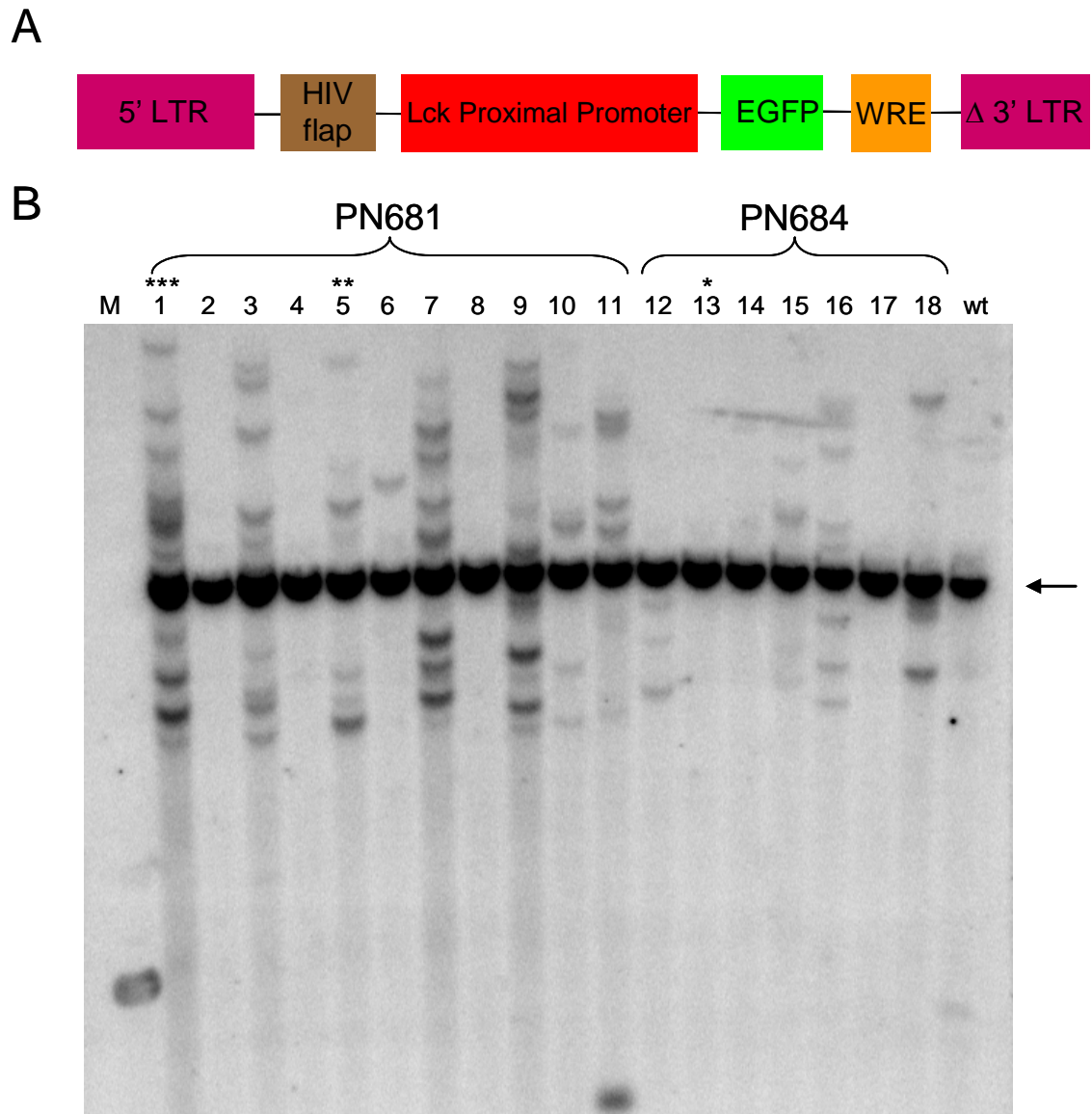


**Figure 4-2. The structure of the FLckGW construct and genomic analysis of transgene integrations.** A) The lentiviral construct FLckGW contains the HIV-1 flap, followed by the Lck proximal promoter, enhanced GFP (EGFP), and the woodchuck response element (WRE), flanked by long terminal repeats (LTR) at the 5' end and a truncated 3' LTR ( $\Delta 3'$  LTR). B) Southern analysis of mice from injection panels PN681 and PN684 (indicated) and flanked by 1 kb DNA marker (M) and C57Bl/6 wild-type (wt) as a negative control. PN684-13(\*NLC), PN681-5 (\*\*low copy), and PN681-1 (\*\*\*) were analyzed further. Transgene detection was by [ $^{32}$ P]-radiolabeled probe specific for EGFP. The arrow indicates a non-specific band that was later determined to be plasmid contamination.

expression.

Analysis of thymocytes revealed that GFP expression was indeed dependent on gene copy number (Figure 4-3). The percentage of GFP<sup>+</sup> cells in the entire thymic population was approximately double in the mouse PN681-1 (\*\*\*) versus the mouse PN681-5 (\*\*). In addition, peak GFP fluorescence was higher in PN681-1 (\*\*\*) thymocytes, indicating that not only does gene copy number affect the percentage of transgene expressing cells, but also affects the level of protein expression. As expected, the normal littermate control (NLC) PN684-13 (\*\*\*) that had received no transgene copies had no GFP-expressing cells.

Both the GFP<sup>+</sup> and GFP<sup>-</sup> population were analyzed for CD4 and CD8 surface expression. This allowed us to determine whether the GFP<sup>-</sup> population was only DN cells that had not initiated expression off the Lck proximal promoter due to immaturity, or if this population was due to variegation in gene expression (Figure 4-3B). Percentages of DP and SP thymocytes were comparable in the two populations, indicating that some cells had indeed not initiated transgene expression, even though Lck expression driven by the Lck proximal promoter had been initiated. The DN population was slightly higher in the GFP<sup>-</sup> population, likely due to a small number of cells that would potentially express the transgene, but had yet to initiate Lck proximal promoter-directed expression. It should be noted as well that presence of the transgene had no effect on normal development of the CD4 or CD8 T cell lineages, as seen in the SP compartment and in the periphery, discussed below.

We also analyzed the peripheral T cell compartment by extracting lymphocytes from the spleen of each transgenic mouse (Figure 4-4). These cells were stained for

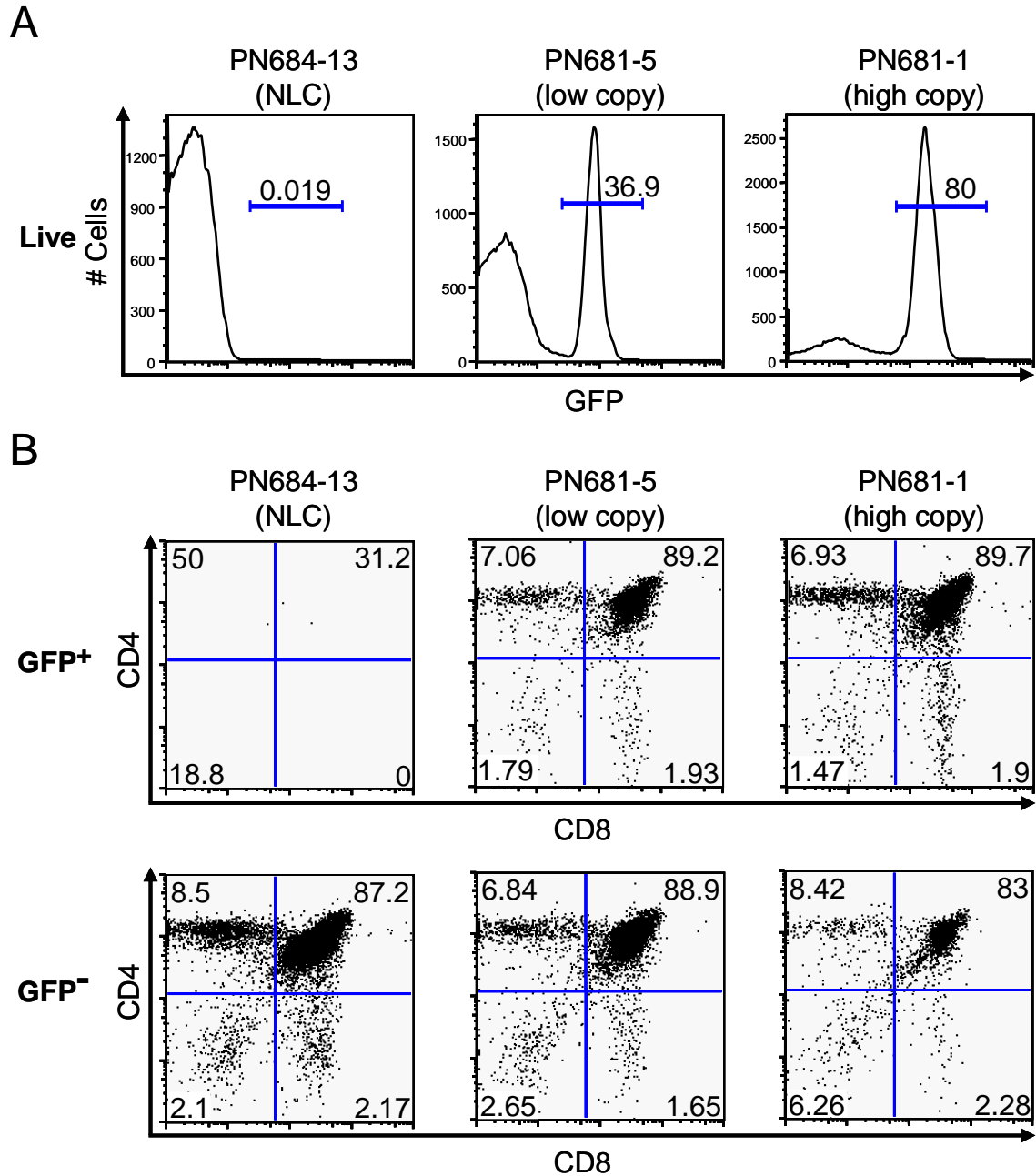


**Figure 4-3. Thymic analysis of 3 mice from injection panel PN681 for GFP expression.** A) Live thymocytes from each mouse were analyzed for GFP expression by flow cytometry. Gates indicate the percentage of GFP<sup>+</sup> cells in each population. B) CD4/CD8 analysis of cells gated on GFP expression, as indicated by GFP<sup>+</sup> and GFP<sup>-</sup>. Percentages of DN, DP, and SP populations are indicated in the corner of each plot. Note that GFP expression has no effect on population percentages.

TCR $\beta$  surface expression to distinguish them from other white blood cells that also inhabit the spleen. As with thymocytes, peripheral T cells were analyzed for GFP expression and stained for CD4 and CD8. GFP was found to be expressed in similar percentages of peripheral T cells as was found in thymocytes, and the level of fluorescence was also comparable. The percentages of CD4 and CD8 T cells were comparable in the PN684-13 (NLC) and PN681-5 (low copy) in both the GFP<sup>+</sup> and GFP<sup>-</sup> populations. In the high copy number mouse PN681-1 (high copy), there seemed to be a skew in the percentage of CD8 T cells in the GFP<sup>+</sup> population, suggesting that high-level transgene expression could cause non-specific effects. This also could be due to an aberrant sample, but should be examined in future experiments. Another odd finding was the presence of GFP<sup>+</sup> T cells in the periphery. Lck expression from the proximal Lck promoter is terminated during the DP $\rightarrow$ SP transition and is then directed by the distal Lck promoter in the SP and peripheral compartments [17, 18]. Other transgenic lines driven by the Lck proximal promoter have shown similar expression in mature cells [19, 20]. It is possible that high GFP expression in mature T cells in FLckGW mice are a result of multiple integration sites, decreasing the ability of cells to silence a given locus.

#### **4.3.2 Variegation in lentiviral gene expression is stable**

To utilize lentiviral transgenesis as an effective tool to study signaling in thymocyte development, variegation in lentiviral gene expression seen in [13] must be stable. Control of transgene expression is crucial, given the importance of different signaling molecules at developmental checkpoints. Should expression of the transgene initiate at one developmental stage and be silenced at a later time, it could drastically

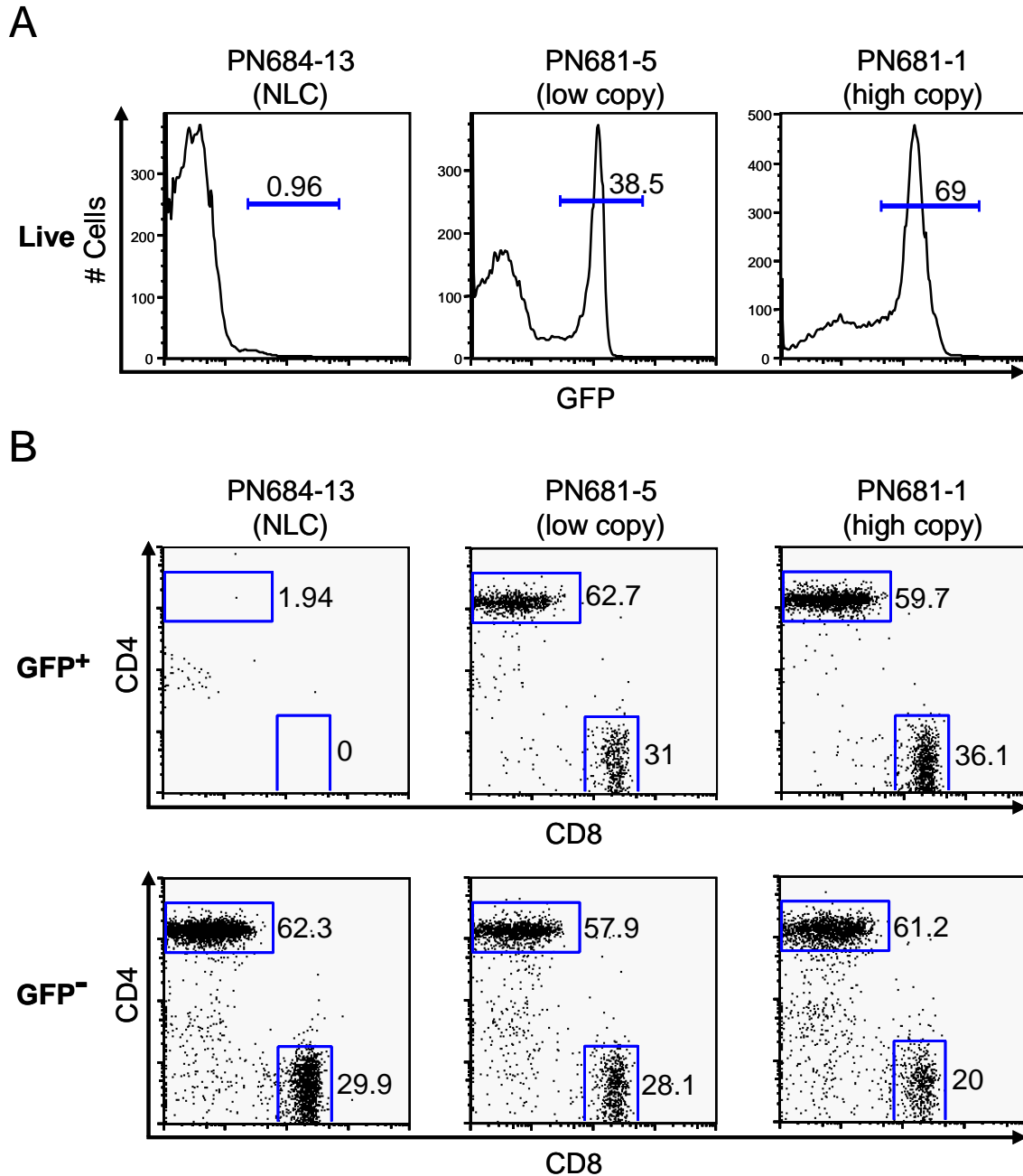


**Figure 4-4. Splenic analysis of 3 mice from injection panel PN681 for GFP expression.** A) Live splenocytes gated for TCRb<sup>hi</sup> expression were analyzed for GFP expression by flow cytometry. Gates indicate the percentage of GFP<sup>+</sup> cells in each population. B) CD4/CD8 analysis of cells gated on GFP expression, as indicated by GFP<sup>+</sup> and GFP<sup>-</sup>. Percentages of DN, DP, and SP populations are indicated in the corner of each plot. Note that GFP expression has no effect on population percentages.

affect the timing of development and the final developmental outcome of a given cell. Alternatively, if transgene expression were to be silenced past the developmental stage in which the tissue-specific promoter should be activated, it could have similar timing and outcome effects. The resulting confusion would greatly decrease the validity of any data derived from or conclusions made about that experiment.

To determine the stability of variegation we designed an experiment using reaggregate Fetal Thymic Organ Culture (RgFTOC) (Figure 4-5). Self-inactivating (SIN) lentivirus coding for GFP under control of the Lck proximal promoter was expressed and packaged in HEK-293T cells and concentrated by ultracentrifugation. C57Bl/6 mouse zygotes were harvested after fertilization, and concentrated lentivirus was delivered by sub-zonal injection with a micropipette. Infected zygotes were implanted into surrogate mothers and day E14.5-E15.5 embryos were harvested. Each fetal thymus was harvested separately, disassociated, and analyzed for GFP expression (Figure 4-6). Lobes containing both GFP-negative (GFP<sup>-</sup>) and GFP-positive (GFP<sup>+</sup>) cells were collected and pooled.

To reduce the possibility of sorting GFP<sup>-</sup> cells that had yet to initiate expression from the Lck proximal promoter, we decided to sort only cells from the DN3 and DN4 populations. Pooled thymocytes were stained with  $\alpha$ -CD25 and  $\alpha$ -CD44, conjugated to phycoerythrin (PE) and allophycocyanin (APC), respectively. The CD25<sup>+</sup>/CD44<sup>-</sup> (DN3) and CD25<sup>-</sup>/CD44<sup>-</sup> (DN4) populations were sorted based on GFP expression. The DN3/DN4/GFP<sup>+</sup> and DN3/DN4/GFP<sup>-</sup> populations were then separately reaggregated with thymic stromal cells derived from treated E14.5 B6D2F1 fetal thymii, which had been depleted of thymocytes by treatment with the nucleotide analog 2'-deoxyguanosine.

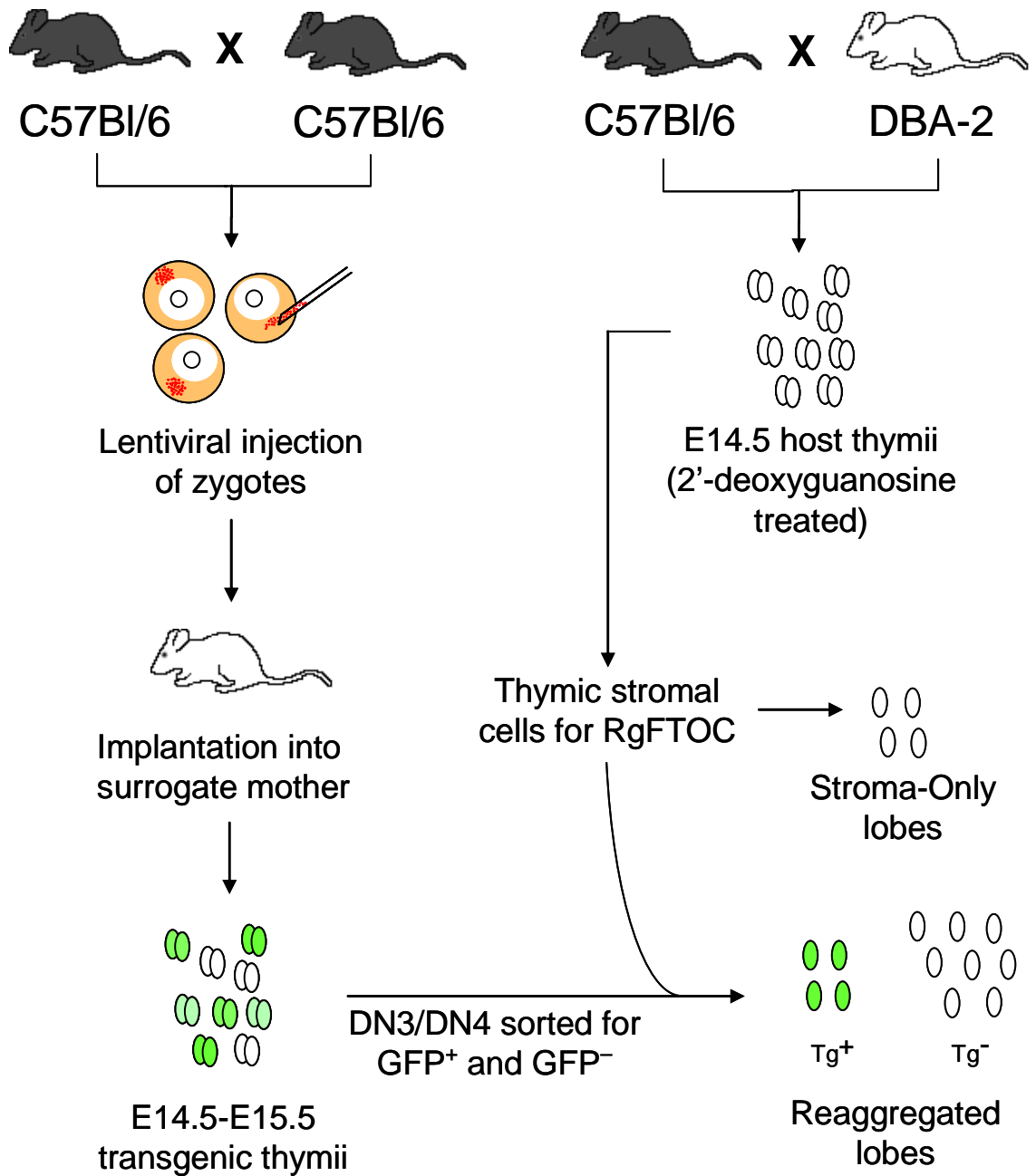


**Figure 4-5. Experimental design to determine stability of variegation in transgene expression.** Transgenic E14.5 thymii were harvested from surrogate mother, and DN3 and DN4 populations were sorted into GFP<sup>+</sup> and GFP<sup>-</sup> populations. Stromal cells from 2'-deoxyguanosine-treated host lobes were dissociated and reagggregated with either GFP<sup>+</sup> (labeled Tg<sup>+</sup>) or GFP<sup>-</sup> (labeled Tg<sup>-</sup>) cells sorted from transgenic lobes or left unseeded (stroma-only). FTOC lobes were then analyzed at 7 and 14 days.

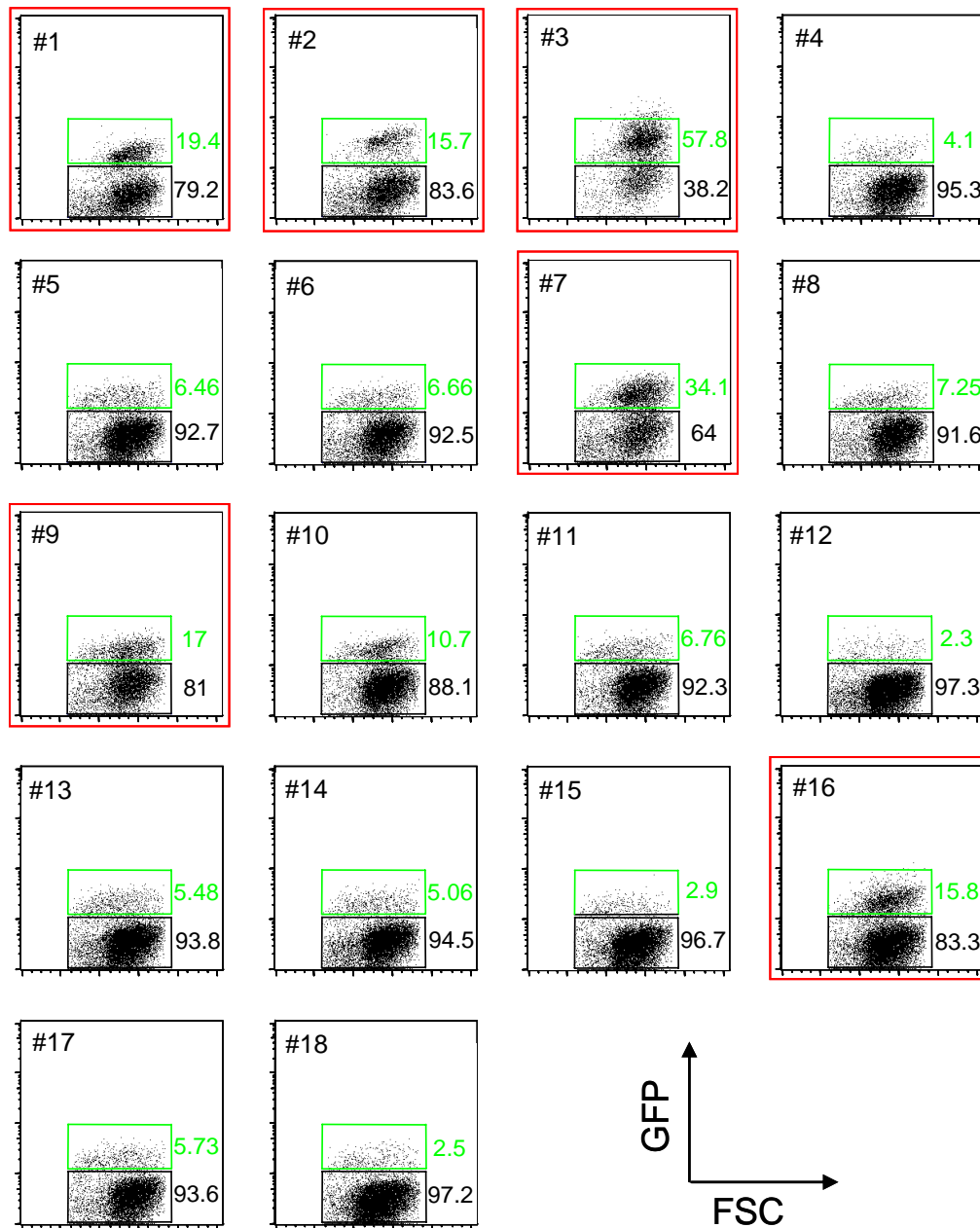


**Figure 4-6. GFP expression in individual fetal thymii from transgenic fetuses.**

Thymocytes from dissociated lobes #1, #2, #3, #7, #9, and #16 (red boxes) were chosen for the variegation experiment based on having  $>15\%$  GFP<sup>+</sup> cells. These cells were pooled, sorted for DN3/DN4/EGFP<sup>+</sup> and DN3/DN4/EGFP<sup>-</sup> populations, and used to seed RgFTOC. Abbr.: green fluorescent protein (GFP), forward scatter (FSC).

This host strain is the F1 cross between C57Bl/6 and DBA2 strains and was chosen because any thymocytes not eliminated by 2'-deoxyguanosine treatment could be distinguished based on expression of different alleles of CD5 and H-2D. This distinction was key, given that any host thymocyte contamination of lobes would be perceived as negative for GFP expression in Tg<sup>+</sup> lobes and confused as a decrease in viral gene expression.

Donor thymocytes were pure C57Bl/6 progeny and only express H-2<sup>b</sup> MHC haplotype and the CD5.2 allele. B6D2F1 progeny express both H-2<sup>b</sup> and H-2<sup>d</sup> haplotypes, as well as CD5.1. Day 7 fetal lobes were analyzed using an  $\alpha$ -H-2D<sup>d</sup> antibody, which failed to effectively distinguish H-2<sup>d+</sup> from H-2<sup>b+</sup> cells (data not shown). Due to the variability in specificity of antibodies to mouse alloantigens we tested an  $\alpha$ -CD5.1 antibody for the ability to distinguish C57Bl/6 and B6D2F1 thymocytes and compared it to the failed  $\alpha$ -H-2D<sup>d</sup> (Figure 4-7). Thymocyte samples from C57Bl/6 and B6D2F1 mice were stained individually and in a 1:1 mixture with  $\alpha$ -H-2D<sup>d</sup> and  $\alpha$ -CD5.1. In contrast to the  $\alpha$ -H-2D<sup>d</sup> antibody,  $\alpha$ -CD5.1 could distinguish host cells from donor cells and was used for day 14 analysis.

Although we were unable to distinguish donor and host thymocyte populations, we analyzed several day 7 lobes for GFP expression and CD4 and CD8 expression within the GFP<sup>+</sup> and GFP<sup>-</sup> populations. GFP expression was absent in stroma-only lobes, with the GFP<sup>-</sup> population in these lobes representing contaminating host thymocytes (Figure 4-8). High percentages of cells from the Tg<sup>+</sup> lobes were GFP expressers, with a small but significant number of GFP<sup>-</sup> cells. These were likely host contaminants, but may also have represented a population of transgenic donor thymocytes that had terminated GFP

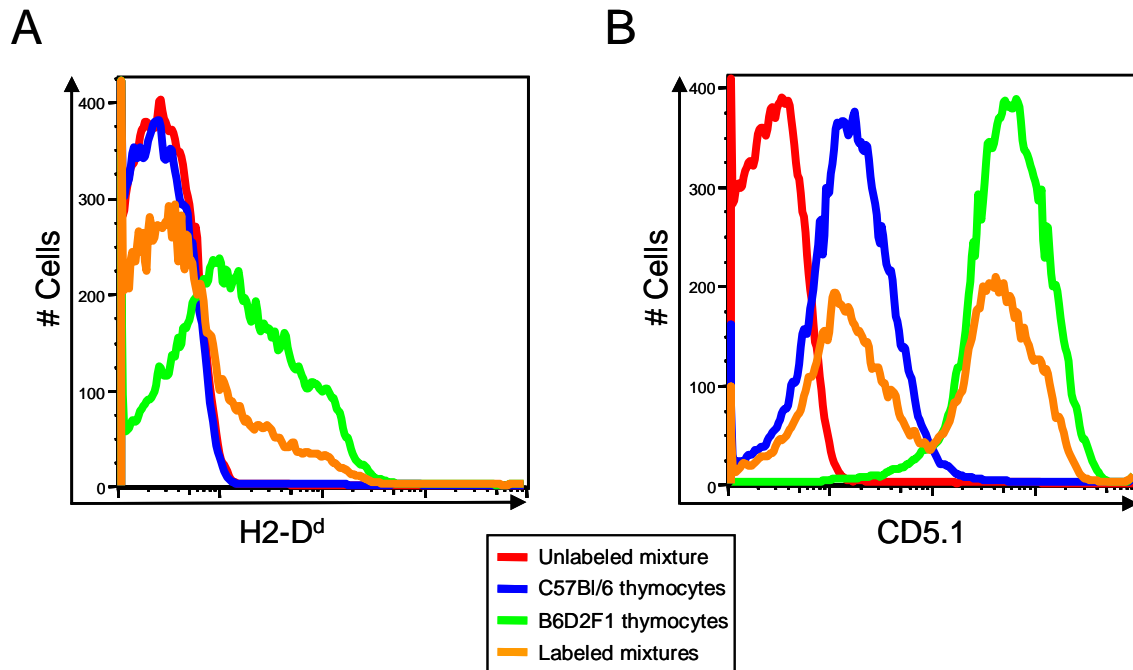


**Figure 4-7. C57Bl/6 and B6D2F1 thymocytes can be distinguished by  $\alpha$ -CD5.1, but not by  $\alpha$ -H-2D<sup>d</sup>.** C57Bl/6 thymocytes, B6D2F1 thymocytes, and a mixture of the two were stained with  $\alpha$ -CD5.1 and  $\alpha$ -H-2D<sup>d</sup>. A) The  $\alpha$ -H-2D<sup>d</sup> staining gives a much smaller peak shift and cannot distinguish a 1:1 mixture of thymocytes. B) The  $\alpha$ -CD5.1 staining gives distinctly separated peaks for C57Bl/6 and B6D2F1 thymocytes and can distinguish the two populations in a 1:1 mixture.  $\alpha$ -CD5.1 was therefore used to distinguish donor versus host in day 14 analysis.

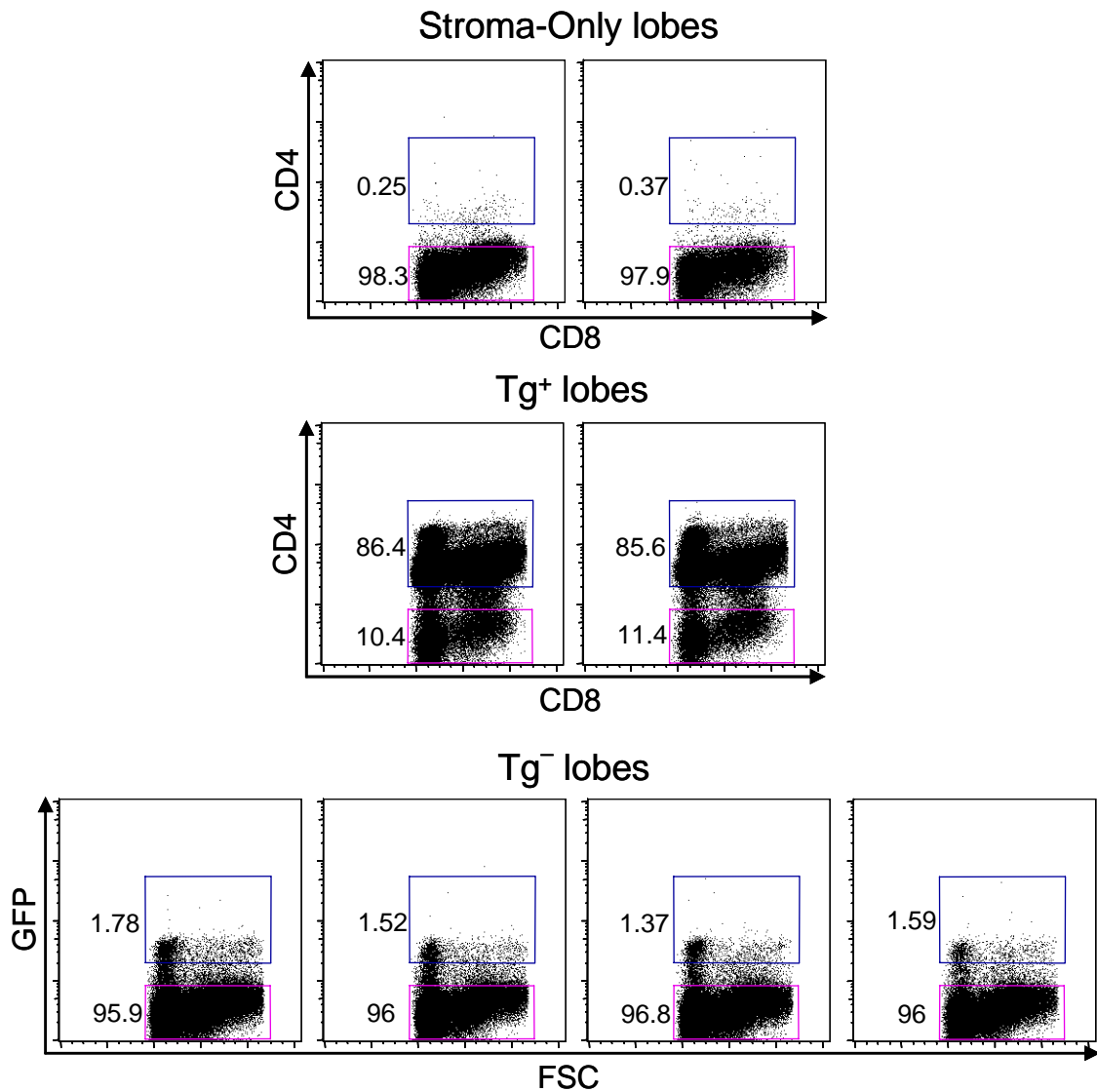


**Figure 4-8. GFP analysis of day 7 RgFTOC lobes.** Each panel indicates the day 7 GFP analysis of one RgFTOC lobe seeded either with no donor thymocytes (stroma-only), GFP<sup>+</sup> donor thymocytes (Tg<sup>+</sup> lobes), or with GFP<sup>-</sup> donor thymocytes (Tg<sup>-</sup> lobes). Pink gates represent the percentage of GFP<sup>-</sup> cells within each lobe, and blue gates represent the percentage of GFP<sup>+</sup> cells within each lobe. The small percentage of GFP<sup>+</sup> cells in the GFP<sup>-</sup> lobes may be due to slight contamination of cells that had very low GFP expression during the sorting phase of this experiment.

expression. Lastly, each of the Tg<sup>-</sup> lobes contained cells that appeared in the GFP<sup>+</sup> gate (Figure 4-8, blue boxes). All of these cells had low GFP fluorescence and represented a small portion of the population. These low expressers may have had too little intracellular GFP during the initial cell-sort and sorted as GFP<sup>-</sup> or may not have initiated transgene expressing despite entering the DN3 stage.

We stained day 7 FTOC samples with  $\alpha$ -CD4 and  $\alpha$ -CD8 fluorescent conjugates for CD4/CD8 analysis. We analyzed the GFP<sup>-</sup> and GFP<sup>+</sup> populations of each lobe separately by the gates established in Figure 4-8. Percentages of DN, DP, and SP populations in the GFP<sup>-</sup> population from the Tg<sup>+</sup> lobes were similar to that of the stroma-only lobes and different than the Tg<sup>-</sup> lobes (Figure 4-9). This would suggest that the GFP<sup>-</sup> cells in the Tg<sup>+</sup> lobes were host cell contaminants, although confirmation of this was not possible until the day 14 analysis, discussed below. CD4/CD8 analysis of the GFP<sup>+</sup> population of Tg<sup>-</sup> lobes, however, correlated with percentages found in the Tg<sup>+</sup> lobes, further indicating that these cells were donor thymocytes that had either initiated GFP expression after cell-sorting or were poor expressers at the time of sorting (Figure 4-10).

Day 14 analysis of Tg<sup>+</sup> lobes showed that a high percentage of the GFP<sup>+</sup> population was CD5.1<sup>-</sup> (Figure 4-11). Conversely, the GFP<sup>-</sup> population was almost entirely CD5.1<sup>+</sup> indicating that this population was made up of contaminating host thymocytes. Two interesting findings were the existence of small populations of GFP<sup>+</sup>/CD5.1<sup>+</sup> and GFP<sup>-</sup>/CD5.1<sup>-</sup>. Theoretically, the transgenic thymocytes could be producing replication-competent virus and infecting the host cells. This is unlikely, however, because the lentiviral construct we used is self-inactivating, and two separate

vectors were used for

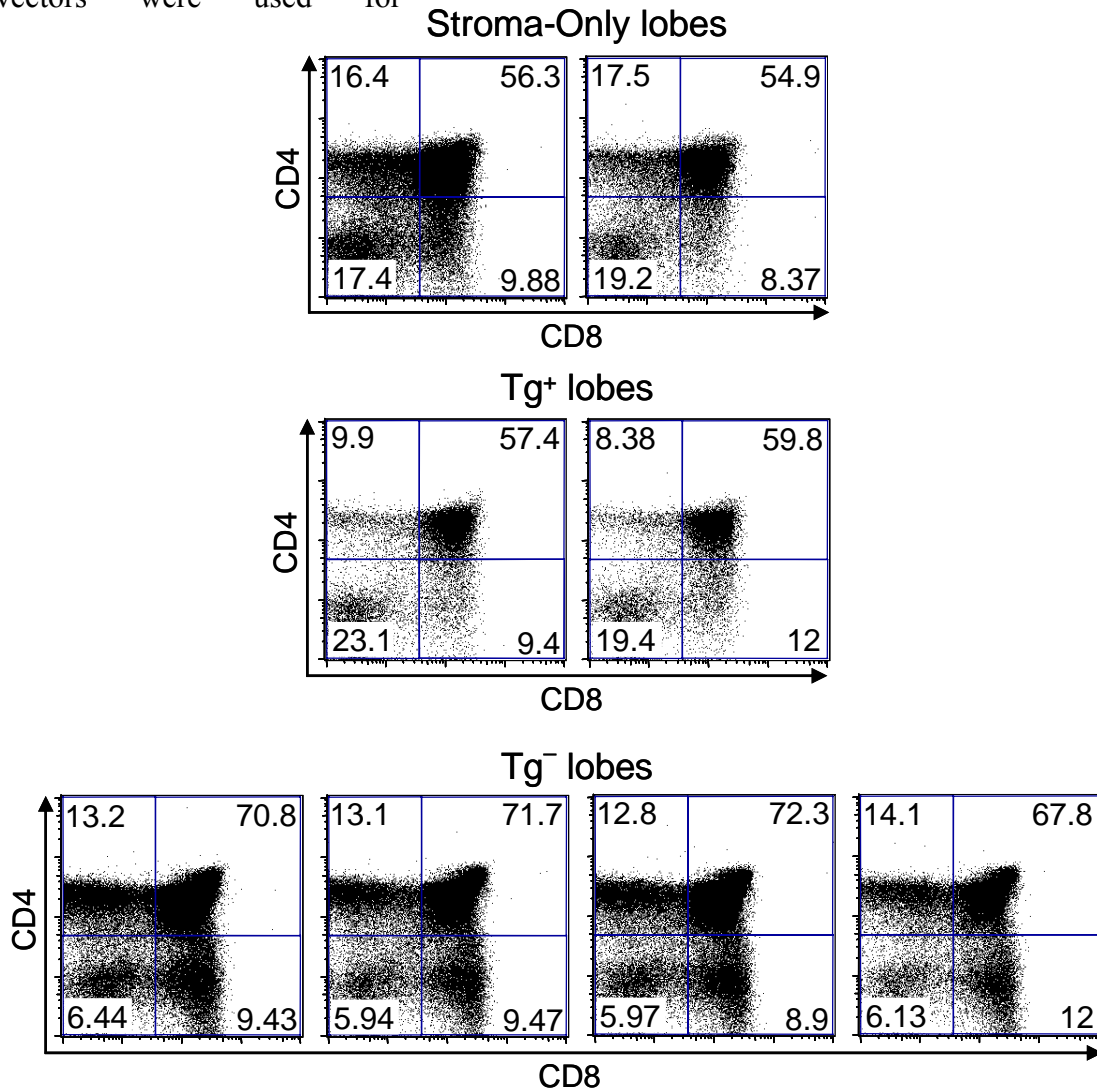


**Figure 4-9. CD4/CD8 analysis of the GFP<sup>-</sup> population from day 7 RgFTOC lobes.**

Each panel indicates the day 7 CD4/CD8 analysis of the GFP<sup>-</sup> population (pink gates in figure 4.8) from one RgFTOC lobe. Percentages of DN, DP, and SP populations are indicated in the four quadrants of each panel. Note that percentages of these populations were similar in the stroma-only lobes and Tg<sup>+</sup> lobes, yet different in the Tg<sup>-</sup> lobes. This indicated that the GFP<sup>-</sup> population in the Tg<sup>+</sup> lobes was likely host thymocyte contamination.

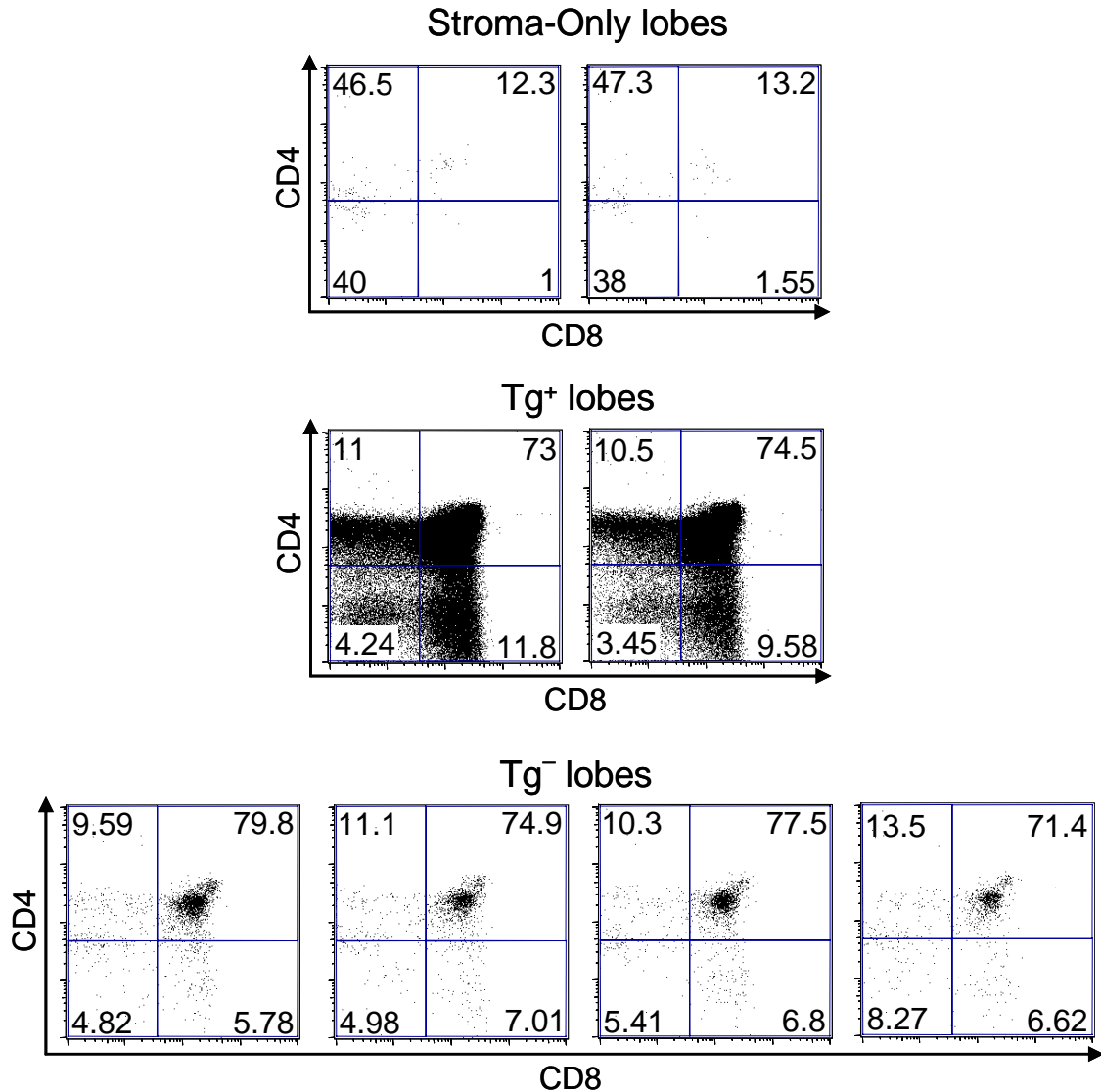


**Figure 4-10. CD4/CD8 analysis of the GFP<sup>+</sup> population from day 7 RgFTOC lobes.**

Each panel indicates the day 7 CD4/CD8 analysis of the GFP<sup>+</sup> population (blue gates in figure 4.8) from one RgFTOC lobe. Percentages of DN, DP, and SP populations are indicated in the four quadrants of each panel. Similar percentages of these populations in both Tg<sup>+</sup> and Tg<sup>-</sup> lobes indicated that they were likely derived from donor thymocytes. The presence of GFP<sup>+</sup> cells in Tg<sup>-</sup> lobes could have been due to very low expression of GFP during initial sorting, or a small percentage of cells in the DN3 population that had not yet initiated expression from the Lck proximal promoter.

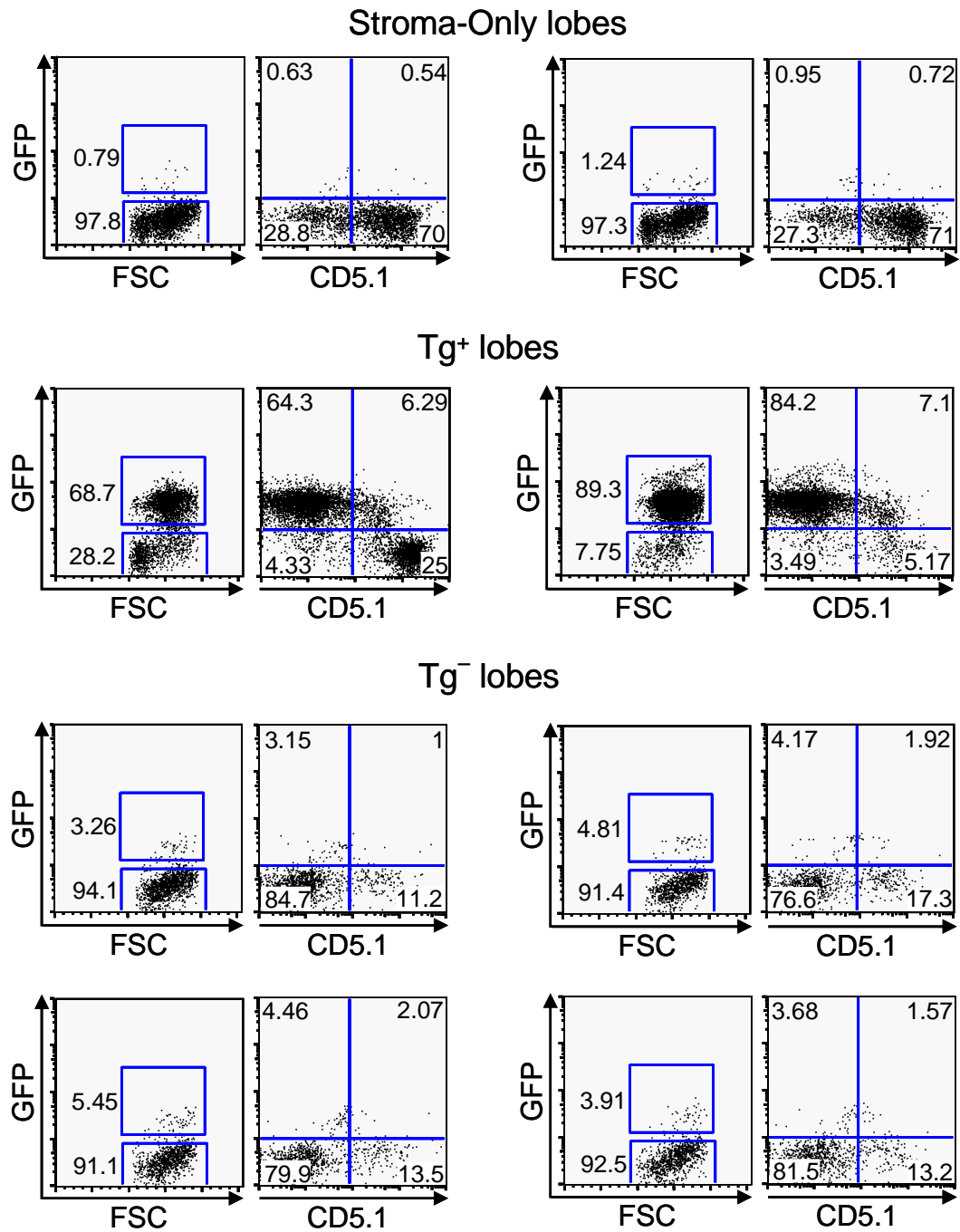


**Figure 4-11. Day 14 analysis of RgFTOC lobes for GFP expression and host contamination.** See next page for caption text.

**Figure 4-11 cont'd:** Each pair of panels represents an individual lobe with percentages for each gate indicated. Stroma-only lobes showed a large percentage of CD5.1<sup>+</sup> cells, indicating the presence of viable host thymocytes even after 2'-deoxyguanosine treatment. Some of these cells were also CD5.1<sup>-</sup> and may represent some of the CD5.1<sup>-</sup>/GFP<sup>-</sup> cells in Tg<sup>+</sup> lobes. The almost all CD5.1<sup>-</sup> cells were also in GFP<sup>+</sup> in Tg<sup>+</sup> lobes, suggesting that expression of the transgene was maintained once transcription was initiated. Conversely, most of the cells in the Tg<sup>-</sup> lobes remained GFP<sup>-</sup>, indicating that spontaneous transgene expression in DN3 or DN4 thymocytes that had not initiated transgene transcription was a rare event.

---

encoding of *gag*, *pol*, and *env* viral genes. These cells have equivalent GFP fluorescence but only an intermediate fluorescence for CD5.1, as compared to host cells. It is likely that these cells are a small portion of the GFP<sup>+</sup> transgenic cells that are staining slightly for CD5.1, possibly due to cross-reactivity.

Tg<sup>-</sup> lobes had a very small percentage of GFP<sup>+</sup> cells, a majority of which were CD5.1 intermediate. The GFP<sup>-</sup> population was mostly CD5.1<sup>-</sup>, but CD5.1<sup>+</sup> host-cell contamination was evident. The close grouping of the “GFP<sup>+</sup>” population at similar fluorescence values for both GFP and CD5.1 indicate a small population of autofluorescent cells, commonly found during RgFTOC analysis (G. Hernandez Hoyos, personal communication). It is likely that these cells do not express GFP or CD5.1, but are broadly autofluorescent. Those few cells that are not in this population could possibly be GFP<sup>+</sup>, indicating that cells initially sorted as GFP<sup>-</sup> had started expressing GFP. Very few cells exhibit this, however, and may be examples of cells that were

sorted but had not yet initiated expression directed by the Lck proximal promoter.

It can be concluded from this experiment that transgene expression is variegated, but relatively stable. The onset of expression is consistent with Lck proximal promoter-driven transgenes, although termination of expression is not, possibly due to the combination of multiple integration sites and the use of the minimal promoter. While the ratio of expressing to non-expressing cells varies from animal to animal and seems to correlate with transgene copy number, the site of integration is also important for transgene expression (L. Yang, personal communication) and likely variegation. An unforeseen advantage of variegation in transgene expression is the effective presence of a control population within each individual transgenic mouse. Those cells that did not initiate transgene expression should develop normally and can be analyzed alongside thymocytes that express the transgene.

#### **4.3.3 Analysis of dMek1 and ROG expression in transgenic mice**

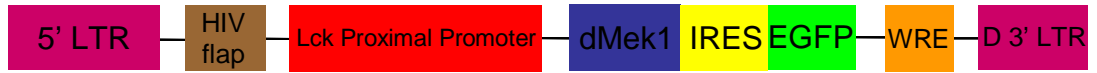
To distinguish thymocytes that had initiated transgene expression from those that had not, we added an internal ribosome entry site (IRES) followed by GFP downstream of the GOI in our lentiviral construct (Figure 4-12A). The IRES-GFP we used was the non-attenuated variant of the IRES derived from the mouse stem cell virus (MSCV) promoter-based vector MIG [21]. We have had much success using MIG in our laboratory for coexpression of GOIs and GFP in thymocytes as well as in murine cell lines [22, 23]. The advantage of this construct is the identification of GOI-expressing cells by flow cytometry. This was particularly important with this lentiviral system because of the variegated transgene expression. Identification of the transgene-

expressing population would be necessary to properly interpret results. The coexpression of GFP would allow us to easily identify transgene-expressing cells without having to perform intracellular staining, which would require us to kill the cells by fixation and permeabilization. That would limit our ability to do *ex-vivo* analysis of the transgene expressing cells.

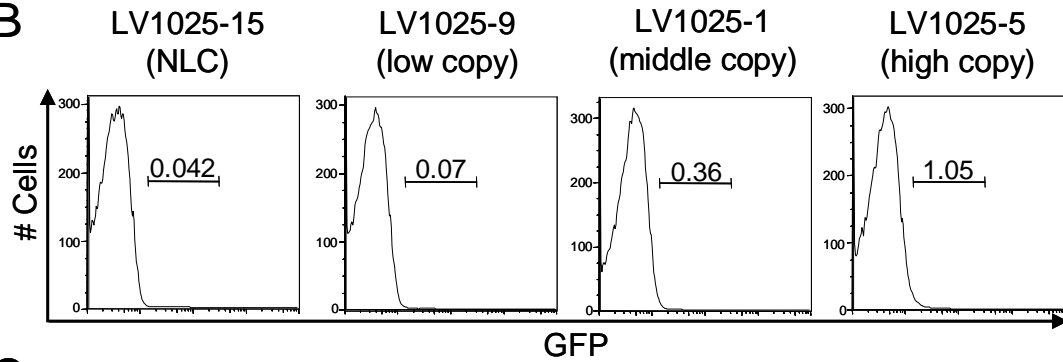
The titer of IRES-GFP-containing virus was approximately 10-fold less than that of FLckGW virus, as tested in 16610D9 cells (data not shown). As a result, infection of embryos was less efficient, and fewer integrations were apparent in transgenic mice that were infected with the IRES-containing construct. We used mice expressing the DO11.10 transgenic TCR, another MHC class II-restricted TCR, for these experiments because the AND<sup>+/+</sup>-Rag2<sup>0</sup> mice had not yet been bred. We infected DO11.10<sup>+</sup> mouse embryos with virus containing the FLP(dMek1)IGW construct (Figure 4-12A). Analysis of 4 FLP(dMek1)IGW mice with a differing number of integrations, as determined by southern blot (data not shown), revealed no discernable GFP<sup>+</sup> populations (Figure 4-12B). There was a slight increase in the “GFP<sup>+</sup>” gated population that correlated with an increase in copy number, but could very well be coincidental. An easily distinguishable GFP<sup>+</sup> population would be required to identify transgene-expressing cells, and it is likely that the IRES is somehow rendered non-functional, as seen with other IRES-containing lentiviral transgenics (L. Yang, personal communication).

We next examined the ability of PMA to stimulate Erk activation as an indirect measure of dMek1 repression (Figure 4-12C). Thymocytes were stimulated with 1 nM PMA for 10 minutes, and pErk level was determined by intracellular staining. Activation of Erk in mice positive for the lentiviral transgene was deficient in a manner correlating

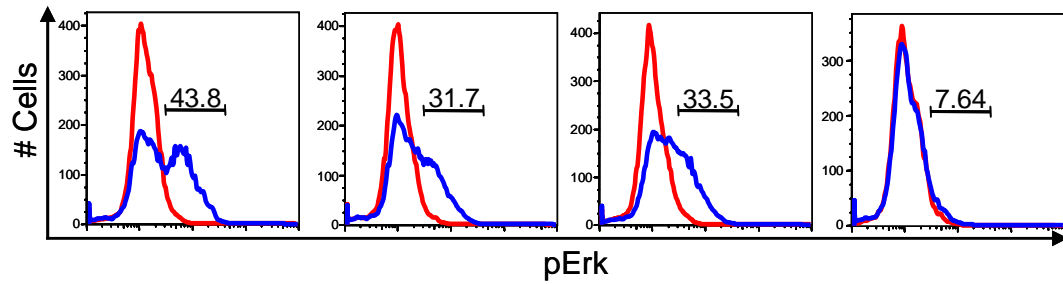
A



B



C



D

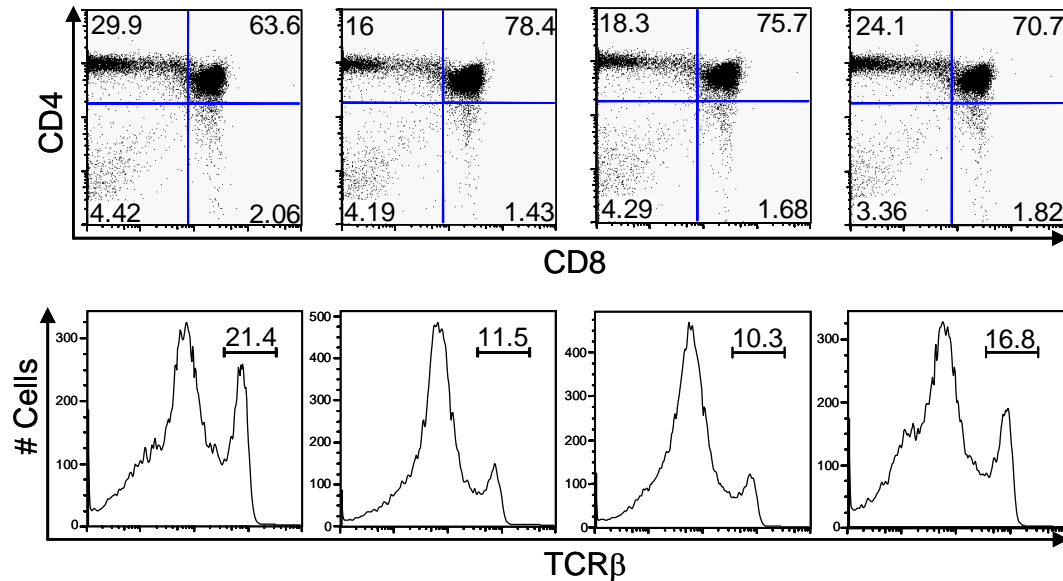


**Figure 4-12. Analysis of FLp(dMek1)IGW mice in a DO11.10 TCR background.**

See next page for caption text.

**Figure 4-12 cont'd:** A) The FLP(dMek1)IGW was derived from FLckGW, containing dMek1 followed by an IRES sequence upstream of GFP. B) GFP expression in transgenic was not detectable by flow cytometry, even with high transgene copy. C) Erk activation was impaired in mice positive for the dMek1 transgene and particularly pronounced in the highest copy mouse. D) Decreased percentages of SP populations, increased DP percentages, and decreased percentages of TCRb<sup>hi</sup> cells indicated impaired positive selection in transgene positive mice, indicative of dMek1 activity. There was no apparent increase in CD8 SPs at the expense of CD4 SPs, suggesting that dMek expression had no effect on lineage determination.

---

to gene copy number.

CD4/CD8 analysis of DO11.10<sup>+</sup> thymocytes from these mice revealed a reduction in positive selection, but no apparent increase in CD8<sup>+</sup> SP cells at the expense of the CD4<sup>+</sup> SP population that would be consistent with a change in lineage choice (Figure 4-12D). This may indicate that while disruption of the Erk MAPK pathway affects survival and maturation, as has been shown [24, 25], it does not play a significant role in CD4/CD8 lineage determination. This result may also be due to the DO11.10 TCR being a poor model for lineage decision studies, as seen in transgenic mice expressing a dominant negative form of Lck in a DO11.10 background that showed only a reduction in positive selection and no effect on lineage choice [26]. Should the latter be the case, it would be important to use a proven lineage choice model, such as the AND TCR [2], for these studies. It should also be noted that the mouse with the highest copy number, LV1025-5, showed the smallest deficiency in positive selection, which is not consistent

with having the highest dMek1 transgene expression.

Some of the data from this experiment revealed technical difficulties that should be pursued. There is no apparent GFP expression off of the IRES sequence from within the lentiviral RNA transcript, and thus we were unable to use GFP fluorescence to identify the cells that were expressing dMek1 as well as the level of expression attained in those cells. The only indication we had was an indirect measure of dMek1 repression by activation of Erk with pharmacological stimulation. Intracellular staining of Mek is not efficient and not a viable option for determining transgene expressing cells (Figure 4-13A). We have produced a dMek1 construct with an N-terminal FLAG-tag and have successfully detected the epitope with intracellular staining using an  $\alpha$ -FLAG antibody (Figure 4-13B). In this manner we will be able to identify transgene-expressing cells, although this will limit our ability to use transgenic cells for *ex vivo* analysis because we must fix and permeabilize the cells for analysis. Conditions for staining, however, have already been optimized as discussed in Chapter 2.

The results from the dMek1-expressing transgenics indicate the possibility that the Erk MAPK pathway does not play a role in lineage determination, but experiments performed thus far are not conclusive. We attempted to address this issue with a better candidate for lineage-decision involvement, Repressor of GATA (ROG) [27]. Our laboratory has recently shown the involvement of the GATA-3 transcription factor in the promotion of CD4<sup>+</sup> lineage choice [23]. As its name implies, ROG is involved in GATA-3 repression and curbs the action of GATA transcription family members if overexpressed [23, 27]. Transgenic mice were generated with a construct containing ROG (FLp(ROG)IGW) in the DO11.10 TCR background. CD4/CD8 analysis of ROG

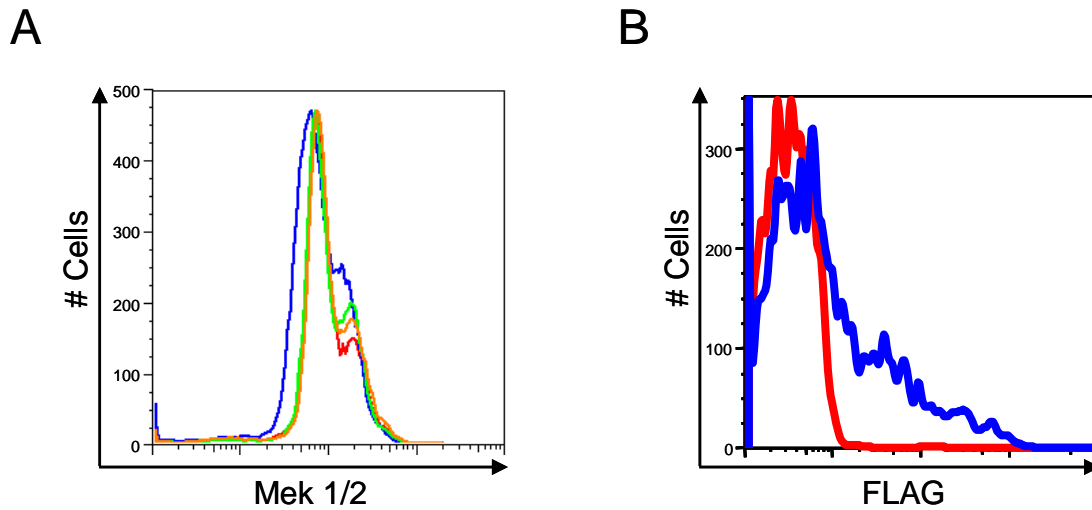


**Figure 4-13. FLAG-tagged proteins are detectable with intracellular staining, whereas Mek 1/2 are not.** A)  $\alpha$ -Mek 1/2 staining of thymocytes from dMek1-positive transgenic mice is ineffective at distinguishing transgene expressing cells. B) HEK-293 cells transfected with FLAG-tagged dMek1 are distinguishable by intracellular staining with an  $\alpha$ -FLAG antibody when compared to an untransfected population.

mice showed no change in lineage decision (Figure 4-14). As with the dMek1 mice, we were unable to see GFP expression and we did not have a working protocol for ROG intracellular staining (data not shown).

Failure to demonstrate any change in lineage determination with these two transgenic systems may be due to a technical difficulty in our approach. It is possible that the DO11.10 TCR background is inadequate for these types of studies. It is also imperative in future studies to be able to distinguish transgene-positive and transgene-negative populations in order to appropriately analyze effect on lineage determination. While co-expression of GFP or any reporter off an IRES sequence does not seem to be plausible, we can most likely overcome this problem by intracellular staining of either the transgenic protein directly or an N-terminal FLAG-tag integrated into the transgene sequence.

#### **4.3.4 Establishing AND<sup>+/+</sup>-Rag2 KO mouse line**

AND<sup>+/+</sup>-Rag2<sup>0</sup> mice are no longer available for purchase, so we decided to establish the line through breeding. To establish this line, we had to cross AND homozygotes and Basel-Rag2 null lines. 6 AND<sup>+/+</sup> males were purchased from The Jackson Laboratory (B10.Cg-Tg(TcrAND)53Hed/J), and each was mated with 2 Basel-Rag2<sup>0</sup> females. The resulting AND<sup>+/-</sup>-Rag2<sup>+/-</sup> F1 progeny were back-crossed with Basel-Rag2<sup>0</sup>, taking care not to mate offspring from the same parental mating pair. Initial screening of the F2 generations was done by tail bleed. At the time of weaning (3-4 weeks post-natal), each mouse had its tail cut, and 5-7 drops of blood were added to 500 $\mu$ l of 1X PBS supplemented with heparin. Blood cells were stained with fluorescent

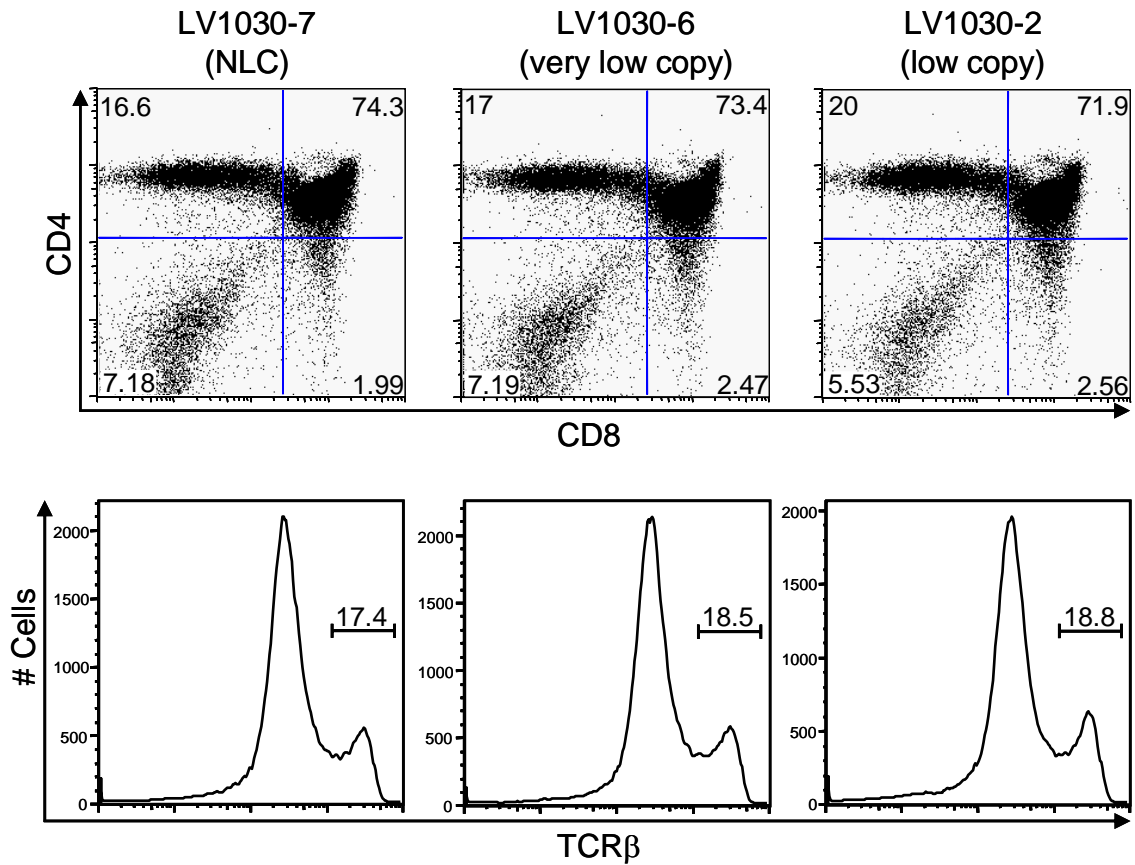


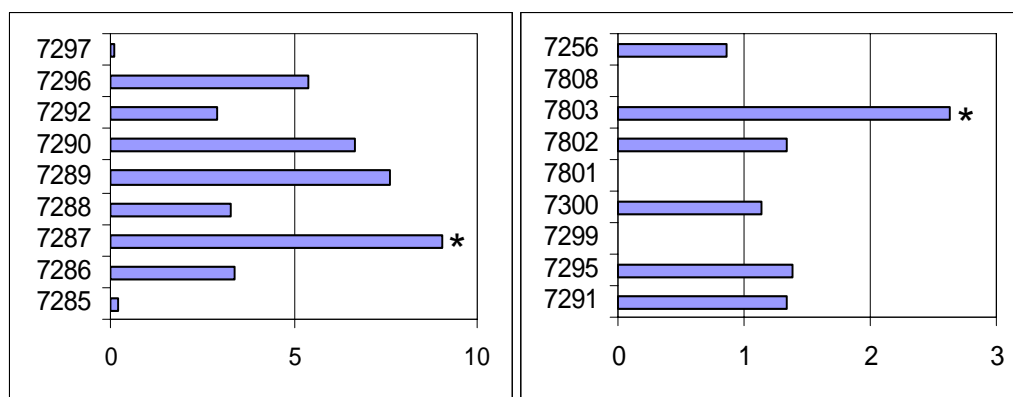
**Figure 4-14. Mice positive for the ROG transgene showed slight enhancement of both the CD4 and CD8 lineages.** A) Mice positive for the ROG transgene had slight increases in both CD4 and CD8 SP percentages, inconsistent with previous data that ROG reduced CD4 development. The percentage of TCRb<sup>hi</sup> was also slightly increased in ROG-Tg<sup>+</sup> mice. There was no apparent bias toward the CD8 lineage consistent with a change in lineage determination. Relative copy numbers were determined by southern blot prior to analysis.

antibodies for the AND transgenic TCR and for B220, a B-cell marker. The latter staining was done to detect the presence of B-cells, which would be indicative of a viable copy of the Rag2 gene.

Stained blood cells were analyzed by flow cytometry. Mice positive for the AND TCR and negative for a B220<sup>+</sup> population were kept for further breeding. All others were culled. These mice were fixed for Rag2<sup>0</sup> locus and heterozygous for the AND TCR. We mated these mice to each other in order to obtain AND TCR homozygotes. Offspring were screened by tail bleeds as above, and 1 cm of tail tissue was collected and frozen for later analysis. All mice were B220<sup>-</sup>, confirming that the Rag2<sup>0</sup> had been fixed. Those mice that were AND<sup>-</sup> by blood screening were culled. Mice that were positive for the AND TCR were analyzed further by Southern blot of genomic DNA extracted from tail tissue mentioned above.

Southern blots were probed with DNA probes specific for the AND TCR transgene and Ets1 as a background loading control. Data was obtained by densitometry of the AND and Ets1 bands and the AND signal was normalized to the Ets1 loading control (Figure 4-15A). The normalized AND signals were compared to select candidates for homozygosity. We expected that mice with two copies of the transgene would have approximately twice the normalized signal of heterozygous mice. We found that several mice had significantly more signal than the others. We chose these as homozygous candidates and used two males in a test-cross to validate that mice with double the signal were indeed homozygous. To speed up our analysis, we decided to sacrifice pregnant females at E12 and harvest and analyze the embryos, rather than wait until they were born and old enough to obtain tissue without having to sacrifice

A



B

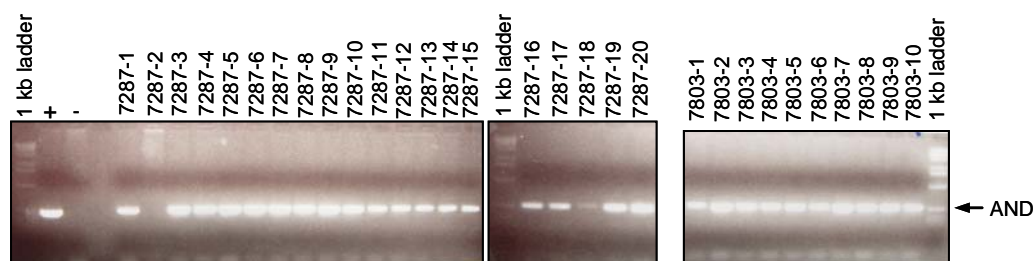


**Figure 4-15. Determination of homozygosity of the AND TCR gene in AND/Rag2<sup>0</sup> mice.** A) Signal from an AND southern analysis was quantitated and normalized to Ets1. Each panel is representative of samples from a single gel. Males with the strongest signal, 7287\* and 7803\*, were used for a test-cross with wild-type C57Bl/6 females. B) Genomic DNA was isolated from resultant test-cross embryos and PCR analysis was performed specifically for the AND TCR transgene. 19/20 embryos from the 7287 test-cross and 10/10 embryos from the 7803 test-cross were positive for the AND transgene. It is possible that one negative from the 7287 test-cross was a false negative due to the apparent absence of the primer band.

them. It is important to note that some of the embryos were not as developed as others, and their small size made them very difficult to harvest.

Embryos were harvested into individual wells of a 96-well plate and genomic DNA was extracted from each. These samples were analyzed by PCR for the AND TCR transgene (Figure 4-15B). 19 out of 20 of the progeny from the #7287 test-cross and 10 out of 10 of the progeny from the #7803 test-cross were positive. While one would expect all of the progeny to be positive by PCR if males #7287 and #7803 were truly homozygous for the AND TCR transgene, it is likely that the one negative sample was either a problem with the PCR reaction or that the “embryo” from that sample was actually maternal tissue harvested accidentally. Based on these results, we concluded that the males that were tested were homozygous for the AND TCR transgene and that mice with similar signal by southern blot were also homozygous. These mice were then used as founders for our AND<sup>+/+</sup>-Rag2<sup>0</sup> line.

#### **4.4 Future Directions**

We were unable to obtain clear results from the transgenic mice we produced. To truly get a sense of whether or not this system can work for our purposes our next step would be to recapitulate the experiment done with a dominant-negative form of Lck in the AND TCR background [2]. Should this be successful, it would not only reconfirm the results seen in that paper, but also show that this method of transgenesis is viable for studying lineage determination. This would, of course, hinge on the ability to stain for Lck by intracellular staining or would require the addition of a FLAG-tag to distinguish transgene-expressing cells.

Once it has been established that our system will work, we would then re-examine the involvement of dMek1 as well as dominant-negative Ras (dnRas). dnRas has been shown to have a more widespread effect on positive selection than dMek1 [25] and could present a bifurcation point for signals originating at the TCR. Transcription factor expression and regulation can also be explored, such as GATA family transcription factors and other factors known to be involved in positive selection [23, 28-30]. Such targets could include Ets family transcription factors, Egr1, Id3, and E-box proteins.

## **4.5 Concluding Remarks**

Our approach using lentiviral transgenesis to study gene dosage effects in transgenic mice could potentially be used as a time and money saving tool for creating and analyzing transgenics. That said, it is quite time and cost inefficient at its current stage and requires further optimizations. Still, the prospect of being able to potentially create a wide range of transgene expressors in a single litter is appealing, since creating many lines of mice by canonical transgenesis is time consuming and costly.

## **4.6 Materials and Methods**

### **4.6.1 Cell staining and flow cytometry**

Cell surface staining was performed in 100  $\mu$ l P4F for 15 minutes on ice. One million cells were resuspended in 50  $\mu$ l of P4F and 50  $\mu$ l of P4F containing indicated antibody. Antibodies were used at the following final concentrations:  $\alpha$ -CD8-APC at 1:100 (eBiosciences),  $\alpha$ -CD4-CyC at 1:200 (eBiosciences),  $\alpha$ -H-2Dd at 1:50 (BD

Pharmingen), and  $\alpha$ -CD5.1-PE at 1:200 (BD Pharmingen). Samples were spun at 500 x g for 3 minutes and washed twice with P4F. After the final wash, cells were resuspended in a minimum of 250  $\mu$ l of P4F and then transferred to FACS tubes. Flow cytometry was conducted on either a FACScalibur or a FACScan (Becton Dickinson) and analyzed using Flowjo software (TreeStar). Intracellular staining was performed as described in Chapter 2. All unlabeled axes are based on a log-scale relative fluorescence.

#### **4.6.2 Production of Lentivirus**

293T-HEK cells were plated on three 10 cm tissue culture dishes (Falcon) at a concentration of  $4 \times 10^6$  cells/dish in DMEM culture medium (Invitrogen). Cells were transfected by CaPO<sub>3</sub> precipitation 24 hours after initial plating with 4  $\mu$ g each of: 1) plasmid containing GOI (FlckGW, FLp(ROG)IGW, or FLp(dMek)IGW), 2) delta 8.9 plasmid, and 3) VSVg plasmid. Precipitates were removed after 4 hours, washed with 1 x PBS, and 10 ml fresh DMEM was added to each plate. Supernatants were collected after 48 hours, pooled together, and filtered through a 0.45  $\mu$ m syringe filter. Lentivirus was concentrated by ultracentrifugation by spinning samples at 4°C for 90 minutes at 25,000 rpm in a Beckman SW-28 rotor. Supernatant was carefully removed and 100  $\mu$ l of 1 x PBS was added to the pellet. Pellet was incubated overnight at 4°C, resuspended by pipetting, and supplied to the mouse facility for perivitteline injection of mouse embryos.

#### **4.6.3 Reaggregate fetal thymic organ culture**

Fetal thymic organ culture was performed as described [23]. Transgenic

thymocytes were sorted as GFP<sup>+</sup> and GFP<sup>-</sup> populations as indicated and lobes were reaggregated with these populations. Lobes were analyzed at 7 and 14 days post-reaggregation.

#### **4.6.4 Southern blotting of genomic DNA**

10µg of tail-derived genomic DNA was digested with 20 units (U) of Pst I for 2 hours at 37°C. An additional 20 U of Pst I was added to each reaction and incubated for 2 additional hours. Samples were loaded on a 0.8% agarose gel supplemented with 200ng/ml ethidium bromide and run at 50 volts overnight. Gels were visualized under ultraviolet light. Gels were treated with 0.25M HCl, followed by 0.4M NaOH and transferred to Hybond N<sup>+</sup> (Amersham) membrane by capillary transfer. Prehybridization was performed for 1 hour at 65°C in Church's buffer supplemented with 100µg/ml salmon sperm DNA. GFP-specific radiolabeled DNA probe was then added to the prehybridization buffer and incubated overnight at 65°C. Membranes were twice washed in 2x SSC buffer for 1 hour at 65°C and exposed to a phosphoscreen. Phosphoscreens were scanned on a Storm 860 (Molecular Dynamics) and analyzed using ImageQuant software.

#### **4.7 References**

1. Alberola-Ila J, Hernandez-Hoyos G: **The Ras/MAPK cascade and the control of positive selection.** *Immunol Rev* 2003, **191**:79-96.

2. Hernandez-Hoyos G, Sohn SJ, Rothenberg EV, Alberola-Ila J: **Lck activity controls CD4/CD8 T cell lineage commitment.** *Immunity* 2000, **12**(3):313-322.
3. Legname G, Seddon B, Lovatt M, Tomlinson P, Sarner N, Tolaini M, Williams K, Norton T, Kioussis D, Zamoyska R: **Inducible expression of a p56Lck transgene reveals a central role for Lck in the differentiation of CD4 SP thymocytes.** *Immunity* 2000, **12**(5):537-546.
4. Adachi S, Iwata M: **Duration of calcineurin and Erk signals regulates CD4/CD8 lineage commitment of thymocytes.** *Cell Immunol* 2002, **215**(1):45-53.
5. Sharp LL, Schwarz DA, Bott CM, Marshall CJ, Hedrick SM: **The influence of the MAPK pathway on T cell lineage commitment.** *Immunity* 1997, **7**(5):609-618.
6. Gordon JW, Scangos GA, Plotkin DJ, Barbosa JA, Ruddle FH: **Genetic transformation of mouse embryos by microinjection of purified DNA.** *Proc Natl Acad Sci U S A* 1980, **77**(12):7380-7384.
7. Wall RJ: **Pronuclear microinjection.** *Cloning Stem Cells* 2001, **3**(4):209-220.
8. Bednarik DP, Cook JA, Pitha PM: **Inactivation of the HIV LTR by DNA CpG methylation: evidence for a role in latency.** *Embo J* 1990, **9**(4):1157-1164.
9. Hoeben RC, Migchielsen AA, van der Jagt RC, van Ormondt H, van der Eb AJ: **Inactivation of the Moloney murine leukemia virus long terminal repeat in murine fibroblast cell lines is associated with methylation and dependent on its chromosomal position.** *J Virol* 1991, **65**(2):904-912.

10. Indraccolo S, Habeler W, Tisato V, Stievano L, Piovan E, Tosello V, Esposito G, Wagner R, Uberla K, Chieco-Bianchi L *et al*: **Gene transfer in ovarian cancer cells: a comparison between retroviral and lentiviral vectors**. *Cancer Res* 2002, **62**(21):6099-6107.
11. Pfeifer A, Ikawa M, Dayn Y, Verma IM: **Transgenesis by lentiviral vectors: lack of gene silencing in mammalian embryonic stem cells and preimplantation embryos**. *Proc Natl Acad Sci U S A* 2002, **99**(4):2140-2145.
12. Puthenveetil G, Scholes J, Carbonell D, Qureshi N, Xia P, Zeng L, Li S, Yu Y, Hiti AL, Yee JK *et al*: **Successful correction of the human beta-thalassemia major phenotype using a lentiviral vector**. *Blood* 2004, **104**(12):3445-3453.
13. Lois C, Hong EJ, Pease S, Brown EJ, Baltimore D: **Germline transmission and tissue-specific expression of transgenes delivered by lentiviral vectors**. *Science* 2002, **295**(5556):868-872.
14. Kaye J, Hsu ML, Sauron ME, Jameson SC, Gascoigne NR, Hedrick SM: **Selective development of CD4+ T cells in transgenic mice expressing a class II MHC-restricted antigen receptor**. *Nature* 1989, **341**(6244):746-749.
15. Goldrath AW, Hogquist KA, Bevan MJ: **CD8 lineage commitment in the absence of CD8**. *Immunity* 1997, **6**(5):633-642.
16. Matechak EO, Killeen N, Hedrick SM, Fowlkes BJ: **MHC class II-specific T cells can develop in the CD8 lineage when CD4 is absent**. *Immunity* 1996, **4**(4):337-347.

17. Wildin RS, Garvin AM, Pawar S, Lewis DB, Abraham KM, Forbush KA, Ziegler SF, Allen JM, Perlmutter RM: **Developmental regulation of lck gene expression in T lymphocytes.** *J Exp Med* 1991, **173**(2):383-393.
18. Garvin AM, Pawar S, Marth JD, Perlmutter RM: **Structure of the murine lck gene and its rearrangement in a murine lymphoma cell line.** *Mol Cell Biol* 1988, **8**(8):3058-3064.
19. Sohn SJ, Forbush KA, Nguyen N, Witthuhn B, Nosaka T, Ihle JN, Perlmutter RM: **Requirement for Jak3 in mature T cells: its role in regulation of T cell homeostasis.** *J Immunol* 1998, **160**(5):2130-2138.
20. Chaffin KE, Beals CR, Wilkie TM, Forbush KA, Simon MI, Perlmutter RM: **Dissection of thymocyte signaling pathways by in vivo expression of pertussis toxin ADP-ribosyltransferase.** *Embo J* 1990, **9**(12):3821-3829.
21. Cherry SR, Binischkiewicz D, van Parijs L, Baltimore D, Jaenisch R: **Retroviral expression in embryonic stem cells and hematopoietic stem cells.** *Mol Cell Biol* 2000, **20**(20):7419-7426.
22. Laurent MN, Ramirez DM, Alberola-Ila J: **Kinase suppressor of Ras couples Ras to the ERK cascade during T cell development.** *J Immunol* 2004, **173**(2):986-992.
23. Hernandez-Hoyos G, Anderson MK, Wang C, Rothenberg EV, Alberola-Ila J: **GATA-3 expression is controlled by TCR signals and regulates CD4/CD8 differentiation.** *Immunity* 2003, **19**(1):83-94.

24. Alberola-Ila J, Hogquist KA, Swan KA, Bevan MJ, Perlmutter RM: **Positive and negative selection invoke distinct signaling pathways.** *J Exp Med* 1996, **184**(1):9-18.
25. Alberola-Ila J, Forbush KA, Seger R, Krebs EG, Perlmutter RM: **Selective requirement for MAP kinase activation in thymocyte differentiation.** *Nature* 1995, **373**(6515):620-623.
26. Hashimoto K, Sohn SJ, Levin SD, Tada T, Perlmutter RM, Nakayama T: **Requirement for p56lck tyrosine kinase activation in T cell receptor-mediated thymic selection.** *J Exp Med* 1996, **184**(3):931-943.
27. Miaw SC, Choi A, Yu E, Kishikawa H, Ho IC: **ROG, repressor of GATA, regulates the expression of cytokine genes.** *Immunity* 2000, **12**(3):323-333.
28. Bain G, Murre C: **The role of E-proteins in B- and T-lymphocyte development.** *Semin Immunol* 1998, **10**(2):143-153.
29. Bettini M, Xi H, Milbrandt J, Kersh GJ: **Thymocyte development in early growth response gene 1-deficient mice.** *J Immunol* 2002, **169**(4):1713-1720.
30. Norton JD, Deed RW, Craggs G, Sablitzky F: **Id helix-loop-helix proteins in cell growth and differentiation.** *Trends Cell Biol* 1998, **8**(2):58-65.

## Chapter 5

# **A General Approach to Detect Protein Expression *In Vivo* Using Fluorescent Puromycin Conjugates**

This chapter has previously appeared as: Starck SR, Green HM, Alberola-Ila J, Roberts RW: **A general approach to detect protein expression in vivo using fluorescent puromycin conjugates.** *Chem Biol* 2004, **11(7)**:999-1008. The formatting of this paper has been adapted to this thesis, while content remains unchanged.

*H. M. Green's contribution to this paper is as follows: in conjunction with S. R. Starck, the design and execution of experiments contributing to Figures 5-4, 5-5, 5-6, and 5-7 as well as comments to the manuscript with regard to these experiments.*

### **5.1 Abstract**

Understanding the expression of known and unknown gene products represents one of the key challenges in the post-genomic world. Here, we have developed a new class of reagents to examine protein expression *in vivo* that does not require transfection,

radiolabeling, or the prior choice of a candidate gene. To do this, we constructed a series of puromycin conjugates bearing various fluorescent and biotin moieties. These compounds are readily incorporated into expressed protein products in cell lysates *in vitro* and efficiently cross cell membranes to function in protein synthesis *in vivo* as indicated by flow cytometry, selective enrichment studies, and western analysis. Overall, this work demonstrates that fluorescent-puromycin conjugates offer a general means to examine protein expression *in vivo*.

## 5.2 Introduction

Complete sequencing of the human genome [1, 2] shows that less than 50% of the putative gene transcripts correspond to known proteins. A complete understanding of the proteome awaits the identification of thousands of unassigned gene products and assignment of their role in signaling cascades [3], membrane trafficking [4], apoptosis [5], and other cellular processes. Currently, there are large-scale techniques to study cellular protein levels indirectly using DNA and mRNA arrays [6]. However, these techniques do not directly monitor the level of protein synthesis. Methods to directly monitor protein expression *in vivo* are extremely useful, particularly in the study of higher organisms with many different cell and tissue types.

Currently, protein expression is studied using pulse-labeling with a radioactive tracer or by transformation with fluorescent reporters based on the green fluorescent protein (GFP) and mutants (BFP, CFP, and YFP) [7]. Pulse-labeling experiments typically require the cell(s) to be destroyed and are not amenable to microscopy experiments with simultaneous protein synthesis detection. Genetically encoded GFP

mutants and fusion proteins have seen broad biological applications including study of  $\text{Ca}^{2+}$  localization [8], protein tyrosine kinase activity [9], and mRNA trafficking and protein synthesis localization in cultured neurons [10, 11]. However, the use of GFP-based constructs is limited to cells that can be efficiently transfected. Additionally, DNA transfection protocols often require several days to produce cells yielding robust GFP-based fluorescent signals and also inundate the protein synthesis machinery with a non-native transcript due to the use of strong upstream promoters. Finally, transfection-based strategies generally require choice of a particular candidate gene product.

We reasoned that puromycin-based reagents might provide a general means to examine protein expression. Puromycin is a structural analogue of aminoacylated-tRNA (aa-tRNA) and participates in peptide-bond formation with the nascent polypeptide chain (Figure 5-1A) [12, 13]. Previously, various puromycin derivatives of the form X-dC-puromycin have been examined and shown to be functional during *in vitro* translation experiments [14-17]. In principle, a fluorescent or biotinylated variant of puromycin should be functional in protein synthesis *in vivo* if it is able to enter cells in a non-destructive fashion (Figure 5-1B). In this way, selective labeling of newly synthesized proteins would enable direct monitoring of protein expression and provide the potential for both spatial and temporal resolution. Here, we demonstrate that a variety of puromycin conjugates can be used as detectors of protein synthesis in live cells. This work shows that puromycin conjugates can easily enter cells and covalently label newly synthesized proteins, enabling direct detection of protein expression *in vivo*.

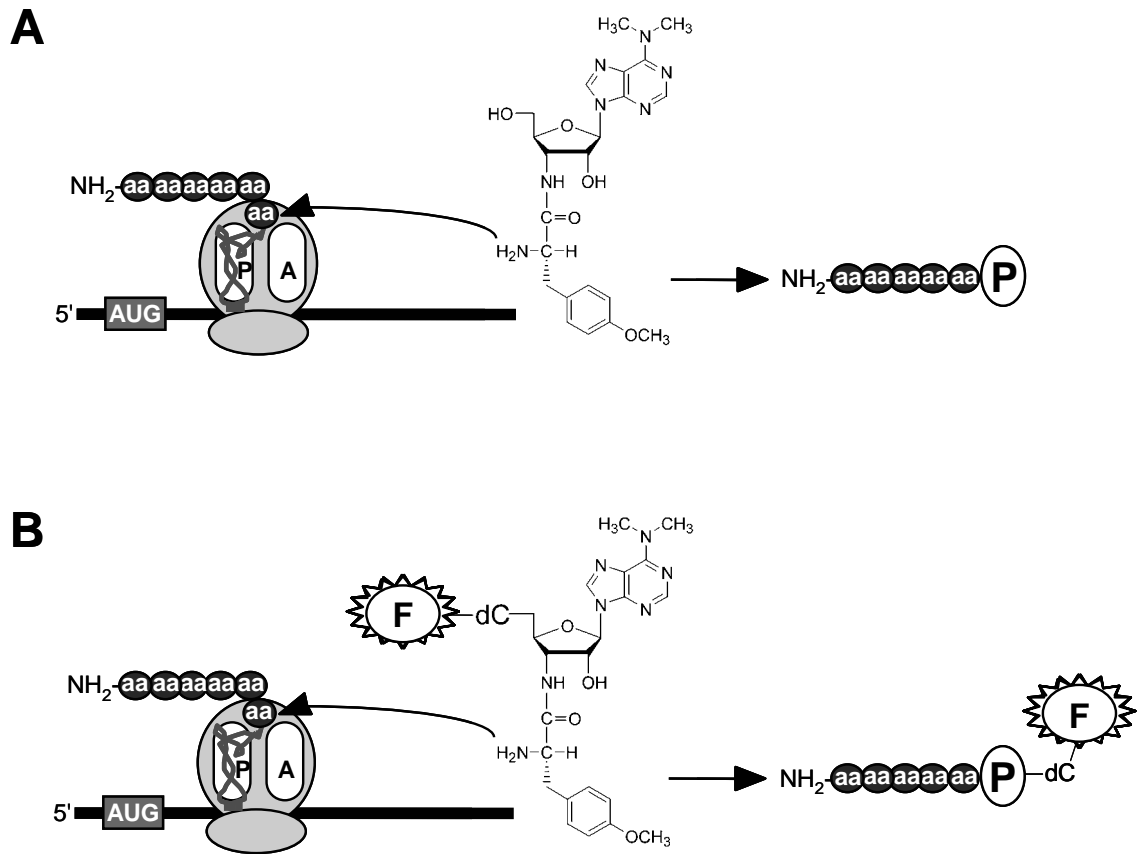


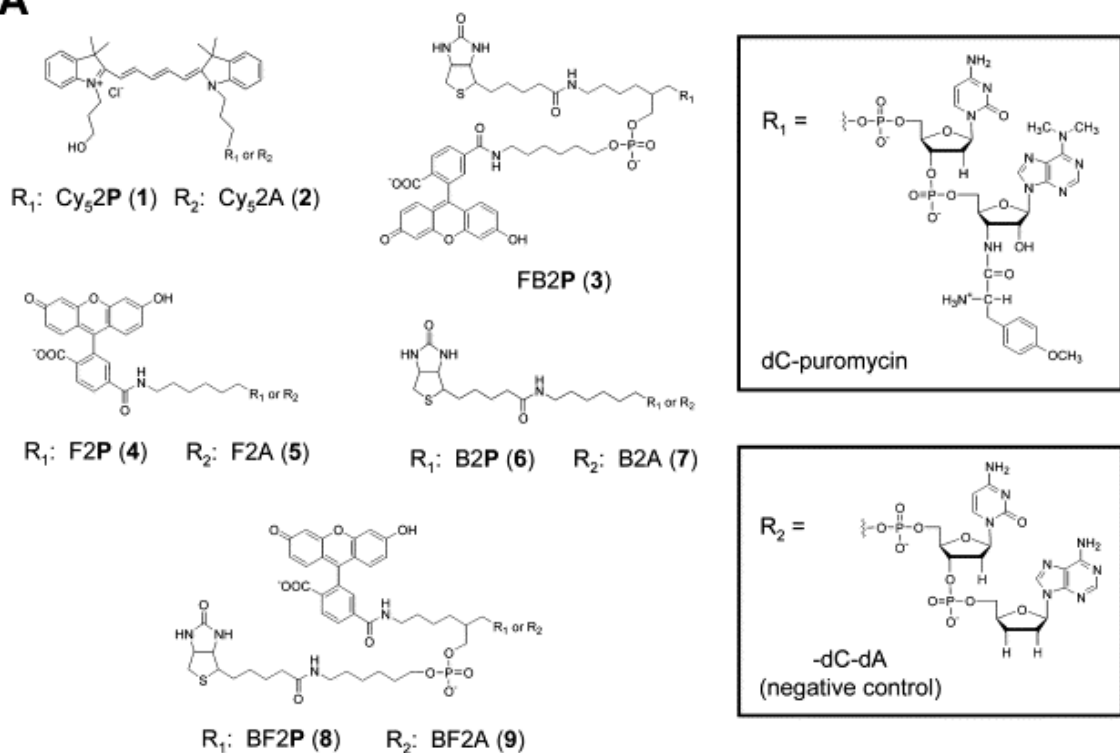
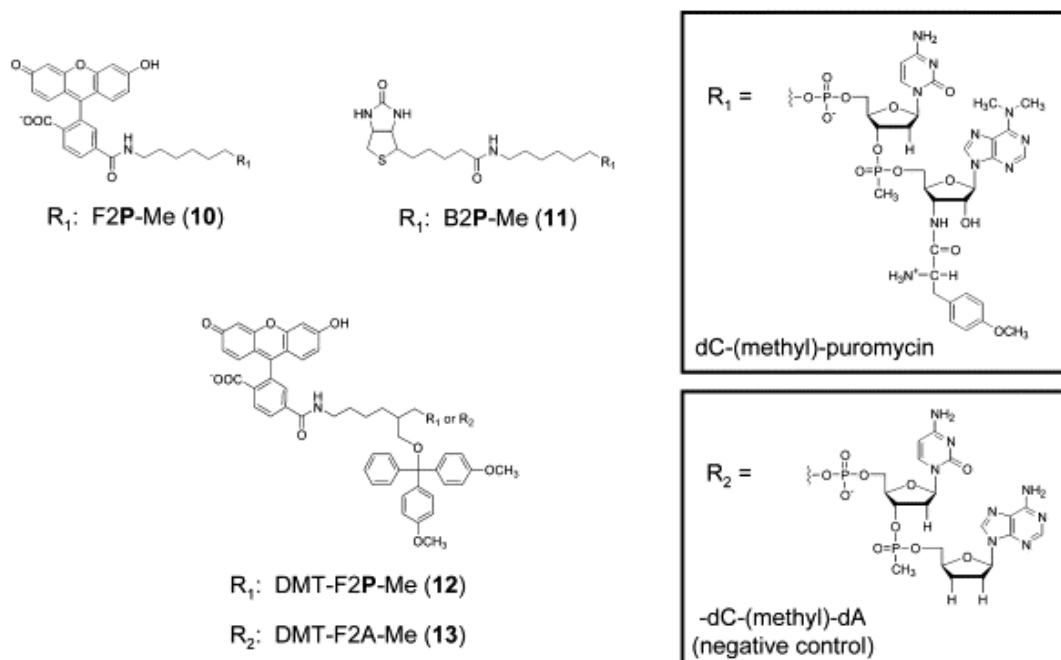
**Figure 5-1.** (A) Puromycin (**P**) participates in peptide bond formation with the nascent polypeptide chain. (B) Puromycin-dye conjugates, of the form X-dC-puromycin where X = fluorescein (**F**), are also active in translation and become covalently linked to protein.

## 5.3 Results

### 5.3.1 Design of puromycin conjugates

To label newly synthesized proteins, our puromycin conjugates would have to satisfy three general criteria: 1) functionality in peptide bond formation, 2) cell permeability, and 3) ready detection in a cellular or biochemical context. In addressing the first issue, it had been previously shown that puromycin derivatives bearing substitutions directly off the 5' OH functioned poorly *in vitro* (e.g., biotin-puromycin  $IC_{50} = 54 \mu\text{M}$ ) [17], whereas conjugates with the general form X-dC-puromycin (e.g., biotin-dC-puromycin) were substantially more effective ( $IC_{50} = 11 \mu\text{M}$ ) [17]. We therefore chose to design molecules by varying the substituents appended to dC-puromycin (Figure 5-2A).

In order to facilitate cellular entry and detection, we considered a number of factors including: 1) type and position of the label, 2) the linker between the label and dC-puromycin, 3) background fluorescence properties, and 4) membrane permeability including net charge and hydrophobicity. We then designed and synthesized various dC-puromycin conjugates to address these issues systematically. The first series of puromycin conjugates (**1**, **3**, **4**, **6**, **8**; Figure 5-2A) either contain fluorescent dyes (compounds **1** and **4**), biotin (compound **6**), or both (compounds **3** and **8**). Two different fluorescent dyes were utilized (Cy<sub>5</sub> and fluorescein) to provide detection at a range of emissions. Biotin labels were introduced to enable detection via western blot analysis or affinity purification. We also prepared a series of compounds (**2**, **5**, **7**, **9**; Figure 5-2A), which lack the 3'-amino acid moiety to serve as negative controls.

**A****B**

**Figure 5-2.** (A) Structure of puromycin conjugates and negative control conjugates. (B) Structure of phosphonate-based puromycin and negative control conjugates.

A second series of conjugates with a phosphonate linkage between dC and puromycin was prepared to examine whether reduction of charge would enhance cell membrane solubility and facilitate cellular entry (Figure 5-2B). Three compounds (**10**, **11**, **12**; Figure 5-2B) were constructed bearing fluorescein (**10**, F2P-Me), biotin (**11**, B2P-Me), or the hydrophobic dimethoxytrityl group (DMT) and fluorescein (**12**, DMT-F2P-Me). A DMT-bearing fluorescein-dC-dA conjugate (DMT-F2A-Me) served as a negative control (**13**; Figure 5-2B). The DMT group was added to gauge whether the addition of a hydrophobic group would further enhance entry into cells.

### 5.3.2 Analysis of puromycin-conjugate activity *in vitro*

We began our analysis by examining the activity of each of our conjugates *in vitro* for their ability to inhibit protein translation. Previously, we had used this activity assay to measure the IC<sub>50</sub> for various puromycin conjugates [17] and analogues [18], as well as demonstrate a direct relationship between the IC<sub>50</sub> and the efficiency of protein labeling [17]. High resolution tricine-SDS gel data corresponding to a typical IC<sub>50</sub> determination is shown for Cy<sub>5</sub>2P (**1**) and Cy<sub>5</sub>2A (**2**) (Figure 5-3A). Using this approach, we measured IC<sub>50</sub> values for the compounds in Figure 5-2A and 5-2B (Figure 5-3B). Generally, the activity of conjugates with the form X-dC-puromycin falls over a fairly narrow range *in vitro*, with IC<sub>50</sub> values ranging from ~4 to ~30 μM (Table 1). Also, control conjugates that lack the amino acid moiety, e.g., Cy<sub>5</sub>2A (**2**) and BF2A (**9**), show little ability to inhibit protein synthesis even at high concentrations.

We next wished to confirm that our puromycin conjugates could become covalently attached to protein *in vitro*. To do this, we translated globin mRNA in the

presence of increasing concentrations of FB2P (**3**), a conjugate containing fluorescein and biotin moieties (Figure 5-3C). Next, the concentration-dependent incorporation of FB2P was analyzed using neutravidin affinity chromatography of these same translation reactions (Figure 5-3D). These data indicate that puromycin conjugates are incorporated efficiently over a broad concentration range ranging from 2- to 3-fold below the  $IC_{50}$  to well above it. Thus labeling is possible even at concentrations where protein synthesis is not greatly inhibited.

These observations support the development of a broad range of puromycin-based reagents for two reasons. First, compounds of the form X-dC-puromycin appear tolerant to a wide variety of substitutions, including molecules containing more than one detection handle (e.g., BF2P and FB2P). Interestingly, even the methyl phosphonate versions (F2P-Me, **10**; B2P-Me, **11**; DMT-F2P-Me, **12**) showed good levels of *in vitro* activity. Second, the  $IC_{50}$  values indicate that even modest concentrations of each of these reagents in the low micromolar range will be sufficient to achieve good levels of protein labeling. This is because our data here (Table 1, Figure 5-3), as well as previous data [17, 18], demonstrate that protein labeling is achieved at or below the  $IC_{50}$  value. Thus, these *in vitro* translation and protein labeling assays provide a starting concentration range for analysis in live cells.

### **5.3.3 Analysis of puromycin-conjugate activity *in vivo***

In order to analyze the activity of puromycin conjugates *in vivo*, we needed to choose both an appropriate cell line and an appropriate quantitation and detection scheme. While microscopy is a powerful means to analyze individual cells and small

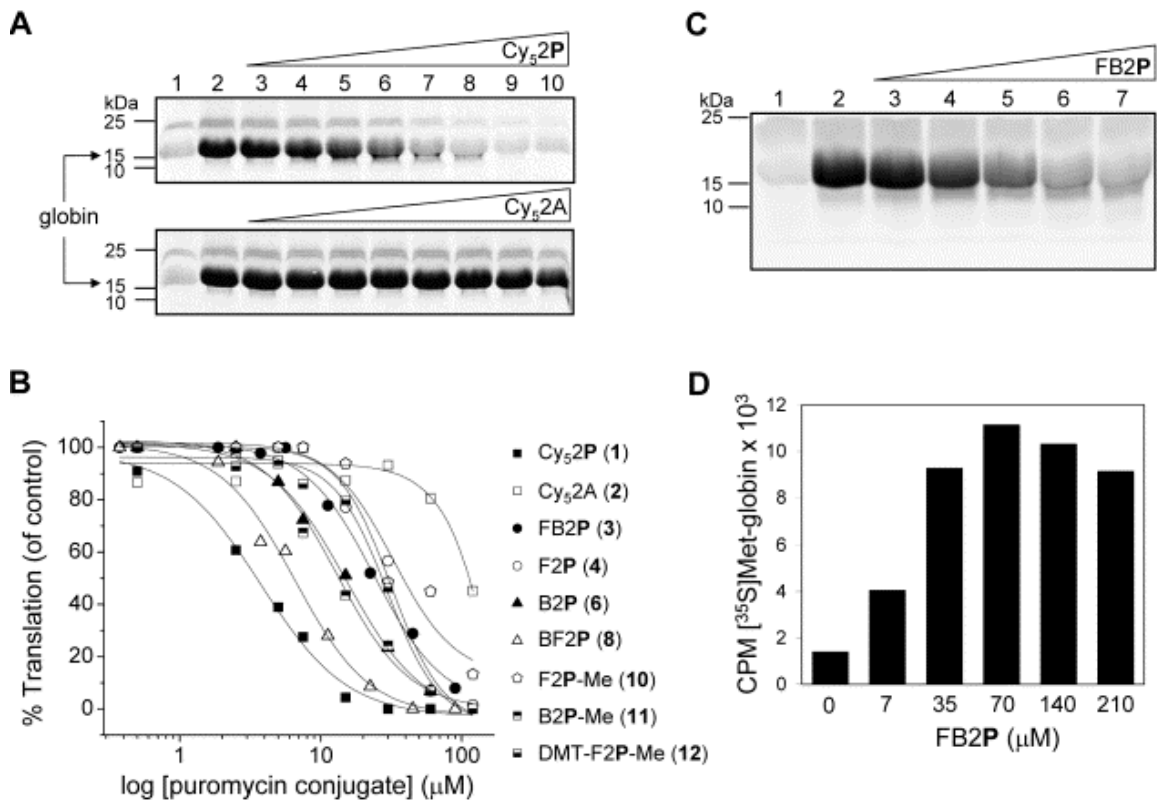


**Figure 5-3.** *In vitro* activity analysis for various puromycin conjugates. (A) Tricine-SDS-PAGE analysis of globin translation reactions in the presence of Cy<sub>5</sub>2P (1) (top) and Cy<sub>5</sub>2A (2) (bottom): Lane 1, no template and no conjugate; lane 2, globin alone; lanes 3-10, conjugate concentrations from 0.5 μM to 120 μM. (B) Percent of globin translation relative to the no conjugate control for compounds 1, 2, 3, 4, 6, 8, 10, 11, and 12. (C) Tricine-SDS-PAGE analysis of globin translation reactions incubated with increasing concentrations of FB2P (3): Lane 1, no template, no conjugate; lane 2, globin alone; lane 3, 7 μM; lane 4, 35 μM; lane 5, 70 μM; lane 6, 140 μM; and lane 7, 210 μM. (D) Neutravidin-purified globin-FB2P complexes from translation reactions in (C).

**Table 5-1. The concentration of puromycin conjugate required for 50% inhibition of globin translation (IC<sub>50</sub>).\***

Puromycin conjugate	IC <sub>50</sub> (μM)
(1) <b>Cy<sub>5</sub>2P</b>	<b>3.8</b>
(2) <b>Cy<sub>5</sub>2A</b>	<b>&gt;100</b>
(3) <b>FB2P</b>	<b>24</b>
(4) <b>F2P</b>	<b>22</b>
(6) <b>B2P</b>	<b>15</b>
(8) <b>BF2P</b>	<b>5.8</b>
(10) <b>F2P-Me</b>	<b>25</b>
(11) <b>B2P-Me</b>	<b>16</b>
(12) <b>DMT-F2P-Me</b>	<b>29</b>

**\*In replicate experiments, the standard error is <5%.**

sections of tissue, we wished to perform experiments where thousands to millions of cells could be examined for protein labeling. We therefore chose flow cytometry as our primary means to analyze uptake and incorporation of our conjugates. In addition to providing a quantitative measure of fluorescence and cell size, flow cytometry methods enable live cells and dead cells to be readily distinguished [19]. We chose the mammalian thymocyte D9 cell line (16610D9) [20] for our experiment for four reasons: 1) they have relatively uniform size and shape, 2) they do not aggregate, making single cell detection possible, 3) they are suspension cells, which allow for ready growth in culture with subsequent acquisition of a large number of single cell readings using flow

cytometry, and 4) they are amenable to routine infection techniques to introduce selectable markers and GFP-based tags.

We began by comparing the concentration and time dependence of labeling with **F2P (4)** and the negative control conjugate **F2A (5)** (Figure 5-4A,B). For **F2P**, progressively increased fluorescence is seen with increasing time and the greatest enhancement is seen after the 24 h incubation at both 5  $\mu$ M and 25  $\mu$ M of the conjugate (Figure 5-4A,B). At both concentrations, a substantial population of live cells is detected and demonstrates up to 4-fold enhanced fluorescence relative to the **F2A** control molecule. Longer incubation (48 hours) in the presence of **F2P** eventually kills the majority of cells at both concentrations tested. In contrast, the background fluorescence from **F2A** reaches a maximum of  $\sim 10^1$  units after a 7 h incubation for both 5 and 25  $\mu$ M incubations (Figure 5-4A,B), and **F2A** has no apparent effect on cell viability. The fluorescence enhancement beyond  $10^1$  units for cells treated with **F2P** is consistent with C-terminal protein labeling by the fluorescein-puromycin conjugate. These experiments also suggest that there is an optimum concentration and incubation time for labeling expressed proteins without killing the cells.

We next wanted to examine the relative level of fluorescence enhancement for a series of conjugates. To do this, a uniform population of D9 cells was split into separate containers, each containing identical concentrations of a different puromycin conjugate, incubated for 24 hours, and analyzed by flow cytometry with a live-cell gate as before (Figure 5-4C). In this series, **DMT-F2P-Me (12)** gives the strongest enhancement, and the rank order of compounds follows **DMT-F2P-Me (12)** > **FB2P (3)**  $\sim$  **BF2P (8)** > **F2P (4)**  $\sim$  **F2P-Me (10)** > **FP**. The  $IC_{50}$  values for all the compounds with the exception of **FP**

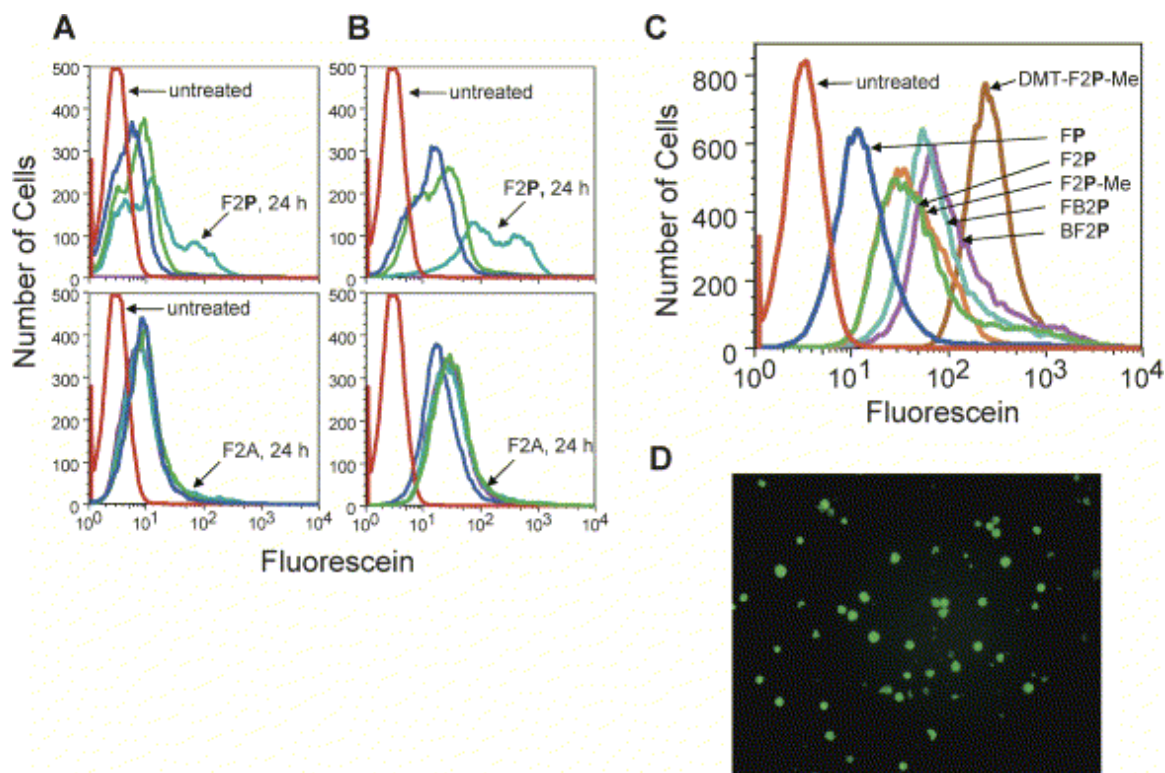


**Figure 5-4.** Analysis of puromycin conjugate activity in 16610D9 thymocyte cells. Dose-response analysis of 16610D9 thymocyte cells treated with F2P or F2A at (A) 5  $\mu\text{M}$  and (B) 25  $\mu\text{M}$ . Incubation times are 1 (■), 7 (■), 24 (■), and 48 h (■). Untreated cells incubated for 1h are indicated with (■). Cells were analyzed using a flow cytometer and gated on a live cell population according to forward and side scatter plots. (C) Flow cytometry analysis of untreated cells (■); Fluorescein-puromycin, FP (■); F2P, 4 (■); F2P-Me, 10 (■); FB2P, 1 (■); BF2P, 8 (■); DMT-F2P-Me, 12 (■). Cells were incubated for 24 hour with puromycin conjugates at 50  $\mu\text{M}$ . Analysis was performed using flow cytometry using a live cell gate as in A and B. (D) Epi-fluorescence microscopy of D9 cells treated with DMT-F2P-Me (25  $\mu\text{M}$ ) with 200 X magnification.

(IC<sub>50</sub> = 120 μM [17]) are relatively similar, while addition of the DMT group in compound (**12**) would be expected to confer increased hydrophobicity and membrane permeability. Compounds containing a phosphate (F2P (**4**)) or a methylphosphonate (F2P-Me (**10**)) bridging the puromycin and dC residue show little difference in IC<sub>50</sub> values (Figure 5-3B, Table 1) and *in vivo* labeling (Figure 5-4C), arguing that charge at this position does not play a key role in either the activity as a substrate or entry into the cell. The poor IC<sub>50</sub> for FP *in vitro* [17] correlates with the small fluorescence enhancement seen for this compound *in vivo* (Figure 5-4C). Epi-fluorescence microscopy confirms that the conjugate DMT-F2P-Me (**12**) readily enters and labels D9 cells brightly (Figure 5-4D).

Following these experiments, we next wished to confirm that two of the best compounds, BF2P (**8**) and DMT-F2P-Me (**12**), also showed fluorescence enhancement *in vivo* relative to control molecules containing only a terminal adenosine. Indeed, comparison of cells treated with BF2P (**8**) versus BF2A (**9**) (Figure 5-5A) and DMT-F2P-Me (**12**) versus DMT-F2A-Me (**13**) (Figure 5-5B) indicates that compounds bearing the terminal puromycin moiety show a 3- to 4-fold fluorescence enhancement as compared with the control molecules. This shift in fluorescence is consistent with labeling protein during rounds of translation. Overall, the combination of our *in vitro* and *in vivo* observations is consistent with the notion that the overall fluorescence enhancement reflects both the efficacy and the cellular permeability of the compounds.

#### 5.3.4 Mechanism of puromycin conjugate activity *in vivo*

We next wished to demonstrate that the puromycin conjugates we had constructed

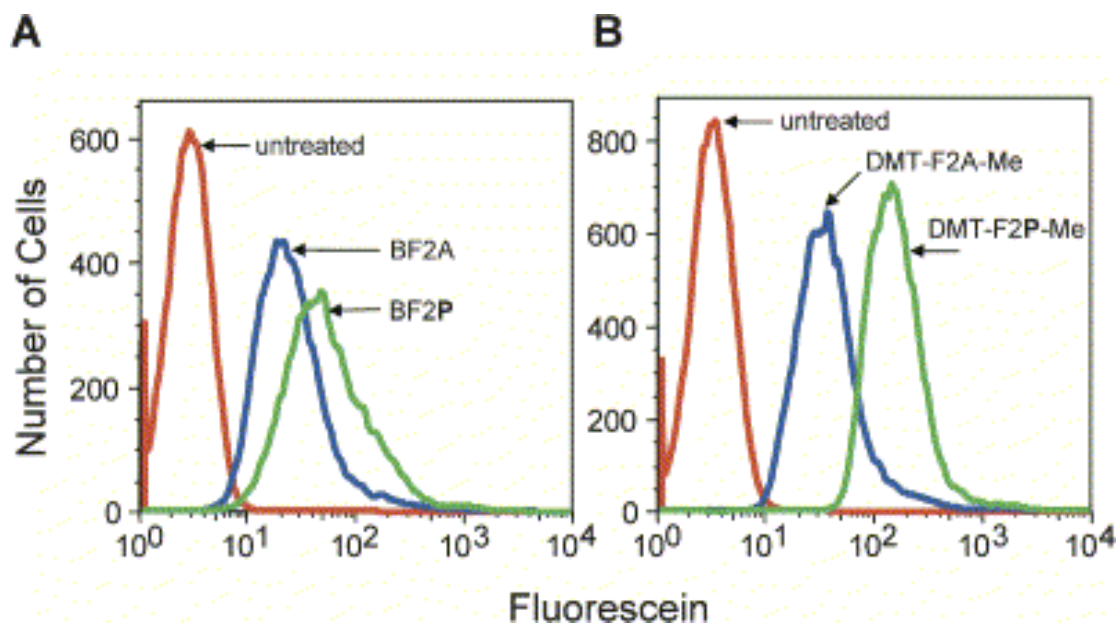


**Figure 5-5.** Fluorescence shift analysis for puromycin conjugates versus negative control molecules in 16610D9 thymocyte cells. (A) Untreated cells (■); BF2A, **9** (■); BF2P, **8** (■). (B) Untreated cells (■); DMT-F2A-Me, **13** (■); DMT-F2P-Me, **12** (■). Analysis was performed using flow cytometry using a live cell gate as described for Figure 5.

were acting *in vivo* by the same mechanism as puromycin itself. Puromycin can be used as a selection agent in mammalian cell culture to kill cells that lack the resistance gene encoding puromycin *N*-acetyl-transferase (PAC) [21]. This enzyme *N*-acetylates the reactive amine on puromycin and blocks its ability to participate in peptide bond formation [22, 23]. In a mixed population of cells, those that lack a vector expressing PAC can be selectively killed by long incubations ( $\geq 48$  hours) with puromycin, leaving only vector-containing cells alive. Previously, we showed that chemical acylation inactivates puromycin-mediated translation inhibition *in vitro* [17]. Thus, we wished to see if the D9 cells bearing PAC would be resistant to killing (and thus enriched in the mixed population) by long incubations with puromycin itself or our puromycin conjugates *in vivo*.

Foreign genes can be inserted into D9 cells by infection with a viral vector (see Experimental Procedures). Vectors that express GFP provide a straightforward means to measure the fraction of cells that become infected and a direct means to monitor any vector-mediated enrichment. We infected D9 cells with a viral vector driven by a mouse stem cell virus promoter (MSCV) containing an internal ribosome entry site (IRES) upstream from enhanced green fluorescent protein (EGFP) referred to as MIG (MIG = **MSCV-IRES-GFP**; Figure 5-6) [24]. MIG expresses GFP so that infection efficiency can be monitored by GFP fluorescence (Figure 5-6). A second vector containing the PAC gene was also constructed (MIG<sub>PAC</sub>; Figure 5-6) and results in a bicistronic mRNA in which both PAC and GFP can be translated (Figure 5-6).

Flow cytometry was used to examine both the infection efficiency and confirm the ability to perform puromycin-based enrichment. After infection with the MIG or

MIG<sub>PAC</sub> vectors, 5.0 % and 4.3 % of the D9 cells were infected and alive based on GFP expression, respectively (Figure 5-6B; upper panels). In both cases, the other 95% of the cells showed no GFP-based signal. Puromycin was then added to both MIG and MIG<sub>PAC</sub> infected cells followed by incubation for 48 hours at 37°C. For MIG infected cells, puromycin results in almost complete killing of both GFP-positive and GFP-negative cells (Figure 5-6B; lower, left panel). For MIG<sub>PAC</sub> infected cells, puromycin selectively kills only those cells lacking GFP, such that after 48 hours the population is totally dominated by GFP-positive cells (94%) (Figure 5-6B; lower, right panel). Enrichment of GFP-positive cells occurs because they express the PAC resistance protein that acylates puromycin, rendering it inactive. These experiments demonstrate that puromycin acylation is sufficient to rescue cells from puromycin toxicity and that *N*-blocked puromycin is non-toxic to D9 cells. The selective enrichment of PAC-expressing cells argues that puromycin exerts its effect on D9 cells by acting on the translation apparatus *in vivo*.

We next wished to examine if B2P (**6**) could act in a biochemically similar fashion as puromycin itself. As with puromycin, flow cytometry indicated that long exposures of B2P (**6**) kills the vast majority of the cells infected with MIG (Figure 5-6C; bottom, left panel), while B2A (**7**), a control molecule lacking the amino acid, had no effect (Figure 5-6C; middle, left panel). Importantly, cells infected with MIG<sub>PAC</sub> show selective enrichment when incubated with B2P (**6**) (Figure 5-6C; bottom, right panel), while B2A shows no change in GFP-positive and negative populations (Figure 5-6C; middle, right panel). These experiments are fully consistent with B2P (**6**) acting by the same mechanism as puromycin itself. Further, these data also provide the first

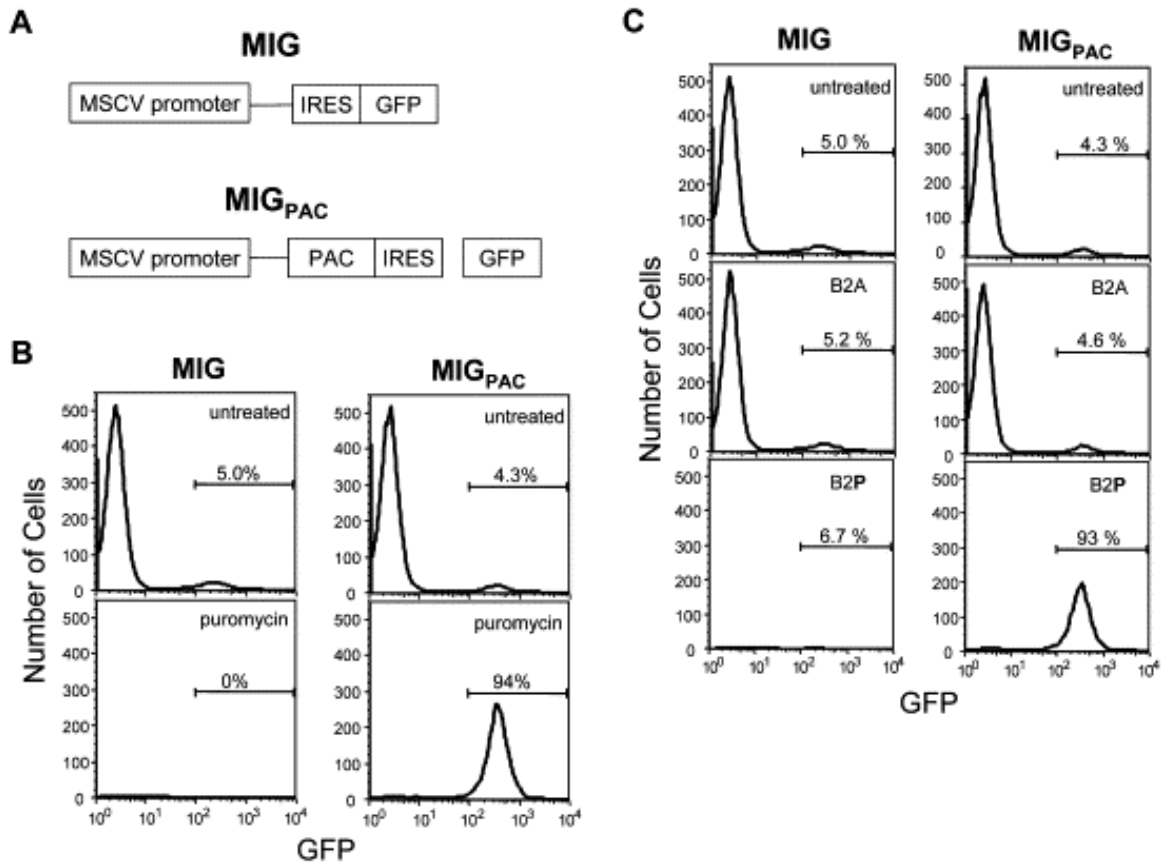


**Figure 5-6.** Mechanism of action of puromycin and puromycin conjugates in 16610D9 thymocyte cells infected with (A) MIG and MIG<sub>PAC</sub> constructs. (B) Cells infected with MIG are sensitive to puromycin action but cells infected with MIG<sub>PAC</sub> are resistant to puromycin. (C) Cells infected with MIG or MIG<sub>PAC</sub> were treated with biotinylated-puromycin conjugates B2A (7) and B2P (6).

demonstration that PAC can act on puromycin conjugates bearing 5'-extensions *in vivo*.

In line with this conclusion, two other puromycin conjugates show similar activity with B2P. We examined a Cy<sub>5</sub>-bearing conjugate Cy<sub>5</sub>2P (**1**) and compared its action with an analogous control molecule, Cy<sub>5</sub>2A (**2**), using both MIG and MIG<sub>PAC</sub> infected cells. Cy<sub>5</sub> provides a useful spectroscopic handle in this context because its red-shifted fluorescence allows the emission of the conjugate to be unambiguously separated from that of GFP. As with B2P versus B2A, MIG-infected cells were insensitive to Cy<sub>5</sub>2A, while long exposure of Cy<sub>5</sub>2P killed both GFP-positive and negative populations, since they lacked the PAC resistance determinant (data not shown). Cy<sub>5</sub>2P also selectively enriched MIG<sub>PAC</sub> infected cells from 4.3 % to 90 % (data not shown). Additionally, B2P-Me (**11**) also resulted in selective enrichment of MIG<sub>PAC</sub>-bearing cells and had similar potency with B2P (**6**) (data not shown). Taken together, these data support the idea that our various X-dC-puromycin conjugates act by the same mechanism as puromycin *in vivo* and that conjugates lacking the 3'-amino acid moiety have no effect.

### 5.3.5 Western blot analysis of puromycin conjugate labeling in live cells

Action of puromycin and our conjugates should result in proteins bearing these compounds at their C-terminus *in vivo*. We chose to use Western blot analysis of cellular lysates to examine if incorporation occurred *in vivo* and to compare the resulting signal with our control conjugates. Cells were incubated with either BF2P (**8**) or the control molecule BF2A (**9**) washed, and a whole-cell lysate was prepared for each sample (see Experimental Procedures). Proteins were run on a SDS-PAGE gel and transferred to nitrocellulose. Equal protein loading was confirmed in each lane using Ponceau S (data

not shown). The Ponceau S stain was rinsed away and the blot was probed with an anti-fluorescein antibody to detect any fluorescein-conjugated protein containing BF2P or BF2A. Cells treated with BF2P (Figure 5-7; lane 2) show good levels of incorporation in this assay, while lanes with cells alone (lane 1), cells treated with BF2A (lane 3), or anisomycin (lane 4) show essentially no signal (Figure 5-7). The Western-blot analysis of BF2P thus shows good correlation with flow cytometry data and is consistent with a model where puromycin conjugates are stably incorporated into proteins *in vivo* during protein synthesis.

## 5.4 Discussion

In the present study, we developed a technique to detect protein synthesis in live cells that does not require gene transfection or radiolabeling. Our strategy thus provides an important potential alternative to these methods for studying protein expression *in vivo*. Generally, a great diversity of reagents of the class X-dC-puromycin, where X can be one or two fluorescent or affinity tags, can be constructed and show good activity in protein synthesis *in vitro* and *in vivo*. These reagents all appear to act by the same basic mechanism, entering the ribosomal peptidyl transferase site during translation, followed by covalent attachment to proteins being actively synthesized. Ribosome entry and attachment occurs predominantly at a few discrete sites in the open reading frame including the stop codon, rather than at every position in the chain [17, 25]. Previous work also demonstrates that, over a 50-fold concentration range that brackets the IC<sub>50</sub>, the length of truncated products is the same and that shorter products are favored as the conjugate concentration is increased substantially.

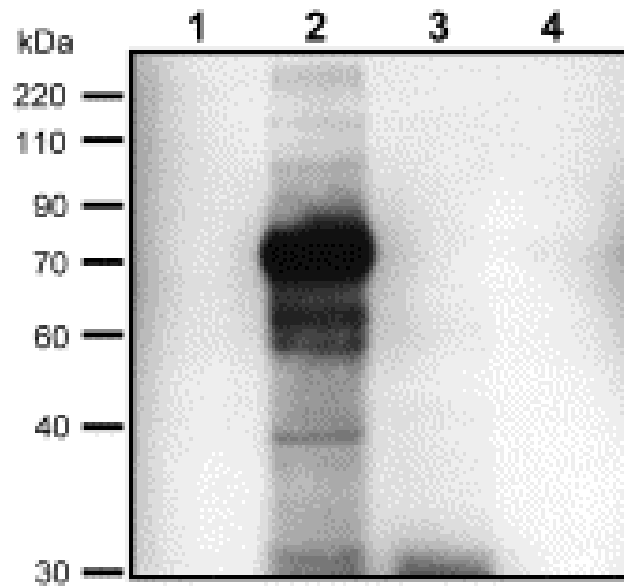


**Figure 5-7.** Western analysis of 16610D9 thymocyte cells treated with a puromycin conjugate and analyzed using an  $\alpha$ -fluorescein antibody: Lane 1, untreated cells; lane 2, BF2P, **8** (25  $\mu$ M); lane 3, BF2A, **9** (25  $\mu$ M); and, lane4, anisomycin (250 ng/mL). Ponceau S stain was used to confirm equal protein loading. BF2P-conjugated protein is seen at many molecular weights indicating that the conjugate could target all translating ribosomes.

Despite the intermediate size of these molecules (1163 to 1730 Da), all the conjugates appear to be competent to enter the D9 suspension tissue culture cells used here and to act at modest concentrations (5 – 25  $\mu$ M). Experiments with other mammalian and insect cell types support the idea that the ability of these compounds to cross membranes and act in protein synthesis is a general phenomenon (W. B. Smith, E. Schuman, B. Hay, unpublished observations). All of the conjugates we have examined show a significant and measurable shift in the fluorescence intensity of live cells as compared to the control conjugates. Western analysis and selective enrichment studies support the idea that this shift is due to the specific covalent attachment of the conjugates to nascent proteins during translation. Demonstration that affinity tags may be inserted into expressed proteins *in vivo* provides the future opportunity to examine protein expression in response to various cellular stimuli and subsequent identification of the individual polypeptides through a combination of affinity purification and mass spectrometry-based sequence analysis.

In the short term (~24 hours), these compounds are non-toxic based on the proportion of live cells seen in our flow cytometry experiments. The robust labeling and signal to noise we observe thus makes these compounds useful for a great diversity of cell, tissue, and organism-level experiments. The long-term toxicity of the present set of compounds may provide some limitations for their use. In that context, non-toxic variants that can be photoactivated or presented as pro-drugs may provide useful paths for future conjugate development. The general class of compounds described here should therefore serve as useful cell biology tools to evaluate *in vivo* protein synthesis in areas such as nuclear protein synthesis [26, 27], neuron dendritic protein synthesis [10],

dendritic cell aggresome-like induced structures (DALIS) [28], and other novel proteome functions.

## 5.5 Significance

Existing methods to study *in vivo* protein synthesis generally require choice of a candidate gene, radioactivity, or the destruction of cells. To overcome these limitations, we have developed a new class of reagents that enable detection of protein synthesis in live cells using fluorescent and biotinylated puromycin conjugates. These reagents, of the general form X-dC-puromycin, are active *in vitro* and *in vivo* and provide a non-toxic alternative for the study of protein synthesis in live cells. A wide variety of detection moieties appears to be accommodated at the X-position allowing for facile custom reagent design and development. Initial *in vitro* studies correlate the function of our compounds in peptide bond formation during protein synthesis. Subsequent *in vivo* experiments in a mouse thymocyte cell line demonstrate the usefulness of these molecules as indicators of protein synthesis in live cells. Selective enrichment studies with several conjugates as well as western analysis demonstrate that these compounds all label protein in cells by the same general mechanism, which is attachment to nascent proteins during translation. The present results thus provide evidence that puromycin conjugates may serve as an alternative to existing tools to elucidate the proteome.

## 5.6 Experimental Procedures

### 5.6.1 Materials

L-Puromycin hydrochloride, rabbit globin mRNA, and carboxypeptidase Y (CPY)

were obtained from Sigma Chemical Co. (St. Louis, MO). Rabbit reticulocyte Red Nova<sup>®</sup> lysate was purchased from Novagen (Madison, WI). L-[<sup>35</sup>S]methionine ([<sup>35</sup>S]Met) (1175 Ci/mmol) was obtained from NEN Life Science Products (Boston, MA). Immunopure<sup>®</sup> immobilized Neutravidin-agarose was from Pierce (Rockford, IL). GF/A glass microfiber filters were from Whatman.

### 5.6.2 Puromycin conjugates

Puromycin conjugates were synthesized using standard phosphoramidite chemistry at the California Institute of Technology oligonucleotide synthesis facility. Puromycin-CPG was obtained from Glen Research (Sterling, VA). Oligonucleotides were synthesized with the 5'-trityl intact, desalted via OPC cartridge chromatography (Glen Research) (DNA oligonucleotides only), cleaved, and evaporated to dryness. 5'-Biotin phosphoramidite, Biotin phosphoramidite, 5'-Fluorescein phosphoramidite, 6-Fluorescein phosphoramidite (Glen Research) were used to make the biotin- and dye-puromycin conjugates. Ac-dC-Me-phosphoramidite (Glen Research) was used to prepare the phosphonate puromycin conjugates. The dried samples were resuspended and desalted on Sephadex G-10 (Sigma). Puromycin, puromycin-conjugate, and control molecule concentrations were determined with the following extinction coefficients ( $M^{-1}cm^{-1}$ ): puromycin ( $\epsilon_{260} = 11,790$ ; in H<sub>2</sub>O); B2P and B2P-Me ( $\epsilon_{260} = 19,100$ ; in H<sub>2</sub>O); F2P, F2P-Me, DMT-F2P-Me, FB2P, BF2P, F2A, and BF2A ( $\epsilon_{491} = 66,000$ ; in 1X PBS); Cy<sub>5</sub>2P and Cy<sub>5</sub>2A ( $\epsilon_{650} = 250,000$ ; in 1X PBS).

### 5.6.3 *In vitro* potency determination for puromycin conjugates

Translation reactions containing [<sup>35</sup>S]Met were mixed in batch on ice and added in aliquots to microcentrifuge tubes containing an appropriate amount of puromycin-conjugate (or control molecule) dried *in vacuo*. Typically, a 20 µL translation mixture consisted of 0.8 µL of 2.5 M KCl, 0.4 µL of 25 mM MgOAc, and 1.6 µL of 12.5X translation mixture without methionine, (25 mM dithiothreitol (DTT), 250 mM HEPES (pH 7.6), 100 mM creatine phosphate, and 312.5 µM of 19 amino acids, except methionine), 3.6 µL of nuclease-free water, 0.6 µL (6.1 µCi) of [<sup>35</sup>S]Met (1175 Ci/mmol), 8 µL of Red Nova nuclease-treated lysate, and 5 µL of 0.05 µg/µL globin mRNA. Inhibitor, lysate preparation (including all components except template) and globin mRNA were mixed simultaneously and incubated at 30°C for 60 min. Each reaction (2 µL) was combined with 8 µL of tricine loading buffer (80 mM Tris-Cl (pH 6.8), 200 mM DTT, 24% (v/v) glycerol, 8% sodium dodecyl sulfate (SDS), and 0.02 % (w/v) Coomassie blue G-250), heated to 90 °C for 5 min, and applied entirely to a 4% stacking portion of a 15% tricine-SDS-polyacrylamide gel containing 20% (v/v) glycerol [29] (30 mA for 1h, 30 min). Gels were fixed in 10% acetic acid (v/v) and 50% (v/v) methanol, dried, exposed overnight on a PhosphorImager screen, and analyzed using a Storm PhosphorImager (Molecular Dynamics).

### 5.6.4 Neutravidin capture of *in vitro* translated protein-puromycin-conjugate products

Neutravidin-agarose [50% slurry (v/v)] was washed 3 times with 1X PBS + 0.1% Tween-20 and resuspended in 1 mL of 1X PBS + 0.1% Tween-20. To 200 µL of this

suspension, 12  $\mu$ L of the reaction lysate and 0.8 mL of 1X PBS + Tween-20 were added. The samples were rotated at 4 °C for 3 h and washed with 1X PBS + Tween-20 until the cpm of [<sup>35</sup>S]Met were <500 in the wash. The amount of immobilized [<sup>35</sup>S]Met-puromycin conjugate was determined by scintillation counting of the Neutravidin-agarose beads.

### **5.6.5 Preparation of MIG<sub>PAC</sub> infected 16610D9 cells**

The PAC gene was cloned into MIG using BgII and EcoRI restriction sites to yield MIG<sub>PAC</sub>. 293T-HEK fibroblasts (American Tissue Culture Collection) were co-transfected with pECL-Eco [30] and MIG or MIG<sub>PAC</sub> by calcium phosphate precipitation. After 12 hours, the precipitate was removed, cells were washed once with PBS, and 4 mL of fresh complete Dulbecco's Modified Eagle Medium (DMEM) supplemented with 10% fetal calf serum (FCS). Viral supernatant was removed 24 hours later and used in infection of 16610D9 cells. One million D9 cells were spin-infected with 0.4 mL of viral supernatant supplemented with 5 $\mu$ g/ml Polybrene (Sigma-Aldrich).

### **5.6.6 Enrichment of GFP(+) 16610D9 cells using puromycin and puromycin conjugates**

16610D9 cells infected with either MIG or MIG<sub>PAC</sub> were cultured in RPMI media with 10% FBS and grown at 37 °C in a humidified atmosphere with 5% CO<sub>2</sub>. For each experiment, 16610D9 cells (0.25 x 10<sup>6</sup>/well) were added to 24-well microtiter plates along with puromycin, puromycin-conjugate, and control molecules dissolved in the minimum amount of either media or PBS. After a 48 h incubation, the cells were washed

twice in 2 mL PBS + 4% FCS and resuspended in PBS + 4% FCS supplemented with 2% formaldehyde along with incubation at 37 °C for 10 min. Flow cytometry was carried out on a Beckman FACScalibur Flow Cytometer.

#### **5.6.7 Detection of protein synthesis events *in vivo* using flow cytometry**

16610D9 cells ( $0.5 \text{ million mL}^{-1}$ ) were combined with the various puromycin conjugates and control molecules resuspended in the minimum volume of PBS or media as described above. After a 24 h incubation, the cells were washed twice in 2 mL PBS + 4% FCS and resuspended in PBS + 4% FCS supplemented with 2% formaldehyde followed by incubation at 37 °C for 10 minutes or used directly after washing for immediate flow cytometry analysis.

#### **5.6.8 Western analysis of 16610D9 cells treated with puromycin conjugates**

Cells were prepared as described above, except as indicated anisomycin was added to a final concentration of  $250 \mu\text{g mL}^{-1}$ , and washed twice in PBS. Live cell number was determined using trypan blue exclusion dye, and each sample was adjusted to contain an equal number of live cells. Cell pellets were resuspended in 2X lysis buffer (100 mM  $\beta$ -glycerophosphate, 3 mM EGTA, 2 mM EDTA, 0.2 mM sodium-orthovanadate, 2 mM DTT, 20  $\mu\text{g/ml}$  aprotinin, 20  $\mu\text{g/ml}$  leupeptin, 50  $\mu\text{g/ml}$  trypsin inhibitor, and 4  $\mu\text{g/ml}$  pepstatin, and 1% Triton X-100) and incubated on ice for 30 minutes. Cell debris was removed by centrifugation at  $20,000 \times g$  for 30 minutes. Cell lysate was combined with SDS loading buffer (0.12 M Tris-Cl (pH 6.8), 20% glycerol, 4% (w/v) SDS, 2% (v/v)  $\beta$ -mercaptoethanol, and 0.001% bromophenol blue) and heated

at 90°C for 10 minutes. Samples were applied entirely to a 4% stacking portion of a 10% glycine-SDS-polyacrylamide gel (30 mA for 1h, 30 min). Protein was transferred using standard Western transfer techniques, and the blot was probed with an anti-fluorescein antibody followed by an anti-rabbit-horseradish peroxidase conjugate (Pierce chemicals). The chemiluminescence reaction was carried out using the ECL PLUS Western Blotting Detection System (Amersham Biosciences).

## 5.7 Acknowledgements

We gratefully acknowledge the help and useful discussions from our collaborators Erin Schuman, W. Bryan Smith, and Bruce Hay who have examined puromycin-dye conjugates in various *in vivo* systems. This work was supported by NIH Grant R01 GM60416 (R. W. R.) and by NIH training grant GM 07616 (S. R. S.).

## 5.8 References

1. Lander ES, Linton LM, Birren B, Nusbaum C, Zody MC, Baldwin J, Devon K, Dewar K, Doyle M, FitzHugh W *et al*: **Initial sequencing and analysis of the human genome**. *Nature* 2001, **409**(6822):860-921.
2. Venter JC, Adams MD, Myers EW, Li PW, Mural RJ, Sutton GG, Smith HO, Yandell M, Evans CA, Holt RA *et al*: **The sequence of the human genome**. *Science* 2001, **291**(5507):1304-1351.
3. Duncan RF, Peterson H, Hagedorn CH, Sevanian A: **Oxidative stress increases eukaryotic initiation factor 4E phosphorylation in vascular cells**. *Biochem J* 2003, **369**(Pt 2):213-225.

4. Lipschutz JH, Lingappa VR, Mostov KE: **The exocyst affects protein synthesis by acting on the translocation machinery of the endoplasmic reticulum.** *J Biol Chem* 2003, **278**(23):20954-20960.
5. Constantinou C, Bushell M, Jeffrey IW, Tilleray V, West M, Frost V, Hensold J, Clemens MJ: **p53-induced inhibition of protein synthesis is independent of apoptosis.** *Eur J Biochem* 2003, **270**(15):3122-3132.
6. Lockhart DJ, Winzeler EA: **Genomics, gene expression and DNA arrays.** *Nature* 2000, **405**(6788):827-836.
7. van Roessel P, Brand AH: **Imaging into the future: visualizing gene expression and protein interactions with fluorescent proteins.** *Nat Cell Biol* 2002, **4**(1):E15-20.
8. Miyawaki A, Llopis J, Heim R, McCaffery JM, Adams JA, Ikura M, Tsien RY: **Fluorescent indicators for Ca<sup>2+</sup> based on green fluorescent proteins and calmodulin.** *Nature* 1997, **388**(6645):882-887.
9. Ting AY, Kain KH, Klemke RL, Tsien RY: **Genetically encoded fluorescent reporters of protein tyrosine kinase activities in living cells.** *Proc Natl Acad Sci U S A* 2001, **98**(26):15003-15008.
10. Aakalu G, Smith WB, Nguyen N, Jiang C, Schuman EM: **Dynamic visualization of local protein synthesis in hippocampal neurons.** *Neuron* 2001, **30**(2):489-502.
11. Steward O, Schuman EM: **Protein synthesis at synaptic sites on dendrites.** *Annu Rev Neurosci* 2001, **24**:299-325.

12. Nathans D: **Puromycin Inhibition Of Protein Synthesis: Incorporation Of Puromycin Into Peptide Chains.** *Proc Natl Acad Sci U S A* 1964, **51**:585-592.
13. Yarmolinsky MB, de la Haba G: **Inhibition by puromycin of amino acid incorporation into protein.** *Proc Natl Acad Sci U S A* 1959, **45**:1721-1729.
14. Doi N, Takashima H, Kinjo M, Sakata K, Kawahashi Y, Oishi Y, Oyama R, Miyamoto-Sato E, Sawasaki T, Endo Y *et al*: **Novel fluorescence labeling and high-throughput assay technologies for in vitro analysis of protein interactions.** *Genome Res* 2002, **12**(3):487-492.
15. Kawahashi Y, Doi N, Takashima H, Tsuda C, Oishi Y, Oyama R, Yonezawa M, Miyamoto-Sato E, Yanagawa H: **In vitro protein microarrays for detecting protein-protein interactions: application of a new method for fluorescence labeling of proteins.** *Proteomics* 2003, **3**(7):1236-1243.
16. Nemoto N, Miyamoto-Sato E, Yanagawa H: **Fluorescence labeling of the C-terminus of proteins with a puromycin analogue in cell-free translation systems.** *FEBS Lett* 1999, **462**(1-2):43-46.
17. Starck SR, Roberts RW: **Puromycin oligonucleotides reveal steric restrictions for ribosome entry and multiple modes of translation inhibition.** *Rna* 2002, **8**(7):890-903.
18. Starck SR, Qi X, Olsen BN, Roberts RW: **The puromycin route to assess stereo- and regiochemical constraints on peptide bond formation in eukaryotic ribosomes.** *J Am Chem Soc* 2003, **125**(27):8090-8091.
19. Diamond RA, DeMaggio S: **In living color: protocols in flow cytometry and cell sorting.** Berlin; New York: Springer; 2000.

20. Van Parijs L, Refaeli Y, Lord JD, Nelson BH, Abbas AK, Baltimore D: **Uncoupling IL-2 signals that regulate T cell proliferation, survival, and Fas-mediated activation-induced cell death.** *Immunity* 1999, **11**(3):281-288.
21. de la Luna S, Ortin J: **pac gene as efficient dominant marker and reporter gene in mammalian cells.** *Methods Enzymol* 1992, **216**:376-385.
22. Perez-Gonzalez JA, Vara J, Jimenez A: **Acetylation of puromycin by Streptomyces alboniger the producing organism.** *Biochem Biophys Res Commun* 1983, **113**(3):772-777.
23. Porter JN, Hewitt RI, Hesseltine CW, Krupka G, Lowery JA, Wallace WS, Bohonos N, Williams JH: **Achromycin: A New Antibiotic Having Trypanocidal Properties.** *Antibiotics and Chemotherapy* 1952, **11**:409-410.
24. Bain G, Quong MW, Soloff RS, Hedrick SM, Murre C: **Thymocyte maturation is regulated by the activity of the helix-loop-helix protein, E47.** *J Exp Med* 1999, **190**(11):1605-1616.
25. Wolin SL, Walter P: **Ribosome pausing and stacking during translation of a eukaryotic mRNA.** *Embo J* 1988, **7**(11):3559-3569.
26. Iborra FJ, Jackson DA, Cook PR: **Coupled transcription and translation within nuclei of mammalian cells.** *Science* 2001, **293**(5532):1139-1142.
27. Nathanson L, Xia T, Deutscher MP: **Nuclear protein synthesis: a re-evaluation.** *Rna* 2003, **9**(1):9-13.
28. Lelouard H, Ferrand V, Marguet D, Bania J, Camosseto V, David A, Gatti E, Pierre P: **Dendritic cell aggresome-like induced structures are dedicated areas**

- for ubiquitination and storage of newly synthesized defective proteins. *J Cell Biol* 2004, **164**(5):667-675.**
29. Schagger H, von Jagow G: **Tricine-sodium dodecyl sulfate-polyacrylamide gel electrophoresis for the separation of proteins in the range from 1 to 100 kDa.** *Anal Biochem* 1987, **166**(2):368-379.
30. Naviaux RK, Costanzi E, Haas M, Verma IM: **The pCL vector system: rapid production of helper-free, high-titer, recombinant retroviruses.** *J Virol* 1996, **70**(8):5701-5705.